Aus der Medizinischen Klinik und Poliklinik I
Klinikum der Ludwig-Maximilians-Universität München

Dissertation

zum Erwerb des Doctor of Philosophy (Ph.D.)

an der Medizinischen Fakultät der
Ludwig-Maximilians-Universität München

The role of platelet subsets in inflammation

vorgelegt von:
Afra Anjum

aus:
Dhaka / Bangladesch

Jahr:
2025

Mit Genehmigung der Medizinischen Fakultät der
Ludwig-Maximilians-Universität München

Erstes Gutachten von:	Priv. Doz. Dr. Leo Nicolai
Zweites Gutachten von:	Prof. Dr. Maria del Sagrario Robles Martinez
Drittes Gutachten von:	Prof. Dr. Christian Weber
Viertes Gutachtes:	Prof. Dr. Bernd Engelmann

Dekan: **Prof. Dr. med. Thomas Gudermann**

Datum der Verteidigung:

22.05.2025

LMU LUDWIG-MAXIMILIANS-UNIVERSITÄT MÜNCHEN

Dean's Office Medical Faculty
Faculty of Medicine

Affidavit

Anjum, Afra

Surname, first name

I hereby declare, that the submitted thesis entitled

The role of platelet subsets in inflammation

is my own work. I have only used the sources indicated and have not made unauthorised use of services of a third party. Where the work of others has been quoted or reproduced, the source is always given.

I further declare that the dissertation presented here has not been submitted in the same or similar form to any other institution for the purpose of obtaining an academic degree.

Munich, 28.05.2025

Place, Date

Afra Anjum

Signature doctoral candidate

LMU LUDWIG-MAXIMILIANS-UNIVERSITÄT MÜNCHEN

Dean's Office Medical Faculty
Doctoral Office

Confirmation of congruency between printed and electronic version of the doctoral thesis

Anjum, Afra

Surname, first name

I hereby declare that the electronic version of the submitted thesis, entitled

The role of platelet subsets in inflammation

is congruent with the printed version both in content and format.

Munich, 28.05.2025

Place, Date

Afra Anjum

Signature doctoral candidate

Table of contents

Part I

Abbreviations

ADP	Adenosine diphosphate
AiA	Antigen-induced arthritis
ALI	Acute lung injury
APAF1	Apoptotic protease activating factor 1
APC	Antigen-presenting cell
Arp2/3	Actin related protein 2/3
ATP	Adenosine tri-phosphate
Ca^{2+}	Calcium ion
CD	Cluster of differentiation
CLEC-2	C-type lectin receptor 2
CRP	Collagen-related peptide
CypD	Cyclophilin D
COVID-19	Coronavirus disease 2019
GP	Glycoprotein
HIT	Heparin induced thrombocytopenia
ITAM	Immunoreceptor tyrosine-based activation motif
LAMP	Lysosome-associated membrane protein
L. monocytogenes	*Listeria monocytogenes*
LPS	Lipopolysaccharide
MHC	Major histocompatibility complex
MK	Megakaryocyte
mPTP	Mitochondrial permeability transition pore
MRSA	Methicillin resistant *S. aureus*
NETs	Neutrophil extracellular traps
PA	Procoagulant activation
PMP	Platelet microbicidal proteins
PRR	Pattern recognition receptors
PS	Phosphatidylserine
PSGL-1	P-selectin glycoprotein ligand-1
RNA	Ribonucleic acid
ROS	Reactive oxygen species
S. aureus	*Staphylococcus aureus*
TLRs	Toll-like receptors
TMEM16F	Transmembrane protein 16F
VITT	Vaccine induced thrombotic thrombocytopenia
vWF	von Willebrand factor

Part II

List of Publications

1. **Anjum A,** Mader M, Mahameed S, Muraly A, Denorme F, Kliem FP, et al. Aging platelets shift their hemostatic properties to inflammatory functions. Blood Journal. 2025. doi:10.1182/blood.2024024901

2. Kaiser R, Escaig R, Kranich J, Hoffknecht M-L, **Anjum A**, Polewka V, et al. Procoagulant platelet sentinels prevent inflammatory bleeding through GPIIBIIIA and GPVI. Blood. 2022;140(2):121-39. doi:10.1182/blood.2021014914

3. Kaiser R, **Anjum A**, Kammerer LM, Loew Q, Akhalkatsi A, Rossaro D, et al. Mechanosensing via a GpIIb/Src/14-3-3ζ axis critically regulates platelet migration in vascular inflammation. Blood. 2023. doi:10.1182/blood.2022019210

4. Nicolai L, Leunig A, Pekayvaz K, Esefeld M, **Anjum A**, Rath J, et al. Thrombocytopenia and splenic platelet-directed immune responses after IV ChAdOx1 nCov-19 administration. Blood. 2022;140(5):478-90. doi:10.1182/blood.2021014712

5. Kaiser R, Dewender R, Mulkers M, Stermann J, Rossaro D, Di Fina L, …**Anjum A**… et al. Procoagulant platelet activation promotes venous thrombosis. Blood Journal. 2024. doi:10.1182/blood.2024025476

6. Nicolai L, Kaiser R, Escaig R, Hoffknecht M-L, **Anjum A**, Leunig A, et al. Single platelet and megakaryocyte morpho-dynamics uncovered by multicolor reporter mouse strains in vitro and in vivo</i&gt. Haematologica. 2021;107(7):1669-80. doi:10.3324/haematol.2021.278896

7. Kaiser R, Leunig A, Pekayvaz K, Popp O, Joppich M, Polewka V, …**Anjum A**… et al. Self-sustaining IL-8 loops drive a prothrombotic neutrophil phenotype in severe COVID-19. JCI Insight. 2021;6(18). doi:10.1172/jci.insight.150862

8. Pekayvaz K, Leunig A, Kaiser R, Joppich M, Brambs S, Janjic A, …**Anjum A**… et al. Protective immune trajectories in early viral containment of non-pneumonic SARS-CoV-2 infection. Nature Communications. 2022;13(1). doi:10.1038/s41467-022-28508-0

9. Kaiser R, Gold C, Joppich M, Loew Q, Akhalkatsi A, Mueller TT, …**Anjum A**… et al. Peripheral priming induces plastic transcriptomic and proteomic responses in circulating neutrophils required for pathogen containment. Science Advances. 2024;10(12). doi:10.1126/sciadv.adl1710

Part III

Introduction

The Multifaceted Roles of Platelets

Platelets possess a myriad of roles in vascular biology, from their classical role in hemostasis & thrombosis to their role as mediators of inflammation (Figure 1)[1-3]. Platelets act as sentinels and adapt their behavior to the demands in local microenvironment which has resulted in platelets earning the title of "guardians of the vasculature".

During **hemostasis**, injured vessels undergo vasoconstriction and platelets play a critical role by adhering rapidly to the site of vessel injury, aggregating together to form a platelet plug and allowing stabilization via formation of a dense fibrin mesh brought upon by the coagulation cascade. This cascade of events is crucial to prevent excessive bleeding[4]. Excessive platelet activation can lead to pathological clot formation - **thrombosis**. Arterial thrombosis in arteries of the heart and brain leads to myocardial infarction and stroke whereas thrombus formation in veins may lead to pulmonary embolism and venous thromboembolism[4, 5]. Beyond hemostasis and thrombosis, platelets are also involved in **inflammation**. Platelets provide a first line of defense by preventing entry of pathogens during injury to vessels through the preservation of vascular integrity[1]. Platelets are known to directly interact with microbes. Our group has shown that during inflammation, migrating platelets can bundle pathogens and secrete antimicrobial agents[1, 6-8]. Activated platelets possess a bactericidal function where they can release secretory products via degranulation during direct interaction with *Staphylococcus aureus* (*S. aureus*)[9]. Another way platelets contribute to immunity is through crosstalk with leukocytes which regulates immune responses. Platelets can also directly present costimulatory molecules as well as antigens like an antigen-presenting cell (APC) to leukocytes such as T cells[10]. Platelet crosstalk can initiate immune cell recruitment to sites of infection[11].

Platelets also play a role in development of pathologic acute lung injury (ALI). During, ALI, the body is unable to meet metabolic demands due to insufficient lung oxygenation, which can lead to fatality. ALI is a complication of infection or sterile injury[12]. During ALI, leukocytes infiltrate the lung and cause edema. Studies showed that depleting platelets enhanced organ function and reduced leukocyte infiltration in ALI, hinting towards the pathological role of platelets[13, 14]. Surface receptors P-selectin and CD40L have been associated with this condition[13, 15]. ALI is an important model for studying the role of platelet subsets and specific effector functions in the setting of inflammation.

To summarize, apart from their classical roles, platelets act as sentinels securing the first line of defense and orchestrate immune responses ranging from innate to adaptive immunity. Here, the focus of this dissertation will be on the non-classical immune-related role of platelet subsets.

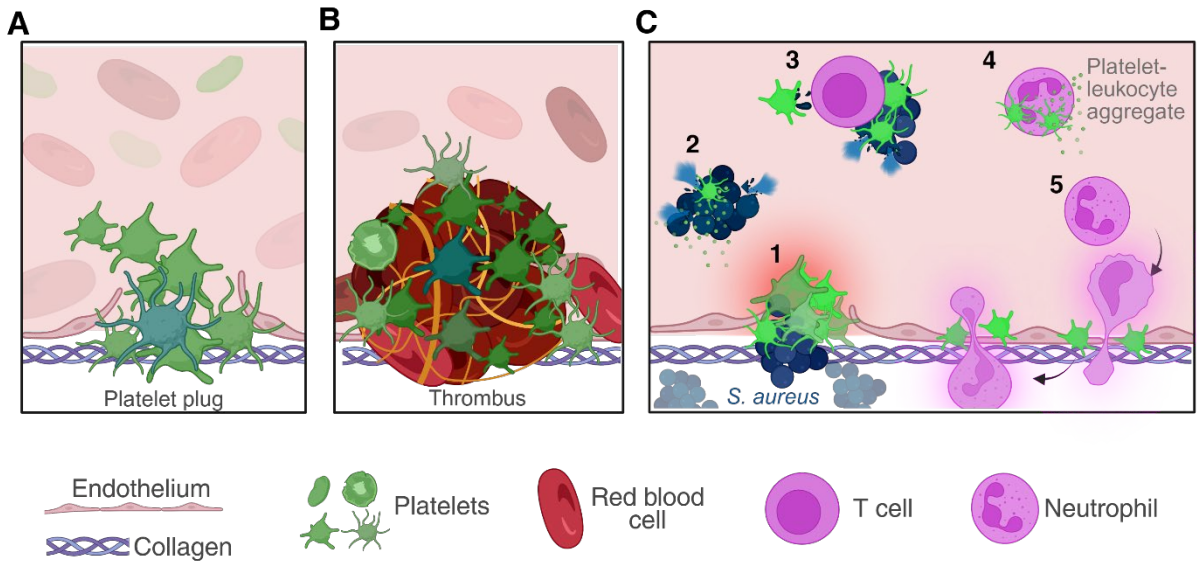

Figure 1. The many roles of platelets. Simplified schematic outline showing diverse roles of platelets. A) Hemostasis - platelets contribute to plug formation at injury sites to prevent bleeding. B) Thrombosis - pathological clot formation can lead to vessel occlusion. C) Inflammation - platelets aid in 1) maintaining vascular integrity, 2) bacterial killing, 3) antigen presentation, 4) platelet-leukocyte crosstalk including platelet-leukocyte aggregates (PLA) and 5) immune cell recruitment to sites of injury. Created in https://BioRender.com.

Platelet Morphology

To understand how platelets can contribute to the myriad processes, and how they have been categorized on their physical properties, we first need to understand the morphology of a platelet. Platelets are very small, approximately 2-5 μm in size with a thickness of 0.5 μm[4, 16-18]. Platelets contain key organelles such as mitochondria, alpha granules (50-80 per platelet), dense granules (3-8 per platelet), lysosomes (<3 per platelet) and sometimes RNA but **no nucleus**[18-20] (Figure 2A).

Platelets do not possess genomic DNA, however, nascent platelets contain residual amounts of megakaryocyte **RNA** which can be used as a platelet age indicator[21, 22]. **Mitochondria** are critical for platelet metabolism, function and signaling[23]. Platelets, when healthy, may contain anywhere between 5-8 mitochondria [23, 24]. Platelet mitochondria have an important role in ATP formation, reactive oxygen species (ROS) generation, calcium homeostasis, procoagulant platelet activation and apoptosis[25, 26]. This means that mitochondrial fitness is intertwined with platelet functions[27]. **α-Granules** consist of both membrane bound proteins and soluble proteins. Membrane bound proteins can be expressed on the platelet surface such as αIIbβ3, GPVI, CD36, or they can be expressed on platelet surfaces following platelet activation, for instance, P-selectin[28]. α-Granules' soluble factors such as CD40L, complement C3, & serpins play a role in inflammation[18, 19]. Platelet **dense granules** originate from the endosomal system rather than from the golgi network, and are lysosome related organelles[29]. They share lysosome-like organelles, as their granule pH is acidic and they contain lysosome related proteins like LAMPs and CD63[19]. Dense granules also contain

ADP, ATP, serotonin, calcium, and magnesium. Platelet **lysosomes** consist of enzymes that are involved in the degradation of lipids, proteins and carbohydrates. LAMP1 can be found on lysosomal membranes and contribute to the protective function of the lysosomes[19].

Platelet Receptors

Platelets express a broad range of receptors to fulfill their diverse tasks. Here, the focus will be on the receptors that we have investigated in more detail in this work. These receptors are crucial for the biological processes that platelets are involved in including: GPIb-IX-V, αIIbβ3, P-selectin, LAMP1, CD40L, CLEC-2, CD47, CD36 and GPVI (Figure 2B).

GPIb-IX-V is an abundant platelet surface receptor complex that is involved in almost all platelet functions[30]. GPIb-IX-V plays a role in hemostasis during the crucial step of platelet adhesion to damaged vessels, where flow shear rate leads to thrombus formation. Each platelet can have anywhere between 25,000 to 35,000 copies of the receptors[30, 31]. They consist of four subunits, namely: GPIbα, GPIbβ, GPIX, and GPV, and exist in a ratio of 1:2:1:1[32]. Constitutively expressed receptor GPIbα can bind to Mac-1 on neutrophils[33]. In the first paper, we used the non-activating, non-depleting platelet specific labeling antibody from Emfret (X488 and X649) that binds to the abundant GPIbβ subunit of the GPIb-IX-V complex.

αIIbβ3 integrins are part of a family of adhesion and signaling molecules which facilitate interaction between cells. Integrins comprise of α and β (β1, β2 and β3 in platelets) subunits[34]. Platelet aggregation is crucial to thrombus formation and is critically dependent on integrin αIIbβ3. This integrin is a receptor for fibrinogen, von Willebrand factor (vWF), vitronectin and fibronectin[35]. Platelet activation by ADP leads to conformational change and allows binding to fibrinogen. Also, GPIIb/IIIa is known as a target of the drug Tirofiban[35].

P-selectin is an integral membrane protein in the α-granules. Platelet activation causes granules to fuse with the cell surface membrane leading to redistribution of P-selectin to the cell surface. P-selectin plays a role in both inflammation and thrombosis[36, 37]. P-selectin expressed by activated platelets can bind to PSGL-1 on leukocytes such as neutrophils, monocytes, dendritic cells and lymphocytes[38, 39]. The rapid interaction and dissociation between the receptor and ligand are the basis for leukocyte tethering and rolling in circulation[38].

Platelets express **CD40L**, a transmembrane protein trimer, on their surface rapidly (within seconds) post stimulation[40]. Platelet CD40L is the ligand for CD40 which is expressed on B-cells, monocytes, macrophages and endothelial cells constitutively. During inflammation, platelets act as guides while binding to neutrophils via CD40L/CD154 surface receptors which trigger P-selectin to cause high affinity conformation in neutrophils that allow the immune cells to pass through the vessel wall[2, 41]. **LAMPs** are membrane-associated proteins found in platelet lysosomes (LAMP1 or CD107a) and dense granules (CD63). Degranulated CD8+ T cells express CD107a on their surface post activation, and are capable of cytotoxity[42]. LAMPs are considered as markers of

platelet activation, however, their functions are not well understood[34]. **CD47**, an important integrin-associated protein receptor, has thrombospondin as its ligand. Thrombospondin initiates signaling that enhance the integrin αIIbβ3[36]. CD47 interacts with collagen receptor α2β1. These interactions can result in modification of processes such as platelet activation, cell migration, adhesion and phagocytosis[43]. **CD36** (glycoprotein 4/GPIV) is one of the most abundant membrane receptors. Platelets have around 16,700 copies of CD36 in platelets[44]. Collagen and thrombospondins are some of the ligands for CD36. Also, one important function of CD36 is being a scavenger for oxidized lipoproteins[45].

Glycoprotein VI is an important surface receptor in the superfamily of immunoglobulin receptors on platelets[46]. GPVI is a receptor for collagen and fibrin[47]. GPVI can be activated by endogenous ligands such as collagen, fibrin, fibrinogen (only in humans) and exogenous ligands such as convulxin and CRP[46]. Afterwards, GPVI can initiate platelet activation by signaling using the ITAM. **CLEC-2** is expressed in high numbers on platelets[46]. CLEC-2 shares the same signaling pathways as GPVI downstream of the hemi-immunoreceptor tyrosine-base activation motif. CLEC-2 on platelets can also interact with podoplanin on macrophages which leads to platelet activation[48]. CLEC-2 knockout in mice showed significant reduction in platelets' ability in preventing inflammation-induced hemorrhage highlighting the importance of platelet CLEC-2 in maintaining vascular integrity and thrombosis during inflammation[46, 49-51].

Platelets possess a myriad of receptors that allow them to interact with immune cells & endothelial cells and become involved in immune functions[52]. Platelet-leukocyte interactions under steady state is minimal but important for the maintenance of vascular integrity[53]. The most important components that aid platelets in their variety of tasks via stable platelet interactions with immune cells and maintenance of vascular integrity include P-selectin, CD40L/CD154, CLEC-2, GPVI and GPIIb/IIIA[52].

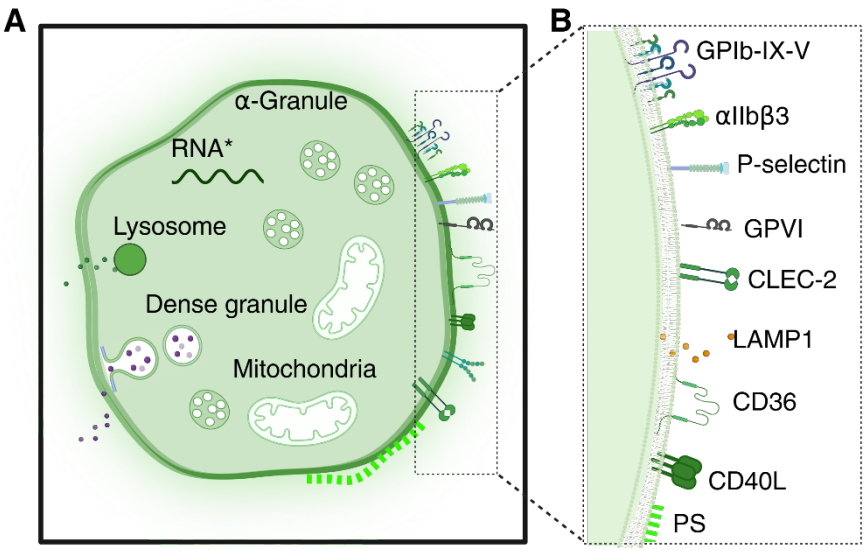

Figure 2. Overview of a platelet. A) Simplified schematic outline of a platelet's key organelles. B) Major platelet components involved in platelet effector functions. Created in https://BioRender.com.

Platelet Effector Functions

Through their diverse receptor repertoire, platelets can be recruited to sites of vessel injury, but also inflammation. Upon recruitment, platelets possess a range of abilities on how to respond to the respective challenge. The platelet effector repertoire consists of diverse mechanisms and pathways that aids in classical hemostasis and non-classical immune related effector activity (Figure 3).

Platelets are primarily effectors of hemostasis which involves prevention of excessive blood loss. During hemostasis, exposed endothelial matrix proteins, collagen and vWF, at the site of injury aids in platelet recruitment which leads to platelet **adhesion**, **activation** and prevention of bleeding[54]. Interaction between platelet GPIb-IX-V and vWF bound to collagen results in platelet retention close to the vessel wall, which in turn facilitates interaction between GPVI and collagen[55]. GPVI is also responsible for initial activation of platelets and granule release[56]. To ensure tight adhesion of platelets at site of injury, inactivated (low affinity) integrin αIIbβ3 in resting platelets undergo activation and conformation shift (high affinity) via the process of "inside-out" signaling[54, 57]. Platelet-platelet interaction and adhesion, mediated by ligand (fibrinogen/vWF) binding to αIIbβ3, triggers "outside-in" signaling which results in platelet **aggregation** and **clot retraction**[58]. Platelet retraction contributes to stabilization of platelet plug and is mediated by shape change via cytoskeleton reorganization. Gα13 subunit is a critical component in the "outside-in" signaling[59].

Platelets also play a role as vascular sentinels, and are at the forefront in the **first line of defense**. Platelets prevent pathogen entry by maintaining vascular integrity. Platelets, like other granulocytes, consist of granules such as α-granules which contain adhesion molecules, platelet microbicidal proteins (PMPs) and kinocidins which aid in their **antimicrobial response**[60]. Platelets can recognize and respond to pathogens using the pattern recognition receptors (PRRs) such as toll-like receptors (TLRs), C-type lectin receptors and NOD-like receptors[7]. Platelet TLR4 is potent in lipopolysaccharide (LPS) recognition, and is essential for **neutrophil activation** and trapping of bacteria via neutrophil extracellular trap formation or NETs.[61]. CLEC-2 deletion in mice showed significant reduction in platelets' ability in preventing inflammation-induced hemorrhage[46, 49-51]. Platelet **migration** also plays a crucial role during infection. We have previously reported that migrating platelets act as scavengers by bundling bacteria and enable neutrophil activation[8]. Genetic deletion of actin related protein 2/3 (Arp2/3) complex, which is responsible for platelet directional motility, resulted in augmented spread of bacteria[62]. Platelets also possess **bactericidal property** that allows them to confront pathogens directly. Thrombin stimulated platelets co-cultured with methicillin resistant *S. aureus* (MRSA) were capable of killing more than 40% of the bacteria in a period of two hours in absence of any immune cells. It was also reported that platelets facilitated *S. aureus* phagocytosis by macrophages via secretion of IL-1β[9]. **Procoagulant activation (PA)** of platelets play an important role during inflammation and has been associated with COVID-19, heparin induced thrombocytopenia (HIT) and vaccine induced thrombotic thrombocytopenia (VITT). Procoagulant platelets are characterized by their presence of P-selectin,

inactivated αIIbβ3 integrin, cytosolic calcium (Ca^{2+}) rise that leads to phosphatidylserine (PS) externalization, and irreversible ballooning[63, 64]. Procoagulant activation occurs when agonists trigger a strong stimulation in platelets causing a rapid increase in intracellular calcium, thus resulting in Ca^{2+} entry into the mitochondria. Once the critical threshold of calcium in mitochondria is reached, Cyclophilin D (CypD) facilitates formation of the mitochondrial permeability transition pore (mPTP). This reduces mitochondrial membrane stability and excess calcium is released back into the cytoplasm, which causes activation of transmembrane protein 16F (TMEM16F). This protein in turn promotes PS exposure on the platelet surface[25]. **Platelet-leukocyte crosstalk** is an essential part of immune response facilitated by an extensive repertoire of receptors in platelets. Platelets crosstalk and guide leukocytes to extravasate using CD40L and P-selectin[41]. The critical role of platelets in guiding neutrophils to the site of injury was exhibited when platelet depletion diminished immune cell extravasation in a model of acute lung injury[13]. In a model of antigen-induced arthritis (AiA), a marked reduction in platelet-leukocyte rolling and adhesion on endothelium was observed in P-selectin knockout mice, which could be rescued by transfusion of wild-type platelets[65]. Platelets also contribute to adaptive immunity via antigen trafficking, and dendritic cell mediated presentation of antigens. Platelets shuttle *Listeria monocytogenes* (*L. monocytogenes*) to CD8α+ dendritic cells in spleen via complement C3 and platelet GPIb which triggers the adaptive immune response. Depleting platelets or blocking aggregation (C3 knockout) sped up pathogen clearance[66]. Platelets also possess major histocompatibility complex class I (MHC class I) which they can use to directly present antigens, along with costimulatory molecules, like an antigen presenting cell (APC) to leukocytes such as T cells[10]. In short, platelet effector functions highlight the myriad roles of platelets that contribute to physiological and pathological settings which includes adhesion, activation, aggregation, migration, clot retraction, procoagulant activation and immune modulation.

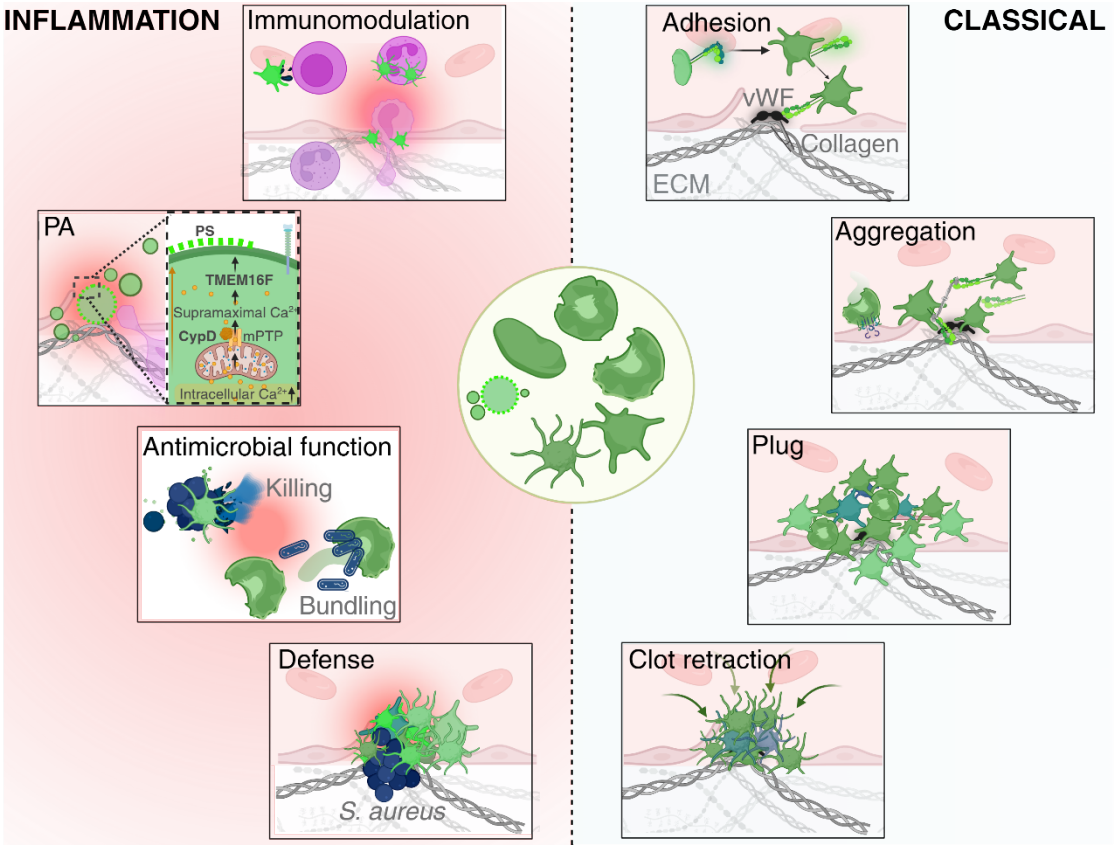

Figure 3. Platelet effector functions. Simplified schematic diagram of classical (right) and non-classical (left) effector functions. Classical functions include platelet **adhesion** to extracellular matrix (ECM) via collagen and von Willebrand Factor (vWF), platelet **aggregation**, formation of hemostatic **plug**, and **clot retraction** for stabilization. Non-classical functions involve **defense** against bacteria like *Staphylococcus aureus* by preventing pathogen entry, **antimicrobial function** through direct killing & bundling of pathogens, **procoagulant activation** (PA) via calcium-dependent (Ca^{2+}) signaling involving TMEM16F & cyclophilin D (CypD) and **immunomodulation** through interaction with leukocytes, supporting antigen presentation & recruitment of immune cells to sites of injury. Created in https://BioRender.com.

Platelet Lifespan

Platelets need to maintain their number in circulation at a steady state, via regular replenishment in order to perform their many roles. **Thrombopoiesis** or platelet production occurs when matured megakaryocytes (MKs) form cytoplasmic extensions called proplatelets that extend through the endothelial barrier, primarily in the bone marrow[67] and also in the lungs (Figure 4A)[68]. Each megakaryocyte may release hundreds of platelets of nearly uniform size into the bloodstream[69]. During situations of heightened platelet demand such as thrombocytopenia or inflammation, platelet release can also occur through the rupture of the mature MK membrane[70]. In both processes, whether by proplatelet formation or MK membrane rupture, megakaryocytes must be positioned adjacent to blood vessels to facilitate platelet release into circulation[71-73]. The vascular

niche consists of extracellular matrix components that enable megakaryocytes to migrate to a microenvironment that supports and guides the final stages of MK maturation, proplatelet formation and finally platelet production[72].

Newly formed platelets that contain residual amounts of RNA are also referred to as immature or **reticulated platelets**[74, 75]. Reticulated platelets can be distinguished from non-reticulated via RNA staining using thiazole orange which facilitates the study of differences in whole blood or isolated platelets[76]. Reticulated platelets show higher adhesion[77], aggregation, response to agonists and higher expression of P-selectin and GPIIb/IIIa[75, 78]. It has also been reported that reticulated platelets contain more cytoskeletal proteins, greater mitochondrial number and are larger in size compared to older platelets, hinting towards platelet metabolic fitness and aptitude which facilitates their primary role in hemostasis and pathological thrombosis[75, 78-80].

Platelets have a lifespan of 7-10 days in humans and 4-5 days in mice[81, 82]. Maintaining a steady number of platelets is crucial as too many platelets can cause thrombocytosis while too low a concentration can cause thrombocytopenia. It is still not well understood how each individual platelet decides to initiate apoptosis and thereby clearance from circulation[82]. As platelets age in circulation, **aged platelets** are considered to undergo a functional decline, characterized by having a smaller size, lesser mitochondria, reduced RNA, a decline in protein content, and overall less reactivity to external stimuli[80]. Interestingly, a recent publication comparing reticulated or large platelet and non-reticulated or small platelet transcriptomics highlighted that aged platelet transcripts were associated with inflammatory processes, such as presence of IL7, complement proteins[80], or more proteins found to be involved in inflammation and immunity[83] which could imply a potential alteration in their role from hemostasis to immune regulation.

When platelets age, they can lose sialic acid from their surfaces, which has been connected to senescent platelet removal[84-86]. **Desialylated platelets** have increased exposure of β-galactose, which can be recognized by the Ashwell-Morell receptor found on the surface of hepatocytes and macrophages (Figure 4B). This in turn induces the clearance of platelets. Desialylation is a great marker for aged platelets that are awaiting clearance[84].

Platelet fate is regulated by mitochondria dependent intrinsic **apoptosis** which is in turn maintained by a fine balance of proapoptotic and pro-survival proteins (Figure 4C)[84, 87]. Under normal conditions, pro-survival Bcl-2 proteins inhibit proapoptotic **BAK** & **BAX**[84, 88]. During stress or damage in platelets, BH3 domain containing proteins are activated which then activate the intrinsic apoptosis pathway in platelets. BH3-only proteins inhibit Bcl-2 and as a result frees BAK & BAX to start mitochondrial membrane damage. Once mitochondria lose their membrane integrity and become permeable, they release cytochrome c into the cytoplasm[87]. Cytochrome c then binds to APAF1 and forms the apoptosome complex leading to activation of caspases[89, 90]. Caspase-3/7 then facilitates phosphatidylserine exposure to the outer side of the cell membrane from the inner side. Phosphatidylserine exposure acts as an "eat me" signal that we also can use as a marker for apoptosis[89]. A model for studying the effects of aged platelets is by using platelet specific BAK

BAX knockout mice, which prolongs platelet lifespan and allows the study of the aged platelet phenotype when compared to wild type.

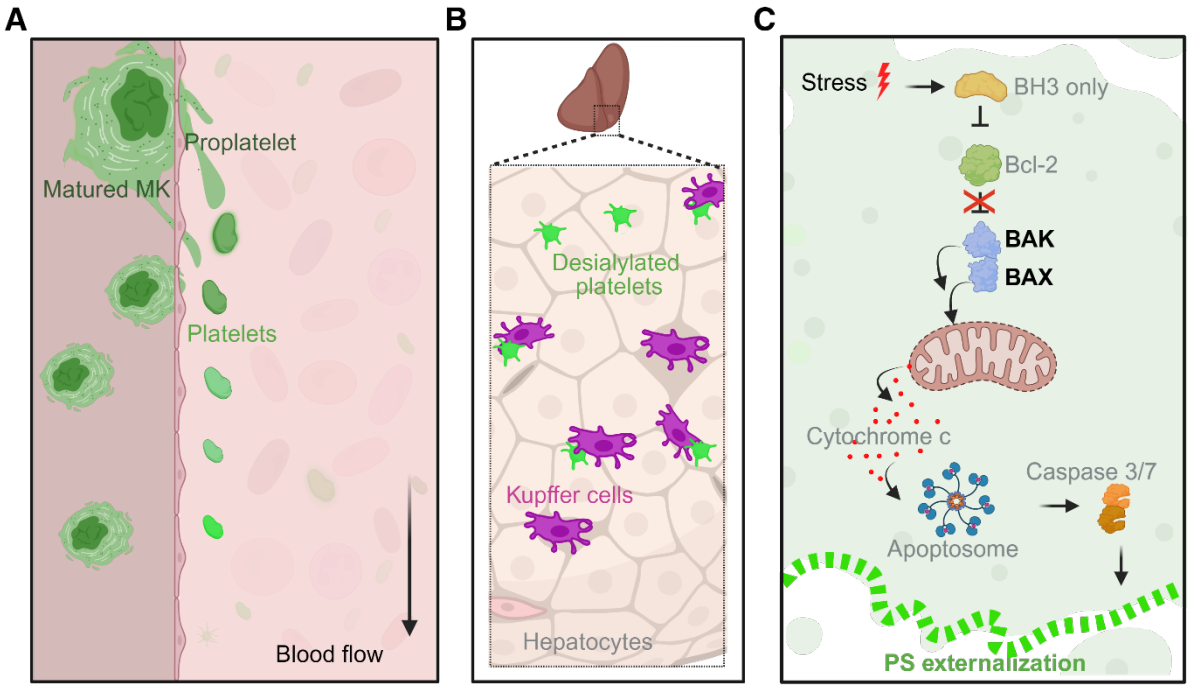

Figure 4. Platelet turnover. A) Schematic representation of platelet production from a matured megakaryocyte (MK) through proplatelet extension and release into the bloodstream. B) Schematic representation of platelet clearance in the liver by Kupffer cells and hepatocytes following desialylation. C) Schematic representation of intrinsic apoptosis in platelets, showing stress-induced BAK BAX activation, mitochondrial cytochrome c release, apoptosome formation and caspase dependent phosphatidylserine (PS) externalization. Created in https://BioRender.com.

Summary

Platelets are well known for possessing multiple roles in vascular biology. Beyond their traditional role in hemostasis and thrombosis during vessel injury, platelets play a critical role in inflammation by supporting leukocyte recruitment at inflammation sites, even confronting pathogens directly. This solidifies platelets' commitment as sentinels that provide host defense and vascular integrity. With these myriad roles to cover, it is comprehensible that platelets developed a specialized distribution of these tasks based on their heterogeneity. This heterogeneity can be due to their age, their phenotype or a combination of both. In this cumulative thesis, I present two studies that our group has investigated which puts emphasis on the specialized roles of platelet subsets: 1) age specific role, and 2) procoagulant platelet dependent role.

In the first article, we have addressed the concept of age dependent platelet heterogeneity and instead proposed **a shift in role from classical hemostasis to inflammatory in aged platelets**. We described this shift in role in detail using an in vivo pulse-labeling method in murine models that allowed the tracking of differently aged platelet cohorts over time. We used in vitro and in vivo assays to define the age specific heterogeneity in platelet functions. We confirmed metabolically fit young platelets were recruited more in clot formation, had stronger response to agonists, and exhibited increased adhesion and retraction. We demonstrated that aged platelets, apart from their propensity to become apoptotic and get cleared, had proclivity for leukocyte aggregation, procoagulant activation, enhanced bactericidal property and showed an upregulation of an arsenal of immune related proteins confirmed by proteomics. During LPS mediated acute lung injury in the BAK BAX mouse model with prolonged platelet half-life, aged platelets were recruited to the lung, and we observed increased inflammation. We also showed immunomodulatory characteristic in in vitro aged human platelet concentrates that was further supported by using a murine model of transfusion highlighting the shift in role of aged platelets with potentially important implications for transfusion medicine.

In the second article, the **role of procoagulant platelets in maintaining vascular integrity** was also investigated using murine models of inflammation. We showed that during pulmonic inflammation, platelets that come across exposed collagen at the site of injury lead to mitochondrial CypD and TMEM16F dependent procoagulant platelet activation. This procoagulant activation further initiates the coagulation cascade and prevents inflammatory bleeding. We were able to demonstrate in vitro that the combination of both integrin αIIbβ3 (GPIIb/IIIa) and GPVI mediated signaling leads to supramaximal calcium bursts and in turn procoagulant transformation.

In both the articles we clarify the complex contribution of platelets to inflammatory disease; in part explained by their heterogenous nature and related effector functions. The first article highlights contribution of young platelets in hemostasis & thrombosis, and a marked role of aged platelets in inflammation. Even though we show in the first article that aged platelets have a proclivity for procoagulant activation, genetic deletion of platelet specific CypD did not hinder the

platelet-neutrophil aggregation, highlighting that aged platelets do not acquire their immunomodulatory property via procoagulant activation. Even though procoagulant activation is not crucial for aged platelets to do their task, an important role of the procoagulant platelet subset is portrayed in the second article. Here we showed that platelet/megakaryocyte specific deletion of CypD in mice which, when treated with LPS intranasally, lead to significant increase in alveolar hemorrhage. In short, I have addressed the important contributions made by heterogenous platelet subsets from **age dependent functional variation** to **procoagulant function critical in maintaining vascular integrity**.

Part IV
Contribution to the Publications

Paper 1: Aging platelets shift their hemostatic properties to inflammatory functions

Co-author contributions

"L.N. initiated the study; L.N. conceptualized the study; L.N. and **A.A.** created the methodology; **A.A.**, M.M., F.D., A.M., F.P.K., R.K., K.P., D.R., R.C., M.S.R. and L.N. conducted the investigation; R.K., F.G, T.B., J.K., J.W.H., K.S., S.M., B.N. and L.N. collected the resources; **A.A.**, M.M., F.P.K., M.S.R., and L.N. conducted formal analysis; L.N. and **A.A.** wrote the original draft; all authors edited the draft; **A.A.** and L.N. handled data curation and software; **A.A.**, F.P.K., and L.N. visualized the study; L.N. provided supervision and project administration; and L.N. administered the funding."

For this paper, I am the **sole first author**. I have created the methodology, conducted the investigations, performed formal analysis, wrote the original draft, handled data curation and visualized the study. All experiments and analysis, except experiments on BAK BAX knockout mouse line, and proteomics were performed by me with the assistance of my coauthors wherever necessary. To follow the 3 R principle (Replace, Reduce and Refine) for ethical animal experimentation, multiple assays were performed on the same day with the assistance of co-authors at different stages of the project. This was done to maximize the amount of data generated from a minimum amount of ethical animal usage post rigorous experimental planning.

Paper 2: Procoagulant platelet sentinels prevent inflammatory bleeding through GPIIBIIIA and GPVI

Co-author contributions

"L.N. initiated the study; R.K. and L.N. conceptualized the study; R.K., R.E., and L.N. created the methodology; R.K., R.E., J.K., M.-L.H., **A.A.**, V.P., M.M., W.H., L.B., C.G., A.T., M.L., and L.N. conducted the **investigation**; R.K., K.P., S.K., F.G, K.S., T.B., S.M., and L.N. collected the resources; R.K., R.E., and L.N. conducted formal analysis; R.K. and L.N. wrote the original draft; all authors **edited the draft**; R.K., R.E., and L.N. handled data curation and software; R.K. visualized the study; R.K., J.K., K.P., K.S., T.B., S.M., and L.N. provided supervision and project administration; and R.K., K.S., S.M., and L.N. administered the funding."

For this project, I have assisted Rainer Kaiser and Leo Nicolai with my experimental expertise wherever necessary. The expertise that I offered included, but not limited to, blood sampling techniques, platelet assays, intravenous injections, acute lung injury, and flow cytometry. I have also edited the manuscript draft.

Part V

Paper I

blood®
Regular Article

PLATELETS AND THROMBOPOIESIS

Aging platelets shift their hemostatic properties to inflammatory functions

Afra Anjum,[1,2] Magdalena Mader,[1,2,*] Shaan Mahameed,[1,*] Abhinaya Muraly,[1,2,*] Frederik Denorme,[3] Fabian P. Kliem,[4] Dario Rossaro,[1,2] Sezer Agköl,[1,2] Lea Di Fina,[1,2] Maité Mulkers,[1,2] Lisa Laun,[1,2] Lukas Li,[1] Nadja Kupper,[1,2] Keyang Yue,[1,2] Marie-Louise Hoffknecht,[1,2] Anastassia Akhalkatsi,[1,2] Quentin Loew,[1,2] Joachim Pircher,[1,2] Raphael Escaig,[1,2] Erwin Strasser,[5] Christian Wichmann,[5] Kami Pekayvaz,[1,2] Bernhard Nieswandt,[6] Christian Schulz,[1,2,7] Maria S. Robles,[4] Rainer Kaiser,[1,2] Steffen Massberg,[1,2] Robert Campbell,[3] and Leo Nicolai[1,2]

[1]Department of Medicine I, Ludwig Maximilian University Hospital, Ludwig Maximilian University Munich, Munich, Germany; [2]German Centre for Cardiovascular Research, Partner Site Munich Heart Alliance, Munich, Germany; [3]Department of Emergency Medicine, Washington University, St. Louis, MO; [4]Institute of Medical Psychology and Biomedical Center, Faculty of Medicine, and [5]Division of Transfusion Medicine, Cell Therapeutics, and Hemostaseology, Ludwig Maximilian University Hospital, Ludwig Maximilian University Munich, Munich, Germany; [6]Institute for Experimental Biomedicine, University Hospital Wuerzburg, Wuerzburg, Germany; and [7]Department of Immunopharmacology, Mannheim Institute for Innate Immunoscience, Medical Faculty Mannheim, Heidelberg University, Mannheim, Germany

KEY POINTS

- **Platelets change their phenotype as they age in circulation, skewing toward inflammatory function over time.**
- **Genetic models of increased platelet half-life and transfusion of in vitro–aged platelets enhance inflammatory responses.**

Platelets are crucial players in hemostasis and thrombosis but also contribute to immune regulation and host defense, using different receptors, signaling pathways, and effector functions, respectively. Whether distinct subsets of platelets specialize in these diverse tasks is insufficiently understood. Here, we used a pulse-labeling method in *Mus musculus* models for tracking in vivo platelet aging and its functional implications. Using in vitro and in vivo assays, we reveal that young, reticulated platelets show heightened responses in the setting of clot formation, with corresponding, increased responses to agonists, adhesion, and retractile function. Unexpectedly, aged platelets lose their hemostatic proficiency but are more prone to react to inflammatory challenge: compared with reticulated platelets, this cohort was more likely to form platelet-leukocyte aggregates and showed increased adhesion to neutrophils in vitro, as well as enhanced bactericidal function. In vivo, this was reflected in increased pulmonary recruitment of aged platelets in an acute lung injury model. Proteomic analyses confirmed the upregulation of immune pathways in this cohort, including enhanced procoagulant function. In mouse models of prolonged platelet half-life, this resulted in increased pulmonary leukocyte infiltration and inflammation upon acute lung injury. Similarly, human platelet concentrates decreased their hemostatic function and elevated their putative immunomodulatory potential in vitro over time, and in a mouse model of platelet transfusion, aged platelet concentrates resulted in augmented inflammation. In summary, we show that platelets exhibit age-dependent phenotypic shifts, allowing them to fulfill their diverse tasks in the vasculature. Because functional alterations of aging platelets extend to platelet concentrates, this may hold important implications for transfusion medicine.

Introduction

Platelets are the major cellular component of hemostasis and are critical for forming a stable plug to prevent bleeding at sites of vascular injury. Because they are also important mediators of thrombosis, this cell type is an attractive and clinically proven pharmacological target in cardiovascular disease. Beyond clot formation, it has become evident that platelets are also important mediators of immunity that arrive first at sites of inflammation, form a tight partnership with innate immune cells, and are instrumental for leukocyte vascular adhesion, immunosurveillance, and extravasation.[1-5] In addition, they serve as guardians of the vasculature, maintaining vascular and lymphatic integrity under steady-state and inflammatory conditions.[4,6-8] Furthermore, platelets have been implicated in cancer development and metastasis, as well as neoangiogenesis, tissue repair, and even adaptive immunity.[9-12] Other cell types with similarly diverse (patho)physiological functions, for example fibroblasts or lymphocytes, have specific subsets that mediate their respective effector function.[13,14] This specialization is frequently fluid and exhibits dynamic plasticity. Even short-lived neutrophils show distinct phenotypes depending on age and context.[15-18] In platelets, it remains insufficiently understood whether there are subsets that mediate the diverse functions outlined earlier. Recently, some environmental influence on platelet biogenesis has been proposed, because there is a contribution of lung and splenic megakaryocytes (MKs) to circulating platelet pools.[19,20]

One subset with ample evidence in basic research but also clinical medicine are young, newly produced platelets. These are termed reticulated platelets due to their elevated content of ribosomal RNA and have been recognized as a highly reactive subset that can contribute to (re-)thrombosis and failure of platelet inhibitory therapies in cardiovascular disease.[21-24] It is thought that platelets lose their functions as they age, and this functional decline leads to defects in hemostasis and thrombosis in models of prolonged platelet half-life.[25,26] Importantly, most of these findings were generated using indirect indicators of platelet age, which leaves key questions, including the dynamics of clearance, phenotype, and function of circulating platelets from birth to their decay, unanswered. Here, using innovative pulse-labeling techniques, single-cell–based functional assays, genetic mouse models, and transfusion experiments, we precisely map phenotypic, functional, and proteomic changes of platelets as they age in circulation. We show that although in vivo aging platelets lose hemostatic potential in vitro and in vivo, they move toward proinflammatory function with important implications in inflammation.

Methods

Platelet pulse-labeling model for tracking specific age cohorts of platelets

To track young platelets as they age in circulation, C57BL/6J mice were injected twice IV (pulse-labeled with a 12-hour interval) with 2.0 μg of glycoprotein Ib (GPIb) antibody conjugated with different fluorophores (X649 and X488) consecutively. Repeated blood sampling (~20 μL) from facial vein was performed to check for the percentage of pulse-labeled platelets (calculated by subtracting the percentage of platelets labeled with the first antibody from those of the second antibody; eg, [% of X488] to [% of X649] of all $CD41^+$ platelets), surface marker expression, and platelet phenotype as they aged. To understand the functional difference between distinct platelet age cohorts, mice were pulse-labeled 108, 60, and 12 hours before blood sampling. Blood was collected terminally from the retro-orbital vein to perform multiple in vitro assays simultaneously.

Generation of young and old platelet age cohorts by ablating platelet production

The PF4-cre;RS26-iDTR model was used to control platelet age by ablating MKs using diphtheria toxin (DT).[27] Administration of 250 ng per mouse of DT on day 1 and 2, and consecutive readministrations of 100 ng per mouse with a 48-hour interval resulted in complete thrombocytopenia after 6 days. A homogeneous population of platelets, aged at least 4 days, was collected by sampling blood via the retro-orbital vein 4 days after repetitive DT injections in Cre^+ mice. Young platelets were isolated by collecting blood 8 days after sequential DT administration, after confirming platelet rejuvenation after a period of thrombocytopenia. A heterogeneous mixed-age (control) population was collected via the vein plexus after repeated DT injection in Cre^- mice.

Sample preparation for mass spectrometry

Platelet-rich plasma samples were incubated with CD45 MicroBeads to deplete $CD45^+$ population to ensure pure platelet populations. Platelet-rich plasma was then diluted 1:2 in Tyrode buffer and centrifuged for 5 minutes at 1200*g* twice. Platelet pellets were lysed with sodium deoxycholate buffer (2% sodium deoxycholate in 100 mM tris[hydroxymethyl]aminomethane pH 8.5) by boiling at 95°C immediately for 5 minutes, followed by 10 cycles of 30 seconds on and 30 seconds off in a Bioruptor Sonicator. Protein samples were reduced and alkylated for 5 minutes at 45°C by adding alkylation buffer (1:10 of 10 mM tris(2-carboxyethyl)phosphine hydrochloride, 40 mM 2-chloroacetamide, pH 7). Next, protein was digested by the addition of 1:100 (enzyme:protein) trypsin and endoproteinase LysC and incubation at 37°C overnight. Samples were supplemented with loading buffer (1% trifluoroacetic acid [TFA] in isopropanol) and loaded onto self-made styrenedivinylbenzene-reverse phase sulfonate StageTips (47 mm; catalog no. 2241; 3M Empore) by centrifugation at 700*g* for 8 minutes. After washing once with loading buffer and once with wash buffer (5% acetonitrile and 0.2% TFA), the peptides were eluted with elution buffer (80% acetonitrile and 0.3125% NH_4OH), concentrated in SpeedVac at 45°C for ~35 minutes and resuspended (2% acetonitrile and 0.1% TFA).

Acute lung injury model

Anesthetized mice were administered 20 μg of lipopolysaccharide (LPS) intranasally. Mice were scored every hour, and blood was sampled every 4 hours. Four or 8 hours after LPS treatment, mice were euthanized via cervical dislocation without damaging the trachea. Bronchoalveolar lavage fluid (BALF) or lung fluid was collected for analysis. BALF (>0.5 mL) was collected by intratracheal flushing with 1× phosphate-buffered saline (with 1% bovine serum albumin and 2 mM EDTA). BALFs were stained with antibodies for flow cytometric analysis. For lung histology, lungs were removed surgically, fixed in 4% paraformaldehyde for 1 hour, dehydrated in 30% sucrose overnight, and cryo-embedded. Lung sections were then stained with CD41 to check for labeled platelet recruitment.

Results

Tracking of platelet cohorts in vivo reveals dynamic changes over their lifetime

To gain insight into platelet aging and adaptation over their lifetime, we used a pulse-labeling method using 2 injections of nonactivating, nondepleting GPIb antibody tagged with a different fluorophore at 0 and 12 hours (Figure 1A-B). We established that the injection of 2.0 μg of antibody per mouse was a nonsaturating dose, leading to efficient labeling of circulating platelets while still allowing for unaffected secondary labeling 5 minutes later (supplemental Figure 1A-E, available on the *Blood* website). MKs were not labeled using this strategy (supplemental Figure 1F-I). Using platelet reporter mice, we showed that labeling with antibody did not affect phenotype, activation, or platelet-leukocyte aggregate (PLA) formation (supplemental Figure 2A-F). The pulse-labeling strategy resulted in a single-positive population of platelets produced in between the 2 injections, that could be followed over their lifetime (Figure 1C-D). This cohort showed an increased half-life and slowed initial clearance compared with the general platelet population, confirming differential clearance dynamics of platelets depending on age (Figure 1E). Furthermore, we found an initial increase in size and activation, as assessed by P-selectin expression, and a gradual increase in phosphatidylserine exposure, confirming prior, indirect findings (Figure 1F).

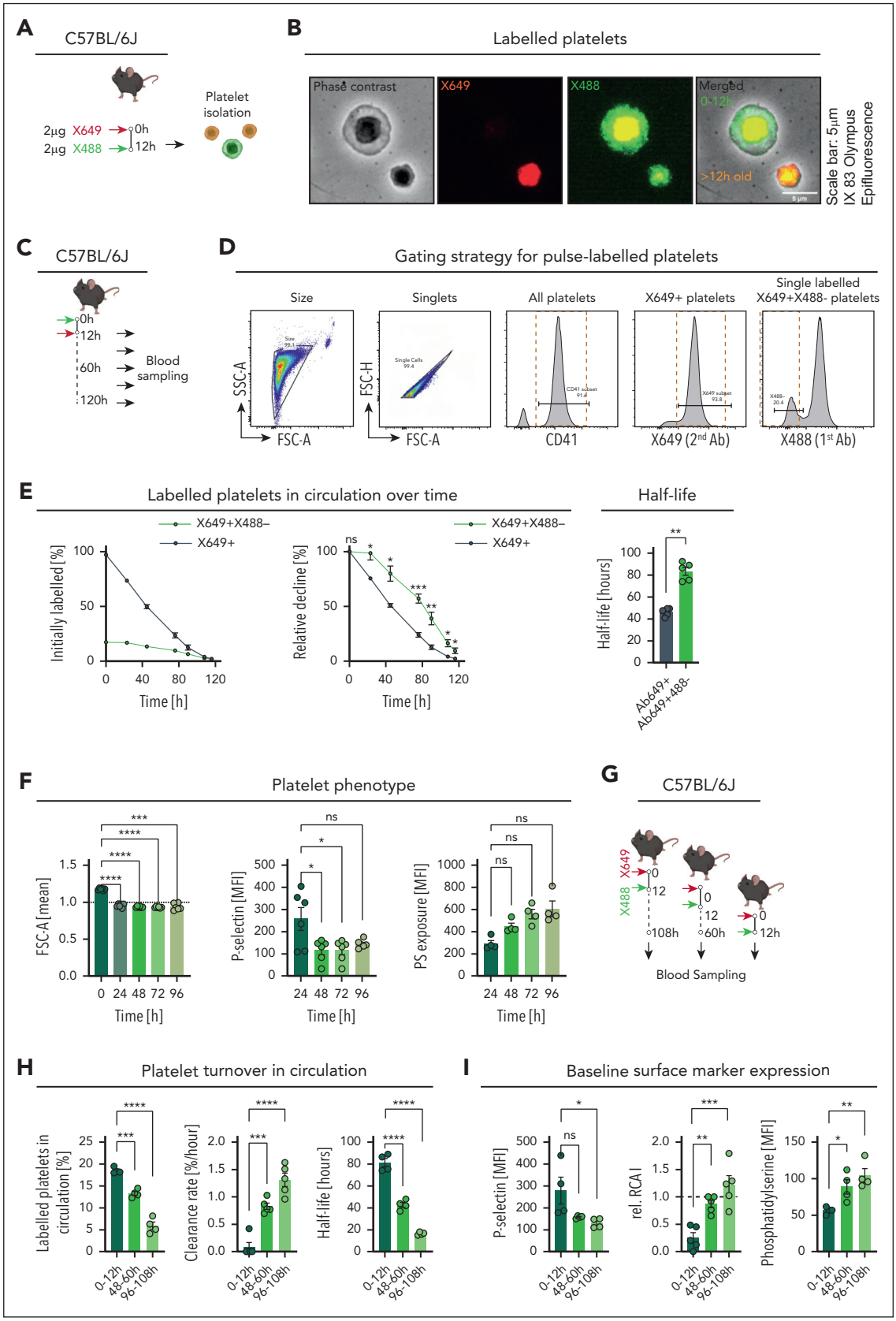

Figure 1. Tracking of platelet age cohorts in vivo. (A) Pulse-labeling scheme in C57BL/6J mice. (B) Representative image of isolated platelets from pulse-labeled mice spread on a fibrinogen-coated chamber. (C) Experimental outline depicting C57BL/6J mice pulse-labeled with X488 and X649 antibodies at 12-hour interval with repetitive blood sampling over time. (D) Representative gating strategy for flow cytometric analysis of pulse-labeled platelets in whole blood. (E) Graph showing percentage of labeled platelets (of all CD41$^+$ platelets) over time, with 2-way repeated measures (RM) analysis of variance (ANOVA), comparison between labeled platelet groups (P = .0008), with the

Next, we deployed this method to generate differently aged cohorts of platelets and compare their phenotype and function at different time points of their life cycle. For this, we collected blood samples 108, 60, and 12 hours after initial pulse labeling, corresponding to platelet cohorts with a mean age of 6 hours, 2 days, and 4 days (Figure 1G).

The aged cohort (mean age, 4 days) showed a significant decline in counts, decreased remaining half-life, and heightened clearance rate (Figure 1H). Correspondingly, this was accompanied by a decrease in P-selectin expression and an increase in desialylation and phosphatidylserine expression, markers of platelet clearance and apoptosis (Figure 1I). In summary, these data directly show dynamic changes in platelets over their lifetime in circulation and allow for functional and phenotypic analysis of age subsets.

Aged platelets exhibit decreased hemostatic and thrombotic potential in vivo

We then used this strategy to compare the function of different platelet age cohorts in vitro. For this, we used assays that allowed for 2-color–based separation of single-positive platelets as well as simultaneous single-cell–based functional analysis (see "Methods"; Figure 2A). Platelets exhibited a time-dependent loss of mitochondrial abundance and function, as measured by MitoTracker intensity (CMTMRos) and tetramethylrhodamine uptake, respectively (Figure 2B).[26] Upon spreading on fibrinogen, younger platelets showed increased surface area coverage, corresponding to their increased size (Figure 2C-D).

Activation with agonists adenosine 5′-diphosphate and thrombin led to greatly enhanced GPIIbIIIa activation and P-selectin expression, a marker of alpha granule release, in the young cohort, with a significant decline in aged platelets (Figure 2E; supplemental Figure 3). Single-cell migration and retraction analyses revealed age-dependent decreases in both assays (Figure 2F-G). This culminated in a significant increase in the recruitment of young platelets in a flow chamber–based thrombosis assay, in which 0- to 12-hour-old platelets were enriched compared with their overall blood concentrations (Figure 2H). These data show maximum hemostatic/clot-forming potential of platelets early after release, which then declines within 48 hours. This substantiates the indirect findings made in humans that reticulated platelets contribute a disproportionately large share to thrombotic risk.

Platelets shift toward thromboinflammatory potential as they age in circulation

Platelet function is not restricted to clot formation but also encompasses the recruitment of the coagulation cascade as well as immunomodulatory function. Interestingly, our pulse-labeling method revealed increased expression of receptors known to be involved in platelet immune function, including C-type lectin-like receptor 2 (CLEC-2), CD40L, and ICAM-1, upon progressive aging in circulation (Figure 3A). Aged platelets already showed heightened phosphatidylserine exposure under steady state (compare with Figure 1I), and this was further enhanced by agonists, in particular, thrombin and convulxin (supplemental Figure 4A). These platelets were P-selectin and Annexin V positive, indicating a bona fide procoagulant phenotype (Figure 3B; supplemental Figure 4B). These results could be reproduced on a collagen matrix, which also triggers procoagulant activation.[8] Again, the 4-day-old cohort showed an almost twofold increase in procoagulant activation compared with young platelets (Figure 3C). Platelet procoagulant activity has been shown to be crucially involved in inflammatory responses.[4,8,28] Another important mechanism of platelet immune function is the formation of PLA. The aged platelet cohort showed a striking increase in PLA formation and in particular, platelet-neutrophil aggregate (PNA) formation in the circulation (Figure 3D; supplemental Figure 4C-D). These observations could solely be based on the longer circulation time and therefore a stochastic increase in the likeliness of interaction with leukocytes in the aged cohort. To address this, we coincubated isolated platelets from the 3 labeled age cohorts with neutrophils in vitro. Again, the 4-day-old cohort showed an increase in interaction, indicating an elevated propensity for interaction upon aging (Figure 3E). Given the increased procoagulant potential of aged platelets, we assessed whether this pathway is also responsible for their heightened interaction with immune cells. Cyclophilin D–deficient platelets still showed unaltered heightened PLA formation and interaction with neutrophils upon aging, despite a decrease in procoagulant transformation on collagen matrices (supplemental Figure 5A-I). This underscores that procoagulant activation is not solely responsible for the observed phenotype, while also underlining that the observed procoagulant propensity is cyclophilin D (CypD) dependent and therefore not solely indicating increased apoptosis of the aged cohort. Interestingly, healthy neutrophils coincubated and forming aggregates with aged platelets showed a more proinflammatory phenotype, indicated by upregulated CD11b, CD66a, and CD177 (Figure 3F). This points toward an enhanced proinflammatory effect of aged compared with young platelets on neutrophils. Next, we assessed whether enhanced leukocyte interaction could be blocked by interfering with established heterotypic platelet-leukocyte receptor-ligand pairs. Blockade of GPIIbIIIa, P-selectin glycoprotein ligand-1 (PSGL-1), and CD40L led to reduced PNA formation, whereas GPIb blockade had no effect (Figure 3G). The strongest effect could be seen with blockade of CD40L, correlating well with the enhanced expression of this receptor by aged platelets (Figure 3G).

Platelets can also directly interact with and kill bacteria.[29] We, therefore, coincubated pulse-labeled platelets with methicillin-susceptible *Staphylococcus aureus*. We observed a

Figure 1 (continued) post hoc Šídák multiple comparisons test; bar graph depicting half-life of labeled platelets; paired *t* test, 2-tailed ($P = .0021$; n = 5). (F) Single-labeled platelet size; RM 1-way ANOVA ($P < .0001$); P-selectin expression over time in single-labeled platelets (RM 1-way ANOVA; $P = .0289$); phosphatidylserine exposure (RM 1-way ANOVA, $P = .0178$), with the post hoc Dunnett multiple comparisons test. (G) Scheme for pulse-labeling mice 108, 60, and 12 hours before sampling to determine platelet phenotype in different age cohorts simultaneously. (H) Graphs depicting single-labeled platelet percentage in circulation (n = 4 per group), platelet clearance rate (n = 5 per group), and platelet half-life (n = 4 per group); ordinary 1-way ANOVA for each graph, $P < .0001$; the post hoc Dunnett multiple comparisons test compared with the 0- to 12-hour group. (I) Platelet surface markers of single-labeled platelets: P-selectin mean fluorescence intensity (MFI; n = 4 per group), desialylation (RCA I binding MFI) relative to MFI of all platelets (n = 5 per group), and phosphatidylserine exposure measured by C1q binding (n = 4 per group); ordinary 1-way ANOVA, $P = .0385$, .0004, and .0063, respectively; the post hoc Dunnett multiple comparisons test compared with the 0- to 12-hour group. *$P < .05$; **$P < .01$; ***$P < .001$; ****$P < .0001$; FSC-A, forward scatter; h, hours; ns, nonsignificant.; rel.RCA I, relative Ricinus Communis Agglutinin I binding; SSC-A, sideward scatter.

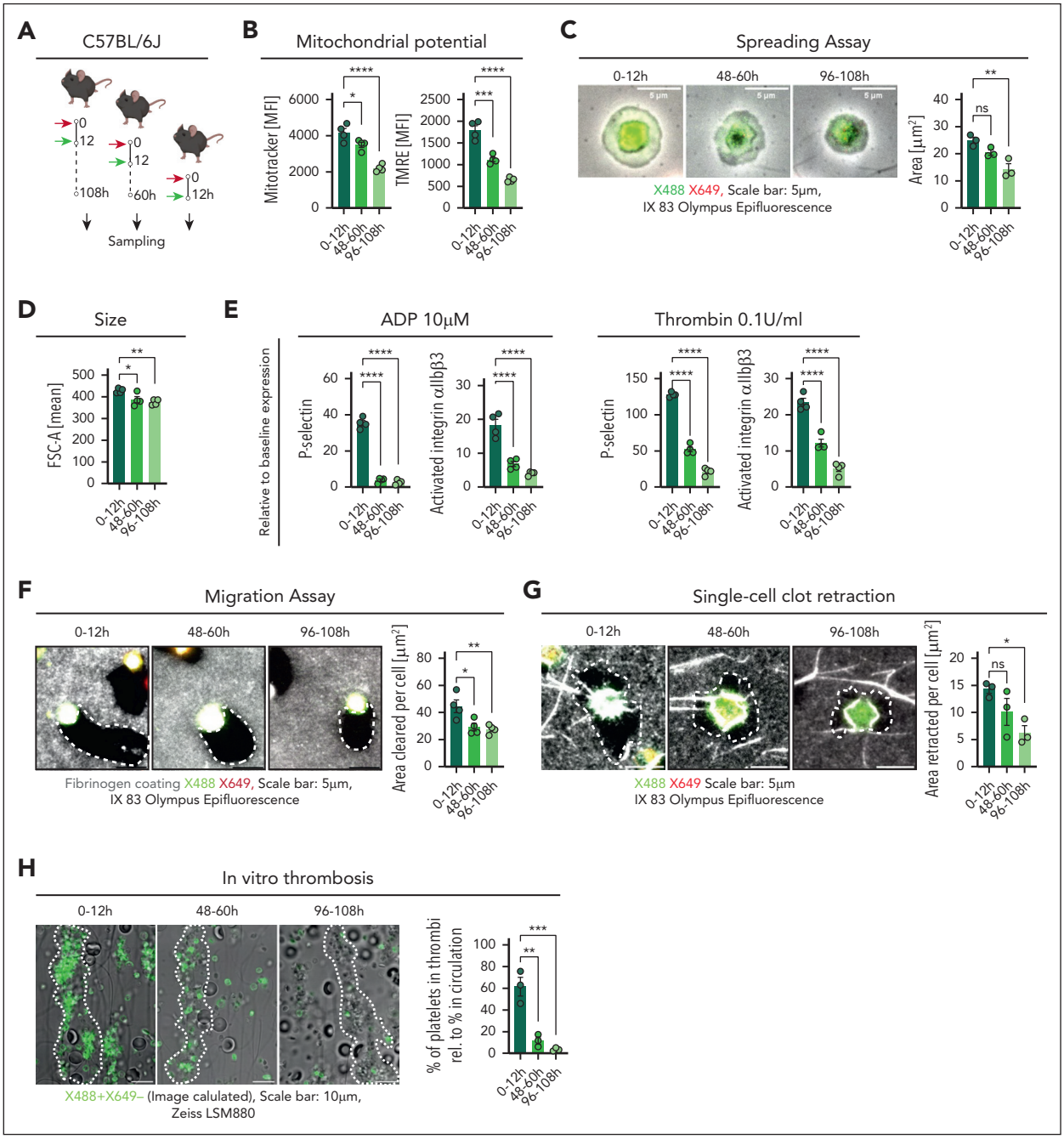

Figure 2. Aged platelets display diminished hemostatic and thrombotic potential in vitro. (A) Schematic outline showing pulse-labeled C57BL/6J mice (red arrow, X649; green arrow, X488). (B) MitoTracker and tetramethylrhodamine MFI of platelet age cohorts analyzed via flow cytometry (n = 4 per group; both $P < .0001$). (C) Representative micrographs of spread platelets and analysis of platelet size by area (n = 3 per group; $P = .0060$). (D) Platelet size measured by FSC-A (n = 4 per group; $P = .0085$). (E) Flow cytometric measurements of P-selectin expression (MFI) and GPIIbIIIa (αIIbβ3) integrin activation (MFI) in washed platelets after treatment with agonists relative to their expression after phosphate-buffered saline (PBS) treatment (n = 4 per group; all $P < .0001$). (F) Representative images of single-labeled platelet migration on labeled fibrinogen substrate and quantification of migration as cleared area (n = 4 per group; $P = .0094$); outlined area showing cleared substrate. (G) Representative micrographs showing single-cell clot retraction assay of pulse-labeled platelets with fibrinogen and platelet poor plasma (n = 3 per group; $P = .0406$); outlined area showing retracted substrate. (H) Representative micrographs of single-labeled platelets (using Image Calculator in ImageJ: subtracting X649 labeled from X488) showing in vitro thrombus formation with whole blood on collagen I (n = 3 per group); white dotted lines enclose area depicting thrombi; bar graph depicting percentage of single-labeled platelets in thrombus relative to the percentage of single-labeled platelets in blood ($P = .0005$). Statistical tests for all, ordinary 1-way ANOVA with the post hoc Dunnett multiple comparisons test compared with 0- to 12-hour group. *$P < .05$; **$P < .01$; ***$P < .001$; ****$P < .0001$; h, hour; ns, nonsignificant.

strongly enhanced binding of 4-day-old platelets, compared with young platelets, to methicillin-susceptible *S aureus* (Figure 3H; supplemental Figure 6A-D). Moreover, aged platelets showed an increased proficiency in killing *S aureus* (Figure 3H).

These data highlight that platelets do not show unidirectional functional decline upon aging but upregulate certain receptors and effector functions, including procoagulant activation, binding and killing of bacteria, and enhanced interaction with leukocytes.

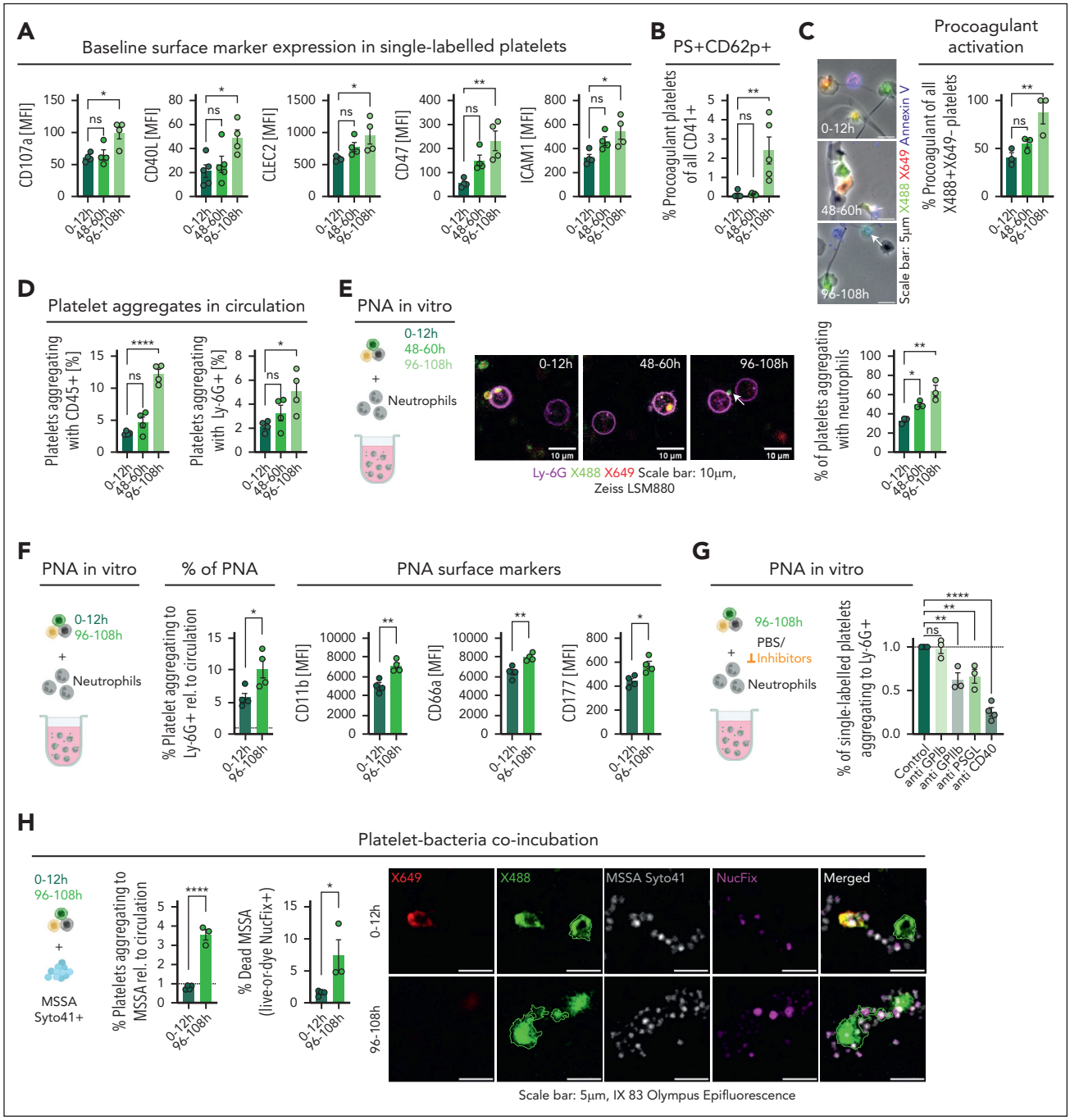

Figure 3. Aged platelets show increased thromboinflammatory potential in vitro. (A) Bar graphs representing flow cytometric analysis of baseline surface markers of platelet age cohorts in whole blood (n = 4 per group; *P* = .0106, .0291, .0484, .0216, .0047, and .0216, respectively). (B) Bar graph depicting the percentage of single-labeled platelets that are PS^{+}P-selectin–positive (*P* = .0023). (C) Representative micrographs and quantification of procoagulant activation of single-labeled platelets seeded on collagen I/fibrinogen matrix (n = 3 per group); graph showing percentage of single-labeled procoagulant platelets (*P* = .0145). (D) Bar graphs showing PLA (percentage of single-labeled platelets aggregating with leukocytes; *P* < .0001) and PNA (percentage of single-labeled platelets aggregating with neutrophils; *P* = .0318) in mouse whole blood (n = 4 per group). (E) Schematic outline, representative micrographs, and quantification of isolated platelets from pulse-labeled mice coincubated with isolated neutrophils (n = 3 per group); bar graph representing percentage of single-labeled platelets of total platelets aggregating with neutrophils (*P* = .0038). (F) Schematic outline of isolated platelet-rich plasma from pulse-labeled C57BL/6J mice coincubated (n = 4 per group) with isolated neutrophils (nonlabeled C57BL/6J mice, n = 2); bar graph representing the percentage of single-labeled platelets out of total platelets aggregating with neutrophils relative to their percentage in circulation (*P* = .0322); bar graphs depicting surface marker expressions in neutrophils post aggregation with pulse-labeled platelets: CD11b (*P* = .0030), CD66a (*P* = .0054), CD177 (*P* = .0143); statistical tests, unpaired *t* tests, 2-tailed. (G) Platelets isolated from mice pulse-labeled 108 hours before experiment treated with anti-GPIb, anti-GPIIbIIIa, anti-PSGL, and anti-CD40 Fab fragments/antibodies coincubated with isolated neutrophils; quantification of single-labeled platelets aggregating with neutrophils relative to control depicted in a bar graph (*P* < .0001). Statistical tests for panels A-E and 3G, ordinary 1-way ANOVA with the post hoc Dunnett multiple comparisons test. (H) Schematic outline shows pulse-labeled platelets coincubated with methicillin-susceptible *S aureus* prestained with SYTO 41 dye (5 µM), followed by staining with Live-or-Dye NucFix of killed bacteria; bar graphs depicting percentage of pulse-labeled platelets aggregating to methicillin-susceptible *S aureus* (MSSA) relative to their percentage in circulation (<0.0001) and the percentage of dead bacteria represented by the percentage of MSSA that are positive for NucFix (0.0408); statistical tests, unpaired t tests, 2-tailed. **P* < .05; ***P* < .01; ****P* < .001; *****P* < .0001. h, hour; ns, nonsignificant.

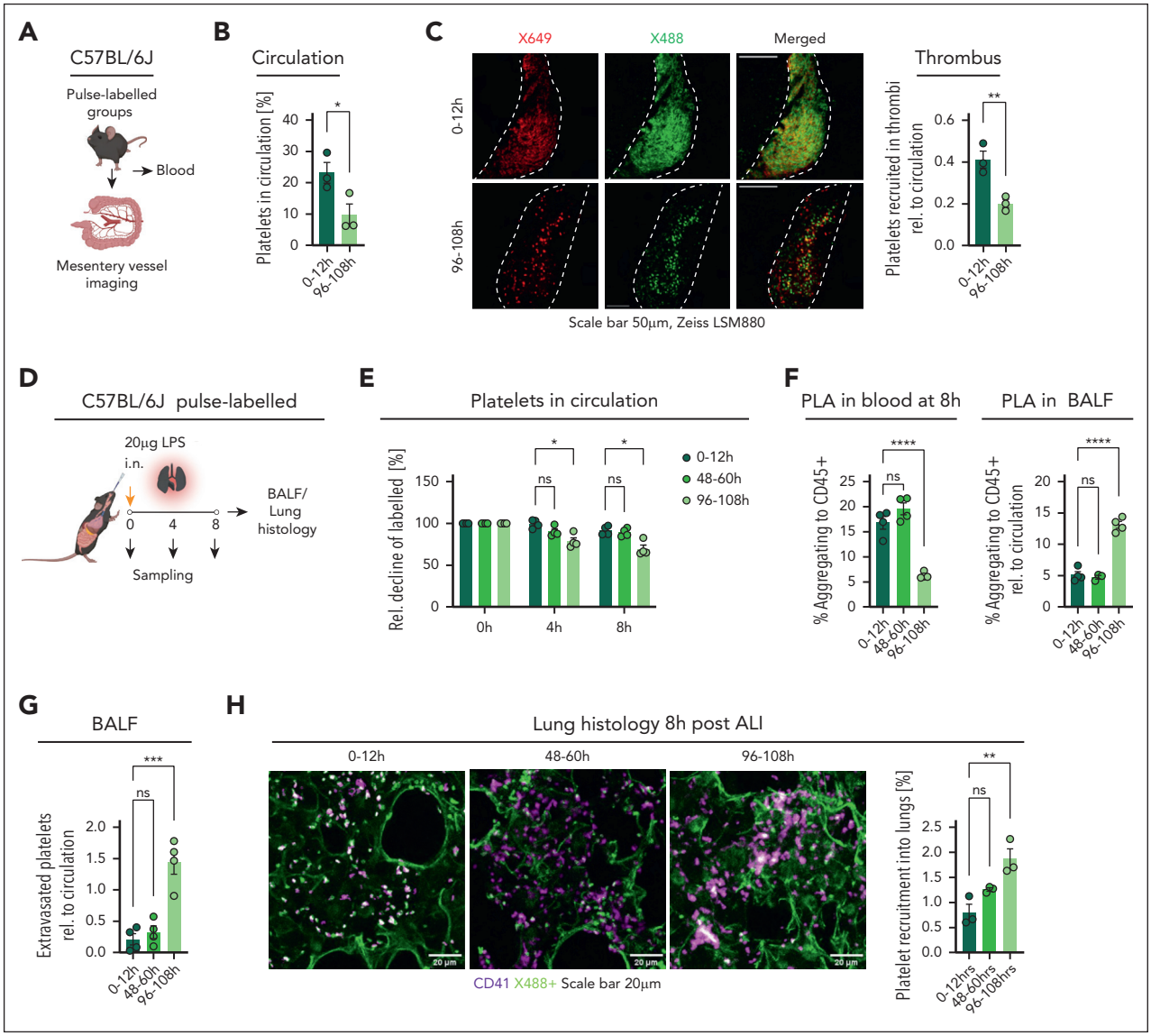

Figure 4. Recruitment of specialized age subsets in thrombosis and inflammation in vivo. (A-C) C57BL/6J mice (n = 3 per group) were pulse labeled 108 hours and 12 hours before blood sampling and mesentery vein imaging; experimental outline (A); percentage of single-labeled platelets in circulation (B; unpaired *t* test, 2-tailed *P* = .0492); Representative micrographs depicting thrombi initiated by exposing mesentery vein to $FeCl_3$ (C); bar graphs depicting the percentage of area covered in thrombus by single-labeled platelets relative to platelet percentage in circulation in panel B (unpaired *t* test, 2-tailed, *P* = .0097). (D-H) Pulse-labeled C57BL/6J mice (E-G; n = 4 per group) were subjected to acute lung injury; experimental outline (D); percentage decline of single-labeled platelets in circulation (E; 2-way RM ANOVA, comparison between labeled platelet groups: *P* = .0022, with the post-hoc Dunnett multiple comparisons test); PLA formation in circulation 8 hour after acute lung injury (ALI) and in BALF (F; both *P* < .0001); percentage of single-labeled platelets recruited in BALF relative to the percentage in circulation 8 hour after ALI (G; *P* = .0002); C57BL/6J mice (n = 3 per group) were euthanized 8 hour after acute lung injury (H); lung histology was performed via staining with CD41; percentage of single-labeled platelets recruitment depicted in the bar graph (*P* = .0072); For panels F-H, the reported *P* values are from ANOVA summary; statistical tests, ordinary 1-way ANOVA with the post-hoc Dunnett multiple comparisons test compared with the 0- to 12-hour group. **P* < .05; ***P* < .01; ****P* < .001; *****P* < .0001; h, hours; ns, nonsignificant.

Specialized platelet subsets are recruited in clot formation and inflammation in vivo

We next aimed to assess whether this age-dependent skewing of effector functions is mirrored in vivo under thrombotic or inflammatory conditions. First, we used a mesenteric thrombosis model to track pulse-labeled platelets using intravital microscopy. Indeed, we confirmed a strong increase in the recruitment of 0- to 12-hour-old platelets in the early phases of thrombus formation, whereas the aged cohort showed a relative defect in recruitment dynamics compared with blood abundance (Figure 4A-C).

Acute lung injury is the common final path of multiple systemic inflammatory syndromes and carries high mortality rates. Moreover, platelets play a decisive role in its pathophysiology by contributing to immune cell recruitment and also maintaining vascular integrity.[5,30,31] We, therefore, assessed pulmonary recruitment dynamics of platelets aged 0 to 12 hours, 48 to 60 hours, and 96 to 108 hours in acute lung injury, using our pulse-labeling approach (Figure 4D). Acute lung injury caused a rapid decline of particularly the aged cohort over 8 hours, which could indicate heightened recruitment (Figure 4E). Particularly, leukocytes aggregated with aged platelets showed a strong

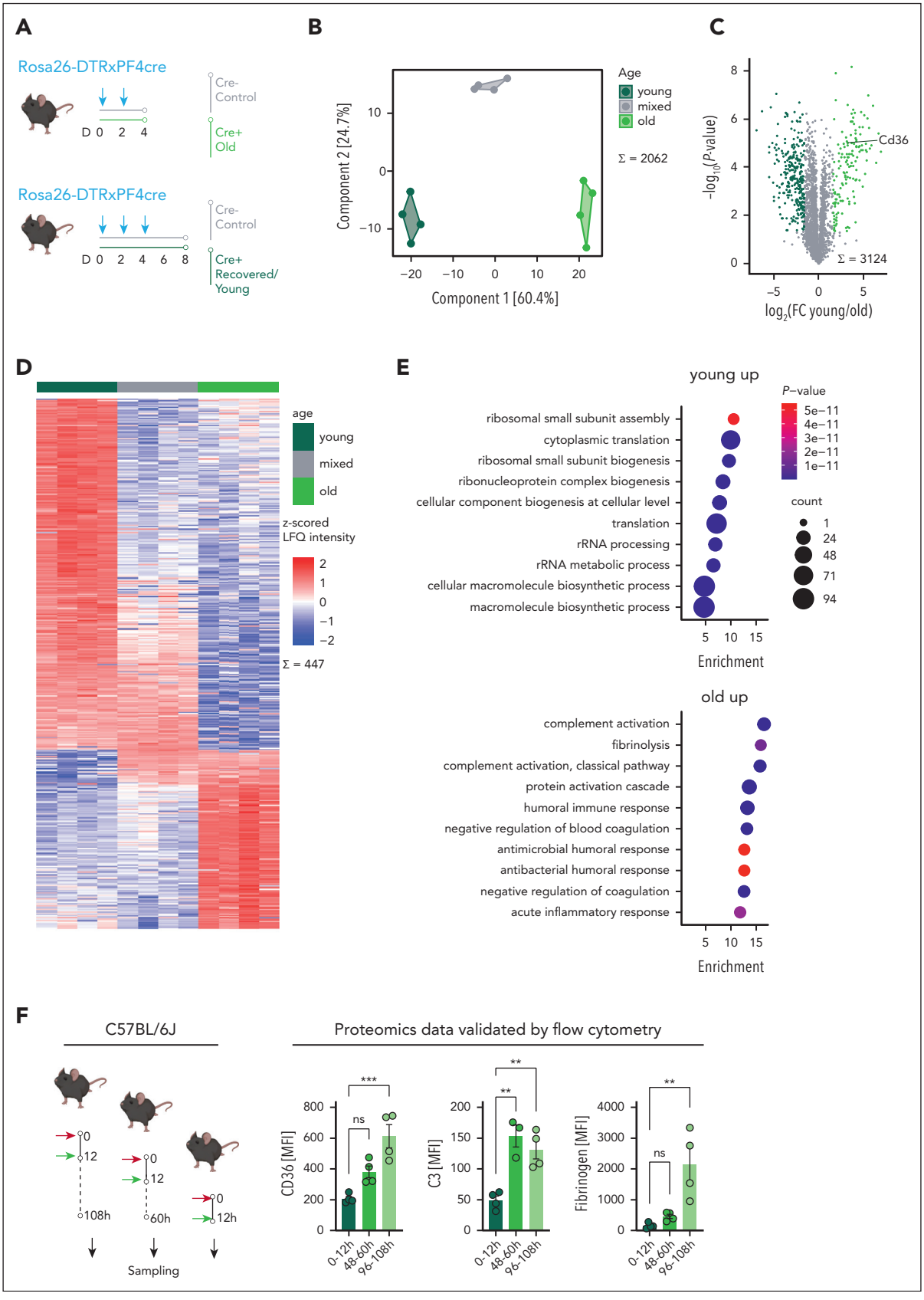

Figure 5. Platelet aging proteomics. (A-E) Rosa26-DTRxPF4cre mice were administered with DT, intraperitoneally every 48 hours; mixed-aged platelet cohorts were isolated from Cre$^-$ mice 4 days after serial DT injections (n = 4); platelets aged >4 days were collected 4 days after serial DT injections in Cre$^+$ mice (n = 4); platelets aged <1 day were collected 8 days after serial DT injections in Cre$^+$ mice during platelet recovery phase (n = 4); schematic outline (A); principal component analysis of all 2062 proteins quantified (n = 4) (B); volcano plot (C) of a student *t* test ($P < .05$; $|\log_2$ fold change$| > 2$) comparing 3124 proteins in the young (left) and old (right) cohorts; heat map (D) of the 447

decline 8 hours after induction (Figure 4F). Indeed, analysis of bronchoalveolar lavage confirmed a strong relative increase in pulmonic extravasation of aged platelets, as well as abundance of PLA in the bronchoalveolar fluid (Figure 4F-G). Lung histology also indicated increased relative recruitment of aged platelets 8 hours after LPS instillation (Figure 4H). In summary, these experiments underpin the obtained in vitro results and highlight that platelet cohorts engage differently upon thrombotic or inflammatory challenges, depending on functional aging.

Aged platelets show proteomic changes corresponding to heightened immunomodulatory function

To better understand the underlying cellular changes accompanying platelet aging in vivo, we aimed to perform state-of-the-art shotgun proteomics. Sorting of marked cohorts led to insufficient protein content as well as signs of platelet activation (data not shown). We, therefore, used the PF4-cre;RS26-iDTR model.[27] This model allows for targeted deletion of MKs via DT application, without affecting already circulating platelets. Platelet counts rebound after 7 days (sampled on day 8) with heightened production, as indicated by increased MK counts (supplemental Figure 7A-C). The produced platelets functionally resemble steady-state young platelets with increased platelet size, heightened recruitment of young platelets in a flow chamber–based thrombosis assay, and an increased mitochondrial potential, whereas the 4-day-old platelets show reduced P-selectin expression and increased CD40L and PS exposure (supplemental Figure 7D-H). We sampled platelets within 4 days of DT injection from both control Cre^- wild-type (WT) mice and Cre^+ mice, representing the aged cohort, because DT treatment led to abolished platelet production; we also sampled rejuvenated platelets after thrombocytopenia from Cre^+ and control platelets from Cre^- on day 8 (Figure 5A; supplemental Figure 8A).

Proteomic analysis of isolated, purified platelets quantified 3495 proteins overall, with 71% proteins quantified in all cohorts (supplemental Figure 8B), and showed clear separation of the respective cohorts in a principal component analysis (Figure 5B). Next, we directly compared the aged platelet cohort with the young platelet cohort with a 2-sample student *t* test ($P < .05$; |log2 fold change| > 1.6), which revealed 296 upregulated proteins in young and 151 upregulated proteins in aged platelets (Figure 5C-D). An enrichment analysis of gene ontology biological processes showed a clear overrepresentation of proteins involved in ribosomal translation in young, reticulated platelets (Figure 5E). Interestingly, in aged platelets, we found inflammation, immunity, and the regulation of coagulation as upregulated processes (Figure 5E). At the protein level, aged platelets showed increases in multiple immunoglobulins, complement factors C3, C5, B, H, and I, coagulation factors II, XII, and XIII, and plasma proteins such as fibrinogen and fibronectin (supplemental Figure 8C-D). These proteins have, in part, been shown to be taken up by circulating platelets, which could explain why aged platelets contain more of these proteins. Furthermore, scavenger receptor CD36 was upregulated (Figure 5C). We confirmed the upregulation of CD36, C3, and fibrinogen via flow cytometry using our pulse-labeling method in unperturbed WT mice (Figure 5F). Furthermore, aged platelets showed increased carbonic anhydrase 1 and 2 content, known to be involved in platelet procoagulant transformation and ballooning, which corresponds well with the heightened procoagulant potential we observed (supplemental Figure 8C-D).[32] Interestingly, aged platelets also showed an increase in multiple serpins, which is a family of protease inhibitors with important roles in regulating vascular function. These included plasma protease C1 inhibitor, alpha-2- antiplasmin, and antithrombin-III, as well as Serpin H1 (supplemental Figure 8C-D).

Taken together, proteomics data confirm changes in protein content over the platelet lifetime, with a relative increase in proteins involved in innate immune function and coagulation over time.

Increased platelet half-life fosters inflammation

Our data indicate that aged platelets are skewed toward immune effector functions and could therefore alter inflammatory disease outcomes. To investigate this further, we used mouse models of increased platelet half-life, the BAK-KO, BAX^{Plt} KO and BAK-KO BAX^{Plt} double KO (DKO) mouse lines.[33] Platelet half-life is significantly increased in these mouse lines, with an almost doubled life span in BAK-KO and DKO strains.[34] These mice show defects in hemostasis and thrombus formation associated with platelet aging (supplemental Figure 9A-B).[25] Given our insights into platelet immune function upon aging, we hypothesized that increased half-life might skew global platelet function toward immune modulatory properties. As expected, we observed increased baseline procoagulant function and PNA formation (Figure 6A-D). We, therefore, sought to investigate whether these mice showed elevated inflammatory propensity in acute lung injury (Figure 6E). Eight hours after LPS application, BAK KO, BAX^{Plt} KO, and DKO mice exhibited increased recruitment of immune cells and PLA in BAL fluid (Figure 6F-G). This was accompanied by an increase in alveolar hemorrhage, as measured by erythrocyte extravasation (Figure 6G). Moreover, proinflammatory cytokines, tumor necrosis factor α and interleukin-6, were significantly higher in BAL fluid from DKO mice than WT controls (Figure 6H; supplemental Figure 9C-D). Importantly, after the rejuvenation of platelets in DKO mice by injecting platelet-depletion antibody and recovery of counts with newly generated platelets, the proinflammatory effect was abrogated, with leukocyte counts, bleeding, and cytokine levels in BAL comparable with WT controls (supplemental Figure 9B-D; Figure 6F-H). This underlines that platelet aging is associated with functional changes rather than strict loss of function, and these functional changes in platelets upon aging can affect inflammation outcomes.

Figure 5 (continued) significant proteins from panel C; Fisher exact test enrichment analysis (false discovery rate <0.02; count ≥10, top 10) of gene ontology biological pathway terms (E) among differential proteins from panel C. (F) Proteomic findings were confirmed by analyzing surface marker expression of single-labeled platelets in pulse-labeled C57BL/6J mice (n = 4 per group) via whole blood flow cytometry; CD36 ($P = .0009$), C3 ($P = .0013$) and fibrinogen ($P = .0035$); statistical tests, ordinary 1-way ANOVA with the post hoc Dunnett multiple comparisons test compared with the 0- to 12-hour group. $^{**}P < .01$; $^{***}P < .001$; FC, fold change; h, hour; LFQ, label-free quantification; ns, nonsignificant; rRNA, ribosomal RNA.

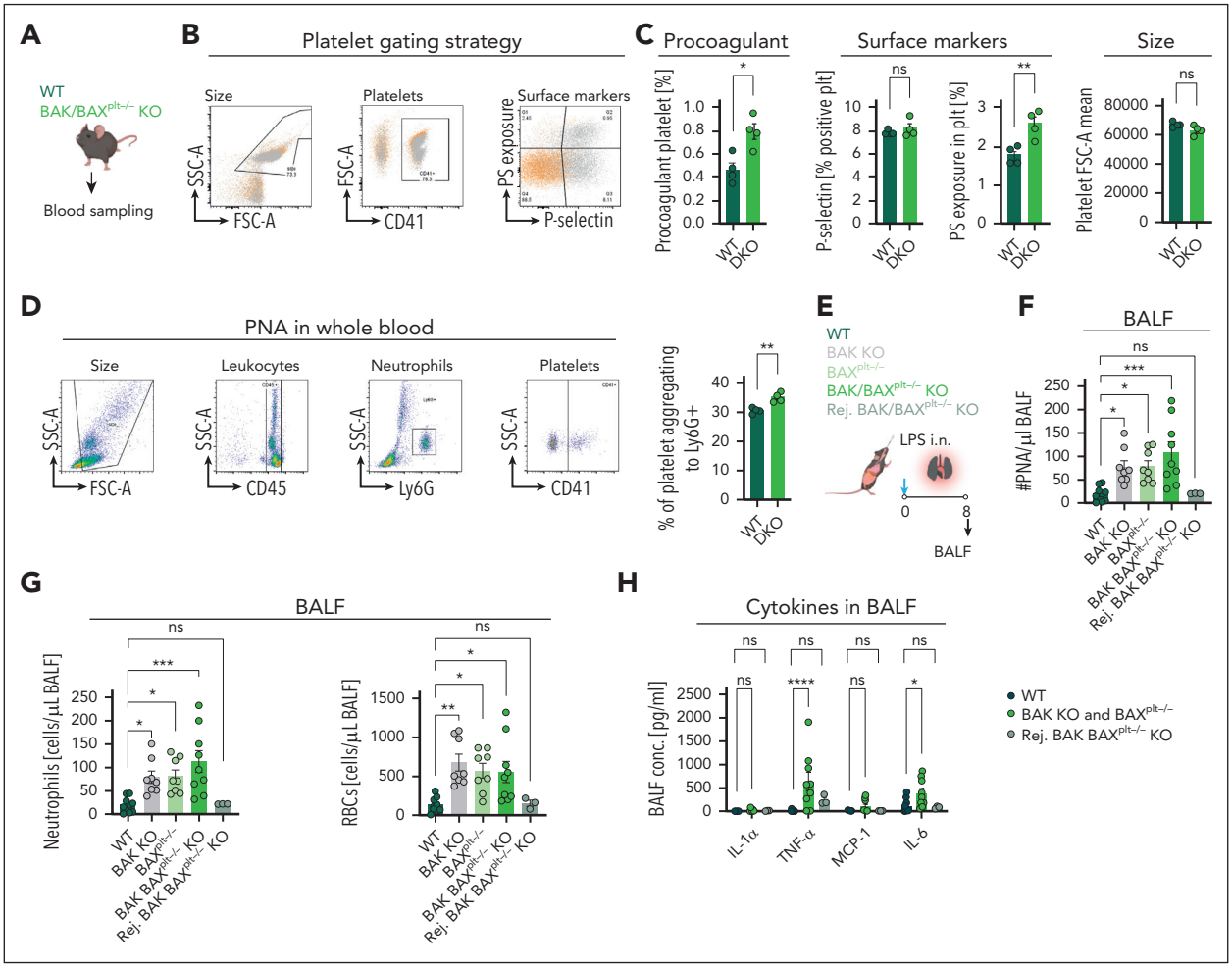

Figure 6. Increased platelet half-life fosters inflammation. (A) Schematic outline showing blood sampling from WT and BAK/BAX$^{plt-/-}$ DKO. (B) Gating strategy for procoagulant platelets. (C) Bar graphs depicting flow cytometric analysis of percentage (%) of procoagulant platelets (P = .0121), P-selectin–positive platelet percentage (0.4077), PS$^+$ platelet percentage (0.0092), and platelet size forward scatter area (0.0915). (D) Gating strategy for PNA in whole blood; bar graph shows the percentage of CD41$^+$ aggregated to Ly-6G$^+$ cells (P = .0031). Statistical tests for panels A-D, unpaired t tests, 2-tailed. (E) Experimental outline of acute lung injury in WT (n = 10), BAK KO (n = 8), BAX$^{plt-/-}$ (n = 10), BAK BAX$^{plt-/-}$ KO (n = 9), and rejuvenated BAK BAX$^{plt-/-}$ KO (n = 4) after antibody-mediated platelet depletion. (F) Bar graphs showing flow cytometric analysis of PNA (P = .0010). (G) RBC count (P = .0017) and neutrophil counts (P = .0009) in BALF. For panels F-G, ordinary 1-way ANOVA with post hoc Dunnett multiple comparisons test compared with WT. (H) Assessment of cytokine measurements in BALF, 2-way ANOVA comparison between mouse strains (P < .0001), with the post hoc Dunnett multiple comparisons test compared with WT. *P < .05; **P < .01; ***P < .001; ****P < .0001; FSC-A; h, hour; IL, interleukin; LPS i.n., lipopolysaccaride intranasally; ns, nonsignificant; SSC-A, sideward scatter; TNF-α, tumor necrosis factor α.

Platelet concentrates shift toward proinflammatory properties over time in vitro and in vivo

Platelet concentrates are fundamental to prevent excessive hemorrhage in patients with thrombocytopenia in a range of diseases. Importantly, it has recently become clear that these transfusion products also confer immunomodulatory function.[35-37] We, therefore, asked whether platelet concentrates would also show functional changes toward decreased hemostatic ability and heightened immune responsiveness over time in vitro. Human platelet concentrates kept under stable conditions in vitro exhibited mostly similar phenotypic changes as observed in murine platelets in vivo, with increased CLEC2, phosphatidylserine exposure, and CD36 and CD47 expression and a decline in RNA content (supplemental Figure 10A; Figure 7A-B). In contrast to in vivo aging, P-selectin expression increased over time, potentially indicating storage-associated activation (supplemental Figure 10B). Functionally, platelets exhibited a significant decline in spreading, aggregation, alpha granule secretion, and adhesion in an in vitro flow chamber–based thrombosis assay (Figure 7C-D; supplemental Figure 10C-D).

Importantly, and in line with our data from mice, in vitro–stored human platelets were polarized toward inflammatory functions: we observed an increase in the procoagulant phenotype at baseline and upon spreading on a collagen matrix, with increased PS$^+$ P-selectin–positive platelets (Figure 7E-F). Furthermore, morphological analysis revealed increased ballooning, confirming bona fide procoagulant phenotype (Figure 7E). Additionally, coincubation at indicated time points with isolated neutrophils showed heightened aggregate formation upon prolonged storage time (Figure 7G; supplemental Figure 10E). In summary, these experiments illustrate that platelets also gradually shift toward immune effector functions in vitro, which affects the phenotype and the effect of platelet concentrates.

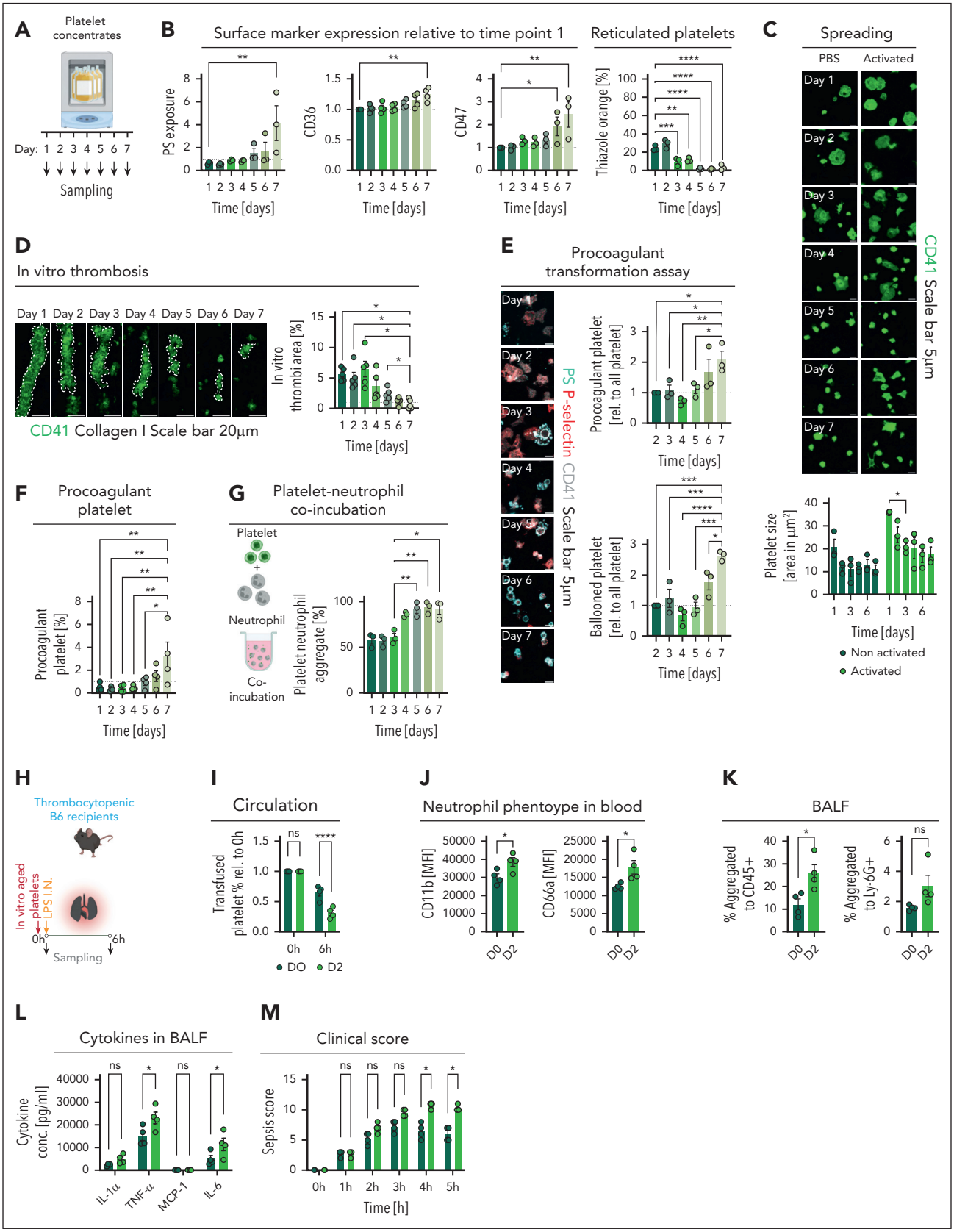

Figure 7. Platelets shift toward inflammatory function during in vitro storage. (A) Schematic outline of platelet concentrate sampling scheme. (B) Flow cytometric analysis of baseline surface marker expression PS exposure (0.0170), CD36 (0.0028), and CD47 (0.0045) relative to time point 1 [TP1]; percentage of reticulated platelets depicted by thiazole orange positive cells (n = 3; $P < .0001$; RM 1-way ANOVA with the post hoc Dunnett multiple comparisons test compared with TP1). (C) Representative micrographs and analysis of spreading of unactivated or stimulated (4-µM adenosine 5′-diphosphate [ADP] + 2-µM U46619) platelets (n = 3); 2-way RM ANOVA (comparison between PBS

To investigate whether in vitro aging of platelet concentrates would affect inflammatory responses in vivo, we optimized in vitro storage of murine platelets and subsequently transfused in vitro–aged and freshly isolated platelets into thrombocytopenic mice and assessed their immune responses in acute lung injury (Figure 7H). In vitro–aged platelets showed an immunomodulatory phenotype (supplemental Figure 11A-H) and exhibited faster decline upon acute lung injury in vivo (Figure 7I). This was accompanied by a proinflammatory phenotype of circulating neutrophils (Figure 7J). In BAL fluid, we observed increased PNA and a stronger cytokine response, indicated by higher interleukin-6 and tumor necrosis factor α levels, similar to the effect witnessed in BAK-KO BAX^{Plt} mice (Figure 7K-L; supplemental Figure 11E-I). In contrast to our genetic models of increased platelet half-life, the effect of transfusing in vitro–aged platelets had a stronger and complex systemic effect on inflammation, causing a more severe clinical disease course (Figure 7M).

This shows that in vitro aging recapitulates major elements of in vivo platelet aging, while also highlighting transfusion-specific effects that might depend on platelet isolation and in vitro storage. It also supports the notion that proinflammatory effects of platelet transfusions could be partly dependent on the age of transfused platelets.

Discussion

Here, using pulse labeling as well as genetically modified mouse models, and combining translational, in vitro, and in vivo studies, we for the first time, to our knowledge, precisely define platelet phenotype and function over their lifetime in the circulation. We confirm previous, mostly indirect findings that young, reticulated platelets newly released from MKs show a distinct phenotype with enhanced hemostatic and thrombotic potential.[21-23] The prowess to form blood clots diminishes as platelets age, and previous studies have therefore described a "functional decline" of platelets, which is exacerbated by interfering with intrinsic apoptosis via Bak/Bax deficiency, leading to enhanced platelet half-life.[25,26]

We demonstrate that platelets change their phenotype and function over time and are, indeed, more prone to certain effector functions that are associated with immunity, including platelet leukocyte aggregate formation, procoagulant transformation, binding and killing of bacteria, and expression of immunoreceptor tyrosine-based activation motif receptors such as CLEC-2 and scavenger receptor CD36, as well as CD40L and C5aR. Importantly, this is reflected in vivo by an increased relative recruitment of aged platelets in a model of lung inflammation. However, it is important to note that the observed changes most likely do not represent bona fide separate populations but rather gradual, relative changes in phenotype over their lifetime in circulation.

Genetic ablation of platelet apoptosis pathways (BAK KO, BAX^{Plt}, or BAK KO/BAX^{Plt} KO), extending platelet half-life, led to a similar, proinflammatory platelet phenotype that enhanced pulmonary leukocyte recruitment and markers of inflammation. Importantly, this could be reversed upon platelet rejuvenation, excluding that immune or tissue alterations in this model play a major role in mediating these effects. These data hold multiple important implications. First, they point toward a potential division of labor by platelet subsets, depending on respective cellular age. It has long been speculated that diverse subsets of platelets exist, which were mostly thought to be derived from specialized MKs. The description of lung-derived platelets, with a distinct transcriptional profile of lung-resident MKs, as well as $CD40L^{hi}$ splenic platelets arising after sepsis, have further driven the idea of a diverse platelet pool in the circulation.[19,20,38] However, recent work has implicated that platelets are overwhelmingly derived from the bone marrow.[39] Moreover, although single-cell RNA sequencing has revealed surprising diversity of MKs, this diversity seems mainly to be based on their roles as immune cells and regulators of stem cell quiescence, whereas the platelet-producing phenotype is relatively homogeneous.[40-42]

Production of a uniform platelet cohort with dynamic, gradual, and cell-intrinsic changes in phenotype and function over time might represent a more constructive strategy to fulfill the diverse requirements that the platelet lineage must meet in the vascular system. Indeed, similar adaptation has also been shown for short-lived neutrophils, with $CXCR4^{hi}$ aged neutrophils showing heightened immune functions such as reactive oxygen species production and NETosis, which are crucial for host defense.[17,43] Importantly, neutrophils contain a nucleus and fully functional transcriptional and translation machinery, making adaptation over their life span more flexible and dynamic than changes observed in anucleate platelets.[18]

Coupling of the aging process with specific effector functions could also be linked to the energetic capacity of platelets. We confirm that young platelets have a superior mitochondrial

Figure 7 (continued) and ADP, $P = .0064$) with post hoc Holm-Šídák multiple comparisons test compared with TP1. (D) Representative micrographs showing in vitro thrombus formation (n = 5); bar graph showing the percentage of thrombus area per field of view ($P = .0058$). (E) Representative micrographs of procoagulant activation of platelets seeded on collagen I/fibrinogen matrix; graphs showing percentage of procoagulant platelets ($P = .0107$) and percentage of ballooned procoagulant platelets relative to TP1 ($P = .001$). (F) Flow cytometric analysis showing percentage of P-selectin–positive PS^+ platelets (n = 4; $P = .0105$). (G) Schematic outline of platelet-neutrophil coincubation (n = 3); flow cytometric analysis showing percentage of platelets aggregating with neutrophils (0.0274); statistical tests for panels D-G, RM 1-way ANOVA with the post hoc Dunnett multiple comparisons test compared with TP7. (H) In vitro aged donor C57BL/6J platelets, freshly isolated (day 0 [D0], n = 4) or stored for 2 days in DSD (day 2 [D2], n = 7) were transfused into thrombocytopenic C57BL/6J recipient mice (n = 4 per group); LPS was given intranasally to induce acute lung injury (ALI) in recipients; blood sampled at 0 and 6 hours after ALI and BALF was collected. (I) Bar graph depicting decline of transfused platelets, mixed-effects model (REML), and comparison between transfused groups ($P = .0015$ with the post hoc Šídák multiple comparisons test). (J) Bar graphs showing surface marker expression: CD11b ($P = .0344$) and CD66a ($P = .0316$) of neutrophils in circulation after ALI (unpaired *t* test, 2-tailed). (K) Bar graphs depicting the percentage of transfused in vitro aged platelets aggregating with $CD45^+$ cells ($P = .0203$) and the percentage of platelets aggregating with $Ly\text{-}6G^+$ cells ($P = .0890$) in BALF (unpaired *t* test, 2-tailed). (L) Assessment of cytokine measurements in BALF (2-way ANOVA, comparison between transfused groups; $P = .0014$, with the post hoc Šídák multiple comparisons test; additional cytokines shown in supplemental Figure 11H. (M) Clinical progression of ALI in recipients that received transfusion with D0 or D2 in vitro–aged platelets (2-way RM ANOVA, comparison between transfused groups; $P < .0001$, with the post hoc Šídák multiple comparisons test). $^*P < .05$; $^{**}P < .01$; $^{***}P < .001$; $^{****}P < .0001$; h, hour; IL, interleukin; LPS I.N., lipopolysaccharide intranasally; ns, nonsignificant; TNF-α, tumor necrosis factor α.

function and show improved force generation, as assessed by retractile function.[26] Therefore, it is well conceivable that this cohort is more suitable to form a stable plug to prevent bleeding, a process that requires energy-consuming clot retraction and stabilization, particularly under high-shear conditions.[44] On the contrary, the baseline increase in phosphatidylserine exposure in aging platelets contributes to the clearance of this population, while potentially also predisposing to procoagulant function, which we found upregulated in this cohort, with important functional implications in thromboinflammation.[28,45] Beyond inflammation, it has also been found that platelet subsets are generated in thrombosis, with some stabilizing the clot via GPIIbIIIa-mediated aggregation, whereas other platelets lose adhesive function, turn procoagulant, and mediate fibrin formation.[46] Whether platelet age contributes to this dichotomous response in thrombosis remains an important question.

Our innovative proteomics approach revealed important differences between platelets aged 0 to 12 hours and those aged 96 to 108 hours. Aged platelets showed a relative increase in proteins involved in procoagulant transformation. Interestingly, some of the functional specialization could be derived by the uptake of plasma proteins, because this cohort showed an increased content of immunoglobulins, as well as complement and coagulation factors. Whether this increase is mediated by specific uptake by this cohort or simply depends on the prolonged circulation time is not clear. Moreover, whether active protein translation plays a role remains to be investigated. Furthermore, it is important to bear in mind that shotgun proteomics captures relative changes in abundance, which limits its value. However, we did confirm crucial hits via flow cytometry, confirming absolute increases in expression. The detected upregulation of Serpins in aged platelets is also of potential relevance. This class of proteins is important in regulating coagulation and fibrinolytic pathways and could hint toward an additional regulatory role of aging platelets.[47] Taken together, our proteome data set is an important resource for further analyses and could help to identify additional targets that are critical in defining platelet (immune) effector function. It remains to be clarified whether there are further subsets within young and aging platelets, a question that could be answered by single-cell omics technology, for example platelet-adapted single-cell proteomics, in the future.

Our findings are potentially relevant for transfusion medicine. It has recently been highlighted that platelet concentrates should be recognized as immunomodulatory treatment.[35-37,48] Because our data show additional proinflammatory changes occurring in platelets stored in vitro over time, it might be beneficial to transfuse freshly isolated, supposedly less proinflammatory platelets in vulnerable populations. Importantly, observational studies examining platelet concentrate age with inflammatory markers will be necessary to contextualize these findings in humans. Along these lines, it will be important to define the cellular and molecular mechanisms that are responsible for the upregulation of their proinflammatory profile. These insights could potentially be used to dampen this effect in vitro and modify the immune profile of stored platelet concentrates.

Acknowledgments

The authors thank all patients included for participation in this study, all laboratory members for technical support, and Benjamin Kile for the Bax/Bak transgenic mice provided in this study. They also thank Hellen Ishikawa-Ankerhold, Zeljka Sisic, Anna Titova, Michael Lorenz, Dominic van den Heuvel, Sebastian Helmer, Nicole Blount, and Beate Jant for excellent technical assistance.

This study was supported by the Deutsche Herzstiftung e.V., Frankfurt am Main (individual grants to L.N.), Deutsche Forschungsgemeinschaft (DFG), the DFG Sonderforschungsbereich (SFB) 1123 (L.N., S. Massberg [B06], and C.S. [A07]) and SCHU 2297/1-1, the DFG SFB 1525 (B.N. [A06]), the German Center for Cardiovascular Research (Clinician Scientist Program [L.N.] and 1.4VD [S.M.]), the DFG Clinician Scientist Program PRIME (413635475, R.K. and K.P.), and the FP7 program (project 260309, PRESTIGE [S. Massberg]). This work was also supported by the Ludwig Maximilians Universität (LMU)excellent program (R.K.), the Else Kröner-Fresenius-Stiftung (R.K.), the European Research Council (ERC-2018-ADG "IMMUNOTHROMBOSIS" [S. Massberg]), and the Corona foundation (L.N.). Work of M.S.R. was supported by LMU Munich's Institutional Strategy LMUexcellent within the framework of the German Excellence Initiative, the German Research Foundation DFG (INST 86/1800-1 FUGG). Additional funding for this work was supported by grants from the National Institutes of Health, National Heart, Lung, and Blood Institute (R01HL160808 and R01HL163019; R.C.), and the American Heart Association (21POST830138; F.D.).

Authorship

Contribution: L.N. initiated and conceptualized the study; L.N. and A. Anjum created the methodology; A. Anjum, M. Mader, S. Mahameed, F.D., A.M., F.P.K., R.K., K.P., D.R., S.A., L.D., M. Mulkers, L. Laun, L. Li, N.K., K.Y., M-L.H., A. Akhalkatsi, Q.L, J.P., R.E., R.C., M.S.R., and L.N. conducted the investigation; R.K., S. Massberg, B.N., E.S., C.W., C.S., and L.N. collected the resources; A. Anjum, M. Mader, F.P.K., M.S.R., and L.N. conducted formal analysis; L.N. and A. Anjum wrote the original draft; A. Anjum and L.N. handled data curation and software; A. Anjum, F.P.K., and L.N. visualized the study; L.N. provided supervision and project administration, and administered the funding; and all authors edited the draft.

Conflict-of-interest disclosure: The authors declare no competing financial interests.

ORCID profiles: A. Anjum, 0000-0002-1976-4102; A.M., 0000-0003-2114-7696; F.D., 0000-0003-1442-3568; M. Mulkers, 0009-0003-4402-2682; L. Laun, 0009-0002-2563-2920; N.K., 0000-0001-6497-024X; K.Y., 0009-0004-8884-7245; K.P., 0000-0003-4040-650X; B.N., 0000-0003-1454-7413; M.S.R., 0000-0001-9149-8761; R.K., 0000-0003-1750-3395; L.N., 0000-0003-0776-5885.

Correspondence: Leo Nicolai, Department of Medicine I, Ludwig Maximilian University Hospital, Ludwig Maximilian University Munich, Marchioninistr 15, 81377 Munich, Germany; email: leo.nicolai@med.uni-muenchen.de.

Footnotes

Submitted 22 April 2024; accepted 2 December 2024; prepublished online on *Blood* First Edition 22 January 2025. https://doi.org/10.1182/blood.2024024901.

*M. Mader, S. Mahameed, and A.M. contributed equally to this study.

Data are available on request from the corresponding author, Leo Nicolai (leo.nicolai@med.uni-muenchen.de).

The online version of this article contains a data supplement.

There is a *Blood* Commentary on this article in this issue.

The publication costs of this article were defrayed in part by page charge payment. Therefore, and solely to indicate this fact, this article is hereby marked "advertisement" in accordance with 18 USC section 1734.

REFERENCES

1. Nicolai L, Massberg S. Platelets as key players in inflammation and infection. *Curr Opin Hematol*. 2020;27(1):34-40.
2. Stark K, Massberg S. Interplay between inflammation and thrombosis in cardiovascular pathology. *Nat Rev Cardiol*. 2021;18(9):666-682.
3. Guidotti LG, Inverso D, Sironi L, et al. Immunosurveillance of the liver by intravascular effector CD8+ T cells. *Cell*. 2015;161(3):486-500.
4. Kaiser R, Escaig R, Nicolai L. Hemostasis without clot formation–how platelets guard the vasculature in inflammation, infection, and malignancy. *Blood*. 2023;142(17):1413-1425.
5. Nicolai L, Schiefelbein K, Lipsky S, et al. Vascular surveillance by haptotactic blood platelets in inflammation and infection. *Nat Commun*. 2020;11(1):5778.
6. Gupta S, Konradt C, Corken A, et al. Hemostasis vs. homeostasis: platelets are essential for preserving vascular barrier function in the absence of injury or inflammation. *Proc Natl Acad Sci U S A*. 2020;117(39):24316-24325.
7. Hess PR, Rawnsley DR, Jakus Z, et al. Platelets mediate lymphovenous hemostasis to maintain blood-lymphatic separation throughout life. *J Clin Invest*. 2014;124(1):273-284.
8. Kaiser R, Escaig R, Kranich J, et al. Procoagulant platelet sentinels prevent inflammatory bleeding through GPIIBIIIA and GPVI. *Blood*. 2022;140(2):121-139.
9. Nording H, Baron L, Haberthür D, et al. The C5a/C5a receptor 1 axis controls tissue neovascularization through CXCL4 release from platelets. *Nat Commun*. 2021;12(1):3352.
10. Malehmir M, Pfister D, Gallage S, et al. Platelet GPIbα is a mediator and potential interventional target for NASH and subsequent liver cancer. *Nat Med*. 2019;25(4):641-655.
11. Wichaiyo S, Lax S, Montague SJ, et al. Platelet glycoprotein VI and C-type lectin-like receptor 2 deficiency accelerates wound healing by impairing vascular integrity in mice. *Haematologica*. 2019;104(8):1648-1660.
12. von Hundelshausen P, Weber C. Platelets as immune cells: bridging inflammation and cardiovascular disease. *Circ Res*. 2007;100(1):27-40.
13. Appay V, van Lier RAW, Sallusto F, Roederer M. Phenotype and function of human T lymphocyte subsets: consensus and issues. *Cytometry A*. 2008;73(11):975-983.
14. Croft AP, Campos J, Jansen K, et al. Distinct fibroblast subsets drive inflammation and damage in arthritis. *Nature*. 2019;570(7760):246-251.
15. Hidalgo A, Chilvers ER, Summers C, Koenderman L. The neutrophil life cycle. *Trends Immunol*. 2019;40(7):584-597.
16. Adrover JM, Aroca-Crevillén A, Crainiciuc G, et al. Programmed 'disarming'of the neutrophil proteome reduces the magnitude of inflammation. *Nat Immunol*. 2020;21(2):135-144.
17. Zhang D, Chen G, Manwani D, et al. Neutrophil ageing is regulated by the microbiome. *Nature*. 2015;525(7570):528-532.
18. Kaiser R, Gold C, Joppich M, et al. Peripheral priming induces plastic transcriptomic and proteomic responses in circulating neutrophils required for pathogen containment. *Sci Adv*. 2024;10(12):eadl1710.
19. Lefrançais E, Ortiz-Muñoz G, Caudrillier A, et al. The lung is a site of platelet biogenesis and a reservoir for haematopoietic progenitors. *Nature*. 2017;544(7648):105-109.
20. Valet C, Magnen M, Qiu L, et al. Sepsis promotes splenic production of a protective platelet pool with high CD40 ligand expression. *J Clin Invest*. 2022;132(7):e153920.
21. Ault KA, Knowles C. In vivo biotinylation demonstrates that reticulated platelets are the youngest platelets in circulation. *Exp Hematol*. 1995;23(9):996-1001.
22. Armstrong PC, Hoefer T, Knowles RB, et al. Newly formed reticulated platelets undermine pharmacokinetically short-lived antiplatelet therapies. *Arterioscler Thromb Vasc Biol*. 2017;37(5):949-956.
23. Bongiovanni D, Han J, Klug M, et al. Role of reticulated platelets in cardiovascular disease. *Arterioscler Thromb Vasc Biol*. 2022;42(5):527-539.
24. Petzold T, Zhang Z, Ballesteros I, et al. Neutrophil "plucking" on megakaryocytes drives platelet production and boosts cardiovascular disease. *Immunity*. 2022;55(12):2285-2299.e7.
25. Pleines I, Lebois M, Gangatirkar P, et al. Intrinsic apoptosis circumvents the functional decline of circulating platelets but does not cause the storage lesion. *Blood*. 2018;132(2):197-209.
26. Allan HE, Hayman MA, Marcone S, et al. Proteome and functional decline as platelets age in the circulation. *J Thromb Haemost*. 2021;19(12):3095-3112.
27. Salzmann M, Schrottmaier WC, Kral-Pointner JB, et al. Genetic platelet depletion is superior in platelet transfusion compared to current models. *Haematologica*. 2020;105(11):2698.
28. Denorme F, Manne BK, Portier I, et al. Platelet necrosis mediates ischemic stroke outcome in mice. *Blood*. 2020;135(6):429-440.
29. Nicolai L, Pekayvaz K, Massberg S. Platelets: orchestrators of immunity in host defense and beyond. *Immunity*. 2024;57(5):957-972.
30. Zarbock A, Singbartl K, Ley K. Complete reversal of acid-induced acute lung injury by blocking of platelet-neutrophil aggregation. *J Clin Invest*. 2006;116(12):3211-3219.
31. Kaiser R, Anjum A, Kammerer LM, et al. Mechanosensing via a GpIIb/Src/14-3-3ζ axis critically regulates platelet migration in vascular inflammation. *Blood*. 2023;141(24):2973-2992.
32. Agbani EO, Zhao X, Williams CM, et al. Carbonic anhydrase inhibitors suppress platelet procoagulant responses and in vivo thrombosis: carbonic anhydrase inhibitors as antithrombotics. *Platelets*. 2020;31(7):853-859.
33. Mason KD, Carpinelli MR, Fletcher JI, et al. Programmed anuclear cell death delimits platelet life span. *Cell*. 2007;128(6):1173-1186.
34. Josefsson EC, James C, Henley KJ, et al. Megakaryocytes possess a functional intrinsic apoptosis pathway that must be restrained to survive and produce platelets. *J Exp Med*. 2011;208(10):2017-2031.
35. Chen BZ, Xia R. Pro-inflammatory effects after platelet transfusion: a review. *Vox Sang*. 2020;115(5):349-357.
36. Davenport P, Sola-Visner M. Immunologic effects of red blood cell and platelet transfusions in neonates. *Curr Opin Hematol*. 2022;29(6):297-305.
37. Moore CM, O'Reilly D, McCallion N, Curley AE. Changes in inflammatory proteins following platelet transfusion in a neonatal population. *Pediatr Res*. 2023;94(6):1973-1977.
38. Pariser DN, Hilt ZT, Ture SK, et al. Lung megakaryocytes are immune modulatory cells. *J Clin Invest*. 2021;131(1):e137377.
39. Asquith NL, Carminita E, Rodriguez-Romera A, et al. The bone marrow is the primary site of thrombopoiesis [abstract]. *Blood*. 2023;142(suppl 1):5403.
40. Puhm F, Laroche A, Boilard E. Diversity of megakaryocytes. *Arterioscler Thromb Vasc Biol*. 2023;43(11):2088-2098.
41. Bruns I, Lucas D, Pinho S, et al. Megakaryocytes regulate hematopoietic stem cell quiescence through CXCL4 secretion. *Nat Med*. 2014;20(11):1315-1320.
42. Sun S, Jin C, Si J, et al. Single-cell analysis of ploidy and the transcriptome reveals functional and spatial divergency in murine megakaryopoiesis. *Blood*. 2021;138(14):1211-1224.
43. Uhl B, Vadlau Y, Zuchtriegel G, et al. Aged neutrophils contribute to the first line of defense in the acute inflammatory response. *Blood*. 2016;128(19):2327-2337.
44. Leon C, Eckly A, Hechler B, et al. Megakaryocyte-restricted MYH9 inactivation dramatically affects hemostasis while preserving platelet aggregation

and secretion. *Blood*. 2007;110(9):3183-3191.

45. Denorme F, Campbell RA. Procoagulant platelets: novel players in thromboinflammation. *Am J Physiol Cell Physiol*. 2022;323(4):C951-C958.

46. Nechipurenko DY, Receveur N, Yakimenko AO, et al. Clot contraction drives the translocation of procoagulant platelets to thrombus surface. *Arterioscler Thromb Vasc Biol*. 2019;39(1):37-47.

47. Rau JC, Beaulieu LM, Huntington JA, Church FC. Serpins in thrombosis, hemostasis and fibrinolysis. *J Thromb Haemost*. 2007;5(suppl 1):102-115.

48. Curley A, Stanworth SJ, Willoughby K, et al. Randomized trial of platelet-transfusion thresholds in neonates. *N Engl J Med*. 2019;380(3):242-251.

Ageing platelets shift their hemostatic properties to inflammatory functions

Afra Anjum[1,2], Magdalena Mader[1,2,*], Shaan Mahameed[1*], Abhinaya Muraly[1,2,*], Frederik Denorme[3], Fabian P. Kliem[4], Dario Rossaro[1,2], Sezer Agköl[1,2], Lea Di Fina[1,2], Maité Mulkers[1,2], Lisa Laun[1,2], Lukas Li[1], Nadja Kupper[1,2], Keyang Yue[1,2], Marie-Louise Hoffknecht[1,2], Anastassia Akhalkatsi[1,2], Quentin Loew[1,2], Joachim Pircher[1,2], Raphael Escaig[1,2], Erwin Strasser[5], Christian Wichmann[5], Kami Pekayvaz[1,2], Bernhard Nieswandt[8], Christian Schulz[1,2,7], Maria S. Robles[4], Rainer Kaiser[1,2], Steffen Massberg[1,2], Robert Campbell[3,] and Leo Nicolai[1,2,#]

[1]Department of Medicine I, LMU University Hospital, LMU Munich

[2]DZHK (German Centre for Cardiovascular Research), partner site Munich Heart Alliance, Germany

[3]Emergency Medicine, Washington University, St. Louis, Missouri, United States[4]Institute of Medical Psychology and Biomedical Center (BMC), Faculty of Medicine, LMU Munich, Munich, Germany

[5]Division of Transfusion Medicine, Cell Therapeutics and Haemostaseology, University Hospital, LMU Munich, Munich, Germany

[6]Institute for Experimental Biomedicine, University Hospital Wuerzburg, Wuerzburg, Germany

[7]Department of Immunopharmacology, Mannheim Institute for Innate Immunoscience (MI3), Medical Faculty Mannheim, Heidelberg University, Mannheim, Germany

* Contributed equally, ordered alphabetically

[#]Correspondence to leo.nicolai@med.uni-muenchen.de, Medizinische Klinik und Poliklinik I, University Hospital Ludwig-Maximilian-University Munich, Marchioninistr. 15 81377, Munich, Germany

Table of contents

Supplementary Methods

Human blood donors

Human blood was drawn from healthy male and female voluntary donors after informed consent was obtained from all subjects. Experiments involving human subjects have been approved by the ethical review board (LMU Munich) and complied with relevant regulation for experiments involving human samples.

Murine blood sampling

For repeated blood sampling, pulse-labelled mice were given short inhalation narcosis with isoflurane, and ~30 µl blood was collected from the facial vein in EDTA coated 100 µl microvettes (Sarstedt). Mice were scored for any discomfort. For larger quantities of blood collection, mice were given inhalation narcosis, restrained and anaesthetized with intraperitoneal injection of MMF: Medetomidine (0.5 mg/kg body weight), Midazolam (5 mg/kg body weight) and Fentanyl (0.05 mg/kg body weight). Blood was collected terminally from the retro-orbital vein plexus using capillary tube coated with acid-citrate dextrose (ACD): 39 mM citric acid, 75 mM sodium citrate, 135 mM dextrose.

Whole blood flow cytometry- tracking platelets, PLA, PNA

For tracking pulse labelled platelets over time, whole blood (5 µl for tracking platelets, minimum 20 µl for analysing leukocytes or platelet leukocyte aggregates) was stained with antibodies (Table 1) in 1:100 dilution in 0.5% BSA-PBS and incubated for 15mins. Samples were erylysed and fixed with 1x FACS lysing solution (BD Biosciences #349202) for 5 mins and then stored in 4°C in darkness. Samples were measured via BD LSRFortessa flow cytometer.

Flow Chamber Assay

µ-Ibidi 0.1 chambers (Cat.No:80661) were coated with Collagen HORM (250 µg/ml) for 10 minutes, followed by washing with 1X PBS at 5.61 ml/h for 1 minute. 300-400 µl of blood (or platelet rich plasma count adjusted) collected in ACD was recalcified with 2.4 mM Ca^{2+}. Whole blood, stained with antibodies, was perfused at 5.61 ml/h for 1 minute. Samples were fixed using 4% PFA by perfusion at the above-mentioned rate for 5 minutes, and then washed with PBS for another 5 minutes in Harvard Apparatus Pump 11 Elite. Samples were stored in the fridge in darkness until imaging using the Zeiss LSM 880 confocal microscope with the 40x objective in Airyscan mode.

Platelet isolation

Blood collected in ACD was immediately diluted 1:1 with modified Tyrode's buffer (137 mM NaCl, 2.8 mM KCl, 12 mM NaHCO3, 5.5 mM sucrose, 10 mM HEPES, pH = 6.5). Diluted blood samples were centrifuged at 70g for 15 min (time is adjusted for 1ml blood diluted in 1ml Tyrode´s) at rtp. Platelet rich plasma was taken out carefully and diluted 1:2 in Tyrode's buffer and subsequently centrifuged for 5 min at 1200g. Platelets were resuspended in pH 6.5 Tyrode´s buffer until functional assays were performed, at which point, the pH was adjusted to 7.2.

Platelet isolation for proteomics

Platelet rich plasma was isolated as mentioned in the paragraph above and treated for CD45 depletion to remove any leukocytes. Detailed protocol mentioned in manuscript method: "*Sample preparation for mass spectrometry"*

Platelet sorting

Data not shown here in the paper. Mice were pulse labelled and 5, 3 and 1 day prior to blood sampling. Platelet rich plasma was isolated and single labelled platelets, gated on size and X488+X649- platelets were sorted using Beckman Coulter MoFlow cell sorter using 70 µm nozzle. At least 1 million platelets were sorted (from each pulse labelled mouse), spinned down at 1200g for 5 minutes. However, platelet pellets were not observed, and enough protein concentration was not reached for performing proteomics. Alternatively, we used 4- day old and 1-day old platelet populations generated using Rosa26-DTRxPf4cre mouse model. Detailed protocol mentioned in manuscript method: “Generation of young and old platelet age cohorts by ablating platelet production” and “Sample preparation for mass spectrometry”.

Human platelet concentrates

Human platelet concentrates were provided by the Division of Transfusion Medicine, Cell Therapeutics and Hemostaseology of the LMU hospital. Analysis of these products was started directly after platelet apheresis concentrate production by the division. Concentrates were stored at 22°*C* with a constant agitation rate of 60 per minute. Concentrates were sampled once a day, and platelet count was adjusted to 300,000/µl in PBS after cell count (Sysmex XN-137 V Series XN-1000V). All assays were performed using diluted samples (unless mentioned otherwise).

Platelet Aggregometry

Chrono-Log 700 Aggregometer was turned on and allowed to warm up after using settings: X0.005 Gain 1000 RPM 37°C. Platelets diluted in PBS, were incubated for 3 minutes at 37°C. Aggregation was initiated by 2 µM ADP + 2 mM $CaCl_2$, 1000 rpm at 37°C and recorded for 6 minutes.

Platelet activation assay

Washed platelets were activated in suspension as described previously[1]. In short, human platelet concentrates or murine platelets resuspended in Tyrode´s buffer with 1mM calcium chloride, were incubated with antibodies against platelet activation markers: P-selectin, activated GPIIbIIIa and phosphatidylserine exposure. Agonists (concentrations mentioned in figures) targeting P2Y12, P2Y12, thrombin receptors PAR1/4 (thrombin), thromboxane receptor TXA2-R (U46119) and GPVI (convulxin, collagen) were incubated with platelets for 30 minutes at room temperature. Subsequently platelets were fixated with 1x FACS lysing solution (BD bioscience) and measured via flow cytometry.

Platelet migration/retraction/procoagulant assay

Human platelet concentrates and isolated murine platelets were diluted to 150 000-200 000/µl. For migration assay, platelets were activated by 4 µM ADP, 2 µM U46619 and 0.2 mM calcium chloride (1 mM for procoagulant assay) and loaded into pre-coated chambers with fibrinogen (+collagen for PA) and incubated at 37°C for 15mins. Chambers were washed with buffer containing calcium chloride to remove non-adhering platelets. Antibodies were added and incubated for 30mins to detect platelet activation and procoagulant transformation. Cells were fixed with 2% PFA, 0.005% GDA in PBS. Samples were measured by imaging on Zeiss LSM 880 (per biological replicate: either 6 random images, or 3x4 tilescan stitched images were acquired) or on epifluorescence (Olympus IX83 microscope).

MSSA Bacteria culture

Sterile tryptic soy broth (TSB) medium (Cat no: 22092-500G, Millipore®) was prepared by autoclaving. Methicillin-susceptible *Staphylococcus aureus* (MSSA strain Newman) single colony was taken using a sterile loop and inoculated into 5ml of the TSB medium in a sterile and placed in a 37°C shaking incubator at 150rpm overnight. Next, 0.25ml of the overnight culture was inoculated into 25ml of TSB medium in a sterile Erlenmeyer culture flask and placed in a shaking incubator. 100 µl of the culture was sampled every 30 minutes and diluted to 1000µl (1 in 10) using 1X sterile DPBS (Gibco). The optical density (OD) at 600nm was checked and once the OD_{600} of the undiluted culture reached 1.0, it was poured into a sterile 50 ml falcon tube and stained with the SYTO™ 41 dye (final conc. 5µM for flow cytometry and 50µM for microscopy) for 20 minutes in the dark. Culture was centrifuged at 1200g and rtp for 5 minutes. Supernatant was removed and the pellet was resuspended in 1 ml of 1X sterile DPBS. Centrifugation, supernatant removal and pellet resuspension was done again to remove any excess dye.

Platelet-bacteria co incubation: Imaging

Before sampling the bacteria, cover slips were coated with 0.01% poly-L lysine for 10 minutes, washed with millipore water and was kept in a tilted position until air dried. Once dried coverslips were placed in a 24 well plate. 100µl of platelet rich plasma at ~400 000/µl (from pulse labelled mice) was isolated using protocol mentioned above and placed onto PLL coated coverslips in the 24 well plate and allowed to settle for 5 minutes and then spun down at 250g for 3 minutes. Extra liquid was collected using a micropipette and discarded. Tyrode´s pH 6.5 was added until plate was taken to S2 room for co incubation with bacteria. Before co incubation with bacteria, extra liquid was removed without touching coverslips. 100µl of SYTO41+ MSSA bacteria in PBS (mentioned above) was added to coverslip and co incubated for 15 minutes. Propidium iodide (30µM) / Live-or-Dye NucFix™ Red (1x) was added to coverslip and swirled 5 times gently to mix in with liquid and incubated for 15 minutes. Extra liquid was discarded and 4% PFA was added and incubated for 5 minutes, then discarded and washed with PBS. Extra PBS was taken away and coverslips were taken out carefully with tweezers and coated with one drop fluorescent mounting media and place on a labelled slide and allowed to dry for 20 minutes. Samples were either stored in fridge or measured right away in IX83 Olympus Epifluorescence in 100x. Images were analysed using ImageJ.

Platelet-bacteria co incubation: Flow cytometry

In a FACS tube, 100µl of platelet rich plasma at ~400 000/µl (from pulse labelled mice) were loaded and 100µl of SYTO41+ MSSA bacteria in PBS (mentioned above) was added. Platelet and bacteria were co incubated for 15 minutes. Propidium iodide/ Live-or-Dye NucFix™ Red was added and gently pipetted 5 times to mix in with liquid and incubated for 15 minutes. 300 µl of 1x BD FACS lysing solution was added and incubated for 5 minutes. Samples were measured right away in BD LSR Fortessa.

Bone marrow cells isolation

For neutrophil isolation, femur and tibia were collected from C57BL/6J after cervical dislocation under inhalation narcosis. Bone marrow was collected by cutting end of the femur & tibia and placing in a 0.5ml tube (whole punched in the bottom) with 100 µL of complete CATCH buffer (12.5 mM HEPES, 1.5 mM EDTA, 1.75% (w/v) BSA, 2.5% (v/v) FCS in PBS), placed in a 1.5ml reaction tube and centrifuged for 1 minute at 2600g at RT. Pellet was RBC lysed (155 mMol/L NH4 Cl, 14 mMol/L NaHCO3, 0.1 mMol/L EDTA) and filtered through 70µm filter.

BM cell flow cytometry

Isolated BM cells were counted using Sysmex XN-1000 hematology analyser and diluted to 10 000/µl in FACS buffer: PBS + 1% BSA + 2mM EDTA BM cells from unlabelled mice were used without staining as negative controls, and also stained with either X488 or X649 (1:100) to generated single stain positive control. BM cell samples were analyzed by BD LSR fortessa, and analyzed via flowjo.

Neutrophil isolation

Neutrophils were isolated using anti-mouse neutrophil isolation kit (Miltenyi Biotec #130-097-658). Human neutrophils were isolated from donor blood with EasySep™ Direct Human Neutrophil Isolation Kit (Catalog #19666).

Neutrophil co-incubation with platelets- Imaging based

0.4cm IbiTreat slides were coated with Poly-L-Lysine for 10 minutes at RT and washed 3 times with PBS. 200,000 neutrophils were added per chamber and allowed to settle for 30 minutes at 37°C in the presence of 5% CO2, and then washed with warm RPMI. 4 million platelets loaded on the chamber and incubated for 15 minutes and washed. Antibodies were added and cells were incubated for 15mins (if unlabeled) and then washed. The cells were then incubated for 1 h at 37°C, 5% CO_2. Cells were fixed with 1% PFA for 15 minutes at RT and washed with PBS. Imaging Zeiss LSM 880 confocal microscope using the 40x objective in Airyscan mode. Quantified: *PNA/FOV, % platelet-bound neutrophils and % PNAs with young vs old platelets.*

Neutrophil co-incubation with platelets- flow cytometry based

Isolated neutrophils were stored in RPMI shortly prior to the experiment. RPMI was removed by centrifuging at 300g for 6 minutes. Neutrophils were resuspended in 1% PBS-BSA and transferred to Eppendorf tubes. Platelets were added to neutrophils in a 20:1 ratio and incubated for 45 minutes at room temperature. Cells were incubated with antibody cocktail for 15 minutes to stain neutrophils and platelets. 1X BD FACS lysing solution was added to fix samples. After fixation, samples were stored at 4°C until measured in flow cytometer.

For blocking platelet neutrophil aggregation, isolated platelet rich plasma from C57BL/6J (pulse-labelled 108h prior to experiment) were blocked using vehicle, anti-GPIb (0.5 µg/µl), anti-GPIIb (0.5 µg/µl), CD40 (0.05 µg/µl) or PSGL1 (0.1 µg/µl) for 20 minutes at room temperature. Platelet were isolated by centrifugation at 1200g for 5 minutes. Washed platelets were then resuspended and added to isolated neutrophils in 96-well plate (round bottom) in a 20:1 ratio. Cell suspensions were incubated for 45 minutes at 37°C, 5% CO2. Cells were stained with antibody cocktail for 15 minutes at rtp and fixed using BD FACS lysing solution and analyzed via flow cytometry.

In vivo thrombosis-$FeCl_3$ injury

Mice under narcosis were prepared for mesentery imaging by surgically opening the skin and peritoneum along the midline. Exteriorization of the proximal bowel was done carefully on a glass coverslip to expose the mesenteric vessels. The bowel was stabilized using saline soaked tissue paper. 10% ferric chloride solution was introduced on mesenteric vessel by gently touching with a saturated a 1x1 mm piece of filter paper for 3 minutes. Next, the ensuing thrombus formation was imaged on an inverted Zeiss LSM 880 in AiryScan Fast Mode (20x/0.8 obj., 990 ms/frame, laser power: 0.96%).

Quantification of platelet recruitment

For thrombosis observed using pulse-labelled mice platelets, analysis was performed on recruited single-labelled platelets (percentage area per field of view) relative to their percentage in circulation (of all CD41+ cells).

In vitro aging of platelets and platelet depletion to induce thrombocytopenia in recipients

To age platelets in vitro, platelet rich plasma was isolated and stored in 1.5ml Eppendorf tubes, kept at 25°C, with gentle agitation for 2day, or 2h prior to transfusion. Platelets were depleted in C57BL/6J mice by injecting 2 µg of anti-Gp1b antibody (R300, Emfret) per mouse intravenously, 1h prior to transfusion of in vitro aged platelets. Platelet rich plasma of the 2 groups of in vitro aged platelets were incubated with X649 (1:100) at rtp for 15mins. PRP was then diluted and centrifuged (See platelet isolation) to remove free antibody. Platelet count was adjusted and transfused into thrombocytopenic C57BL/6J recipients. Blood was taken to ensure similar percentages of transfused platelets in both groups. Platelet counts were measured using cell counter (Sysmex XN-137 V Series XN-1000V).

Acute Lung Injury in Bax/Bak mice.

Bak global knockouts (Bak KO), Bax platelet specific knockouts ($Bax^{Plt-/-}$) and double Bak KO and $Bax^{Plt-/-}$ were from Dr. Benjamin Kile (University of Adelaide). Bak KO, $Bax^{Plt-/-}$ Bak KO/ $Bax^{Plt-/-}$ and litter mate wild-type controls were anaesthetized and 20 µg of LPS (Escherichia coli-derived O111:B4; Sigma) was administered intranasally. Eight hours post LPS treatment, whole blood was drawn into 3.2% sodium citrate and mice were then sacrificed via cervical dislocation without damaging the trachea. Bronchoalveolar lavage (BAL) fluid was collected for analysis by intratracheal flushing with 1mL of PBS (1% BSA containing 2 mM EDTA). When at least half of the applied volume was recovered (>0.5 mL) without damaging the lung vasculature, only then the BALF sample was included in the analysis. BALFs were stained with antibodies for flow-cytometric analysis.

Multiplex cytokine measurements

Murine bronchoalveolar lavage fluid was assessed for their cytokine levels using LEGENDplexTM Mouse Inflammation Panel (13-plex (Biolegend, #740446) according to the manufacturer's manuals. Cytokines in BALF were measured on a BD LSRFortessa flow cytometer and analysed using the Data Analysis Softwar LEGENDplexTM to quantify their concentrations.

Histology

Harvested Femur were fixed with 4% PFA for 2h, transferred into 30% sucrose for 2h, and subsequently stored overnight in 15% sucrose. The femur was cryoembedded and stored at -80°C. Cryo-sectioning was done vertically until bone marrow was visible. Thawed bone was permeabilized in an Eppendorf tube with 1:1 mixture of 0.1% Triton-X and 10% natural goat serum for 30 minutes at 4°C. Blocking was done with 1:1 mixture of 3% BSA and 10% Natural goat serum for 4 hours at 4°C. Samples were then stained with antibody against CD41 (Clone:MWReg30) overnight at 4°C in Block solution. The following day, samples were stained with Hoechst (1:1000) for 10 minutes at rtp and washed. The femur was carefully placed on a cover slide and covered with ultrasound gel to maintain moisture. Imaging was done with confocal microscopy (Tilescan images). For lung histology, 1ml tissue tek diluted with PBS (1:1) was perfused intratracheally. Harvested lungs were placed into 4%PFA for 1h, in 30% sucrose overnight and embedded in tissue tek and stored at -80°C.organs were sliced vertically. Lung slices were stained with CD41 for 3h followed by DAPI for 5 minutes and mounted.

LC-MS/MS analysis and data processing

200ng of peptide samples were loaded onto a 50-cm reversed-phase column (diameter 75 mm; packed in-house with 1.9 mm C18 ReproSil particles; Dr. Maisch GmbH). The column was mounted to an UltiMate 3000 HPLC (ThermoFisher Scientific®) and its temperature maintained at 60°C. The peptides were eluted with a binary buffer system consisting of buffer A (0.1% formic acid) and buffer B (80% ACN and 0.1% formic acid). A gradient length of 150min was chosen starting with 5% buffer B for 5min and then ramping to 30%-60%-95% for 95min-5min-1min, keeping constant for 5min and then reducing to 5% for 1min and keeping constant for 30min. Peptides were electrosprayed into a Q Exactive HF-X mass spectrometer (MS) (ThermoFisher Scientific®), obtaining full scans (300 to 1650 m/z, R = 60,000, max. injection time 20ms, normalized AGC target 3e6). Data-dependent acquisition was performed to obtain the top 15 MS2 spectra (R= 15,000, max. injection time 28ms, normalized AGC target 1e5). Raw files were processed using MaxQuant Version 2.1.4.0 using default settings but keeping conditions in separate fractions (difference>3), enabling "Matching between runs" with a time window of 0.7min and activating label-free quantification (LFQ)2. Proteins were identified from fasta files of the UniProt database from mouse with isoforms (April 2020). Further processing was performed using Perseus V 1.6.10.503. LFQ intensities were log2 transformed to fit a normal distribution. For Venn diagram proteins were filtered for 1 valid value in any sample, for PCA 100% valid values and for all other analyses proteins were filtered for ¾ valid values in any of the young or old cohort. Two-sample student's t-test was performed in Perseus (FDR>0.05, S0=1) after imputing missing values from a normal distribution (width 0.3, down shift 1.8). Enrichment analysis was performed using Perseus' Fisher exact test (Threshold value 0.02). Visualizations were realized in Perseus or R using ggplot2.

Statistical analysis

Animal numbers were estimated during ethical approval of planned experiments according to statistical power calculations. Animal experimental groups were coordinated to match age and sex in mouse lines. Platelet cohort percentages were calculated relative to their abundance in blood as measured by flow cytometry (percentage of CD41+ platelets) to assess relative changes in recruitment/activation patterns in in vitro and in vivo assays. Data analyses were performed using FlowJo v10 (BD), Prism v10 (Graphpad), and Excel (Microsoft Office Professional Plus 2019). All error bars in data are ± standard error mean (SEM); in bar graphs, single dots represent single data points measured per biological replicate. All data shown consist of at least 3 biological replicates. Images or flow cytometry plots shown were representative of mean values in respective data. Statistical tests were performed by using t-tests, and ANOVA (analysis of variance), which are specified in figure legends. P-values for t-tests and ANOVA summaries are stated in figure legends. Two tailed tests were always selected for t tests; paired t tests were used in experiments performed on the same biological replicate, otherwise, unpaired t tests were performed. Experiments containing more than two groups were analyzed using one-way ANOVA with post-hoc Dunnett's multiple comparisons test compared to either 0-12h cohort (in pulse-labelled models), WT (genetic knockout models), or specific timepoints (in vitro aged platelets). For two-way ANOVA, post-hoc Holm-Šídák's multiple comparisons tests were performed. Across all statistical tests, 'ns' and asterisks were used to denote p-values according to $p>0.05$ (ns = non-significant), $p\leq0.05$ (*), $p\leq0.01$ (**), $p\leq0.001$ (***), $p\leq0.0001$ (****).

Table 1:

Protein/epitope/Reagents/kits	Clone	Dilution	Manufacturer
anti-mouse GpIb	X488	1:100	Emfret
anti-mouse GpIb	X649	1:100	Emfret
anti-mouse CD41	MWReg30	1:100	Biolegend
anti-mouse Ly6G	RB6-8C5	1:100	Biolegend
anti-mouse CD49b	HMa2	1:100	Biolegend
anti-mouse CD45	30-F11	1:100	Biolegend
anti-mouse CD19	1D3/CD19	1:100	Biolegend
anti-mouse CD115	AFS98	1:100	Biolegend
anti-mouse CD3	17A2	1:100	Biolegend
anti-mouse CD11b	1A8	1:100	Biolegend
Anti-mouse CD66a	MAb-CC1	1:100	Biolegend
Anti-mouse CD177		1:100	Biolegend
Anti-mouse CD184	L276F12	1:100	Biolegend
Anti-mouse CD42d	1C2	1:100	Biolegend
anti-mouse CD107a/LAMP1	1D4B	1:100	Biolegend
anti-mouse CD54	YN1/1.7.4	1:100	Biolegend
anti-mouse CD36	HM36	1:100	Biolegend
anti-mouse Clec2	17D9	1:100	Biolegend
anti-mouse CD88	20/70	1:100	Biolegend
Anti-mouse CD9	MZ3	1:100	Biolegend
Anti-mouse CD40l	MR1	1:100	Biolegend
anti-mouse CD47	miap301	1:100	Biolegend
Anti-mouse CD44	NIM-R8	1:100	Biolegend
Anti-mouse CD62p	RMP-1	1:100	Biolegend
Anti-mouse GPVI	FAB6758P	1:100	Biolegend
anti-mouse ICAM2	CBR-IC2/2	1:100	Biolegend
Anti-mouse JonA	M023-2	1:100	Emfret
anti-mouse P-selectin	RMP-1	1:100	Biolegend
anti-mouse TER-119	TER-119	1:100	Biolegend
Anti-mouse CD45 microbeads	130-052-301	1:100	Miltenyi Biotec
anti-human CD62P	AK4	1:100	Biolegend
anti-human CD41 Antibody	HIP8	1:100	Biolegend
anti-human CD107a (LAMP-1) Antibody	H4A3	1:100	Biolegend
Anti-C3	RmC11H9	1:50	CEDARLANE
Purified anti-mouse CD40 Antibody	HM40-3	0.05 µg/µl	Biolegend
Annexin V	640924	1:50	Biolegend
RCA I		1:100	Invitrogen™
R300	R300	0.09µg/g	Emfret
Neutrophil Isolation Kit, mouse	130-097-658		Miltenyi Biotec
Diphtheria toxin			Merck
Poly-L-Lysine solution	P8920	0.01%	Sigma-Aldrich
CountBright™ Absolute Counting Beads	C36950		Invitrogen™

Lipopolysaccharides from Escherichia coli O111:B4	L2630		Sigma-Aldrich
SYTO™ 41	S11352	5-50µM	Thermofisher
Propidium iodide	BMS500PI	30µM	Invitrogen™
TMRE Kit	ab113852		Abcam
Live-or-Dye NucFix™ Red Staining Kit	#32010		Biotium
Calcium chloride			Sigma-Aldrich
Hoechst 33342	H3570	1:1000	Thermofisher
Diptheria toxin	D0564		Sigma-Aldrich
MitoTracker Green	M7514	50nM	Invitrogen™
Thiazole orange		200 ng/ml	Sigma-Aldrich
Poly-L-lysine solution	P8920-100ML	1:10	Sigma-Aldrich

Supplementary Figure legends

Suppl. Figure 1: **Pulse-labelling method does not have a depleting effect on platelets and does not stain megakaryocytes:** A) Schematic outline of C57BL/6J mice (n=3/group) were labelled with X649 followed by X488 at different concentrations: 0 µg (vehicle), 0.02 µg, 0.2 µg, 2 µg and 20 µg of each antibody. B) Gating strategy for all platelets. C) Histogram overlay and multi plots of X649 and X488 labelled platelet populations (post platelet gating strategy) after injection of aforementioned concentrations of antibodies. D) Bar graph depicting percentage of platelets labelled by X488 and X649 antibodies at the mentioned concentrations, two-way RM ANOVA (no variation in labelled groups, p-value=0.4645, with post-hoc Dunnett's multiple comparisons test compared to 0 µg [vehicle control]). E) Bar graphs depicting platelet counts (p-value=0.9015) and mean platelet volume (0.5983) in blood post double injection; statistical test, one-way ANOVA with post-hoc Dunnett's multiple comparisons test compared to 0 µg (vehicle control). F) Schematic outline of sequential intravenous injections of C57BL/6J mice (n=4 per group) with either 0.9% NaCl (vehicle) or with 2 µg of X649 followed by 2 µg of X488 (pulse-labelled); femur and tibia were collected post second labelling. G) Whole mount staining of femur with CD41 and Hoechst. H) Gating strategy for CD41+ and CD42d+ megakaryocytes in bone marrow (BM) cells from vehicle and pulse-labelled mice. I) Histogram overlay of CD41+CD42d+ MKs of vehicle treated, pulse-labelled and positive controls (stained BM cells); percentage of MKs stained with X488 or X649, two-way RM ANOVA, comparison between vehicle and pulse-labelled groups: p-value=0.3269 with post-hoc Šídák's multiple comparisons test.

Suppl. Figure 2: **Pulse-labelling method validation.** A) Experimental scheme showing platelets isolated from GPIbCre-mTmG cre+ mouse were labelled with X649, and then transfused in C57BL/6J mice (n=4) with repeated blood sampling. B) Flow cytometry scatter plots showing gating strategy for platelets to be transfused; graph showing efficient labelling of $EGFP^{+}$ (mG) platelets with X649. C) Gating strategy for transfused platelets. D) Graph showing dye stability after transfusion in C57BL/6J mice as tracked over time (p-value=0.9813). E) Platelet-leukocyte aggregate gating strategy (p-value= 0.0927). F) P-selectin (p-value=0.5260) and RCA-I (p-value=0.8875) MFI over time in labelled platelets.

Statistical tests for fig. 2D-F, two-way RM ANOVA with post-hoc Holm-Šídák's multiple comparisons test compared between $EGFP^+$ & X649 labelled platelets.

Suppl. Figure 3: **Young platelets show increased activation and mitochondrial potential.** Platelets isolated from pulse-labelled mice were treated with agonists for 30 minutes and stained with antibodies (n=4 per group); bar graphs depicting flow cytometric measurements of P-selectin expression (ADP, p<0.0001 and thrombin, p<0.0001), activated GPIIbIIIa integrin (ADP, p-value=0.0002 and thrombin, p-value=0.0169) relative to their baseline expression in single-labelled platelets; statistical tests for all, ordinary one-way ANOVA with post-hoc Dunnett's multiple comparisons test compared to 0-12h old platelet group.

Suppl. Figure 4: **Gating strategy of PLA and PNA in mouse whole blood.** A-D) Mice pulse-labelled 108h, 60h and 12h prior were sampled for blood; multi-panel antibody staining was done to determine platelet PS exposure, procoagulant platelets and platelet aggregation with leukocyte subsets via flow cytometry; A) Flow cytometric analysis of PS exposure (MFI) in washed platelets after treatment with PBS (p-value=0.0189), 100 µM ADP + 4 µM U46619 (p-value=0.0034) and 0.1 µg/ml Convulxin + 0.1 U/ml Thrombin (p-value=0.0034); absolute MFI of single-labelled population shown for PBS treated platelets; PS MFI of single-labelled population relative to that of PBS treated platelets shown for samples treated with agonists, n=4 per group. B) Procoagulant platelet gating strategy. C) Representative platelet-leukocyte aggregate gating strategy; D) Platelet-neutrophil aggregate gating strategy;

Suppl. Figure 5: **Disrupting procoagulant platelet activation by genetic ablation of mitochondrial cyclophilin D (CypD) does not affect PNA formation in aged platelet cohorts.** A-D) PF4cre-$CypD^{fl/fl}$ mice (n=4 per group) pulse-labelled with 12h interval and blood sampled every 12h; A) Schematic outline; B) Gating strategy of pulse-labelled platelets; C) Percentage of labelled platelets in circulation over time, two-way RM ANOVA (np-value= 0.7503) with post-hoc Holm-Šídák's multiple comparison between mouse strains; D) Bar graphs depicting platelet half-life and baseline phosphatidylserine exposure, unpaired t tests, two-tailed, p-values=0.8236 and 0.4561, respectively. E-I) PF4cre-$CypD^{fl/fl}$ mice (n=4 per group) were pulse-labelled 108h prior to experiment, blood was sampled for whole blood flow cytometry and platelet isolation; E) Schematic outline; F) Representative micrographs and quantification of procoagulant activation of platelets seeded on collagen I and fibrinogen, p-value=0.0135; G) PLA gating strategy and bar graph showing % of 96-108h old platelets aggregating with leukocytes in whole blood, p-value=0.4355; H) PNA gating strategy and bar graph showing % of 96-108h old platelets aggregating with neutrophils in whole blood, p-value=0.0613; I) Washed platelets were co-incubated with isolated neutrophils (from C57BL/6J mice, n=2) on a PLL coated chamber, followed by staining and PFA fixation; representative micrographs of platelet neutrophil aggregation; bar graph depicting percentage of single-labelled platelets of all CD41+ platelets aggregating with neutrophils, p-value=0.4905; statistical tests for fig 4F-I, unpaired t tests, two-tailed.

Suppl. Figure 6: **Aged platelets show increased propensity to aggregate and kill MSSA.** A) Schematic outline shows isolated platelets from pulse-labelled C57BL/6J mice (0-12h or 96-108h) co-incubating with methicillin-susceptible Staphylococcus aureus (MSSA strain Newman) prestained with SYTO™ 41 dye, followed by staining of co-cultured cells with propidium iodide (PI). B) Gating strategy of pulse-labelled platelets co-cultured with MSSA. C) Histogram overlay of staining controls (unstained MSSA: negative control and ethanol killed MSSA: positive control) for PI and pulse-labelled groups. D) Bar graphs depicting percentage of MSSA aggregating with pulse-labelled platelets (p-value=0.0186) and percentage of MSSA that are positive for propidium iodide (p-value=0.0002); statistical tests, unpaired t tests, two-tailed.

Suppl. Figure 7: **Generation of functional young platelets in recovery phase post MK ablation using Rosa26-DTRxPF4cre+.** A) Experimental scheme of Rosa26-DTRxPF4cre mice administered with diphtheria toxin (blue arrows), DT, intraperitoneally every 48h; ~1-day old rejuvenated platelets (Young cohort) from Cre+ and mixed control platelets (WT) from Cre- were collected 8 days after serial DT injections (see Method); n=4 per group. B) Bar graphs depicting platelet counts pre and post DT administration in Cre- and Cre+ mice (DT: dotted blue lines and rejuvenated young platelets: blue box), two-way RM ANOVA, comparison between cre- only and cre+ groups: p-value=0.0002 with post-hoc

Šídák's multiple comparisons test. C) Representative micrographs of whole mounted femur histology on day 8 post serial DT administrations; bar graph showing megakaryocyte (CD41+) count per field of view, p-value=0.0103, unpaired t test, two-tailed. D) Flow cytometric analysis of platelet size by depicting forward scatter-area (FSC-A) mean, unpaired t test, two-tailed, p-value=0.0043. E) Representative micrographs showing in vitro thrombus formation with count adjusted platelet rich plasma on collagen I (n=4 per group); bar graph depicting percentage area covered by thrombus per field of view, p-value=0.0426, unpaired t test, two-tailed. F) Bar graph showing percentages of platelets that are TMRE positive and MitoTracker Green positive, two-way ANOVA comparison between cre+ young, and cre- control: p-value=0.0659 with post-hoc Šídák's multiple comparisons test. G) Experimental scheme showing: Cre- control (wild type) and Cre+ Young cohort (~1-day old) rejuvenated platelets collected 8 days post serial DT injections (n=4 per group); C57BL/6J mice (n=3) were pulse-labelled with 2µg of X649 followed by 2µg X488 (PL 0-12h) and immediately sampled after the second labelling. H) Surface marker expression in platelets: P-selectin (p-value=0.0116), CD40L (0.0072), and PS exposure (<0.0001), ordinary one-way ANOVA with post-hoc Dunnett's multiple comparisons test compared to cre- control group.

Suppl. Figure 8: **Platelet ageing proteomics.** A-D) Rosa26-DTRx PF4cre mice were administered with diphtheria toxin, DT, intraperitoneally every 48h; mixed platelet age cohorts were isolated from cre- mice 4 days after serial DT injections (n=4); >4-day old platelets were collected 4 days after serial DT injections in cre+ mice (n=4); <1-day old platelets were collected 8 days after serial DT injections in cre+ mice during platelet recovery phase (n=4); A) Platelet count and sampling time points for mixed, young and old platelet aged cohorts; B) Venn diagram of all 3495 proteins quantified; C) Boxplots of LFQ intensities of several proteins of interest in the young and old cohorts; D) Heatmap of z-scored LFQ intensities of proteins belonging to several functional groups in the young and old cohorts.

Suppl. Figure 9: **Elevated cytokines in the lung of mice with constitutively aged platelets**. A) Platelets isolated from WT and BAK $BAX^{plt-/-}$ KO were treated and checked for percentage of platelets positive for GPIIbIIIa integrin activation, P-selectin and phosphatidylserine exposure, two-way RM ANOVA (variation between mouse strains, p-value= 0.040, <0.001, and <0.001 respectively) with post-hoc Holm-Šídák's multiple comparison between mouse strains. B) Baseline platelet count in BAK KO, $BAX^{plt-/-}$, BAK $BAX^{plt-/-}$ KO; p-value=0.0002. C) Acute lung injury was induced in BAK KO, $BAX^{plt-/-}$, BAK $BAX^{plt-/-}$ KO and rejuvenated BAK $BAX^{plt-/-}$ KO after antibody-mediated platelet depletion; bar graph showing platelet count in bronchoalveolar lavage fluid; p-value=0.0206. Statistical test for suppl. fig 9B-C, ordinary one-way ANOVA, with post-hoc Dunnett's multiple comparisons test compared to WT. D) Cytokine measurements in BALF 8 hours after ALI statistical tests, two-way ANOVA (variation between strains, p-value= <0.0001), with post-hoc Dunnett's multiple comparisons test compared to WT; data is also depicted in fig 6H.

Suppl. Figure 10: **Proinflammatory effect of human platelet concentrates depends on platelet age.** A-E) Human platelet concentrates sampled every ~24h were adjusted to 300,000/µl for all assays; A) Flow cytometric analysis of baseline CLEC2 (p-value=0.0525); B) Flow cytometric measurements of P-selectin expression under baseline conditions relative to timepoint 1 (n=4), p-value=0.0270; C) Flow cytometric measurements of P-selectin expression after stimulation with 20 µM ADP + 2 mM $CaCl_2$ relative to baseline expression, n=5 (p-value=0.0056); D) Line graph representing platelet aggregation as area under the curve (AUC), p-value=0.0555; Statistical tests for Suppl Fig 7A-D, RM one-way ANOVA with post-hoc Dunnett's multiple comparisons test compared to TP7; E) Schematic outline and representative gating strategy for platelet-neutrophil aggregates in Fig. 7G

Suppl. Figure 11: **Proinflammatory effect of in vitro aged murine platelets.** A) Experimental scheme for the collection of platelet rich plasma from C57BL/6J mice, which were freshly isolated, inside 'PRP Digital Storage Device' (DSD). B) Surface marker expression in platelet rich plasma: CD107a (p-value= 0.6219), CD40L (p-value= 0.5092), CLEC2 (p-value <0.0001), CD47 (p-value= 0.0935), PS exposure (p-value= 0.1335) and P-selectin (p-value= 0.0132). Statistical tests: unpaired t test, two-tailed. C) Isolated platelets were treated with either PBS, ADP (20µM) or convulxin (1µg/ml) + thrombin (0.1U/ml) in the presence of 2mM calcium chloride; bar graphs representing surface markers post treatment with vehicle or agonists; PS exposure (p-value=0.1338), JonA (0.3067) and P-selectin (0.9459); statistical

tests, two-way ANOVA, comparison between in vitro stored groups with post-hoc Šídák's multiple comparisons test. C) Micrographs depict in vitro thrombosis of platelet rich plasma (count adjusted to 300 000/µl); bar graph showing percentage area of thrombi in field of view, unpaired t test, two-tailed, p-value=0.0202. E) In vitro aged donor C57BL/6J platelets (freshly isolated or 2 day old), were transfused into thrombocytopenic C57BL/6J recipient mice (n=4/group) and acute lung injury (ALI) was induced in recipient mice; blood sampled at 0h and 6h post ALI; BALF was collected at 6h post ALI. F) platelet counts; statistical test: two-way ANOVA (comparison between transfused groups, p-value= 0.0689 with post-hoc Šídák's multiple comparisons test. G) Bar graphs depicting immune cells count in blood analysed via flow cytometry: CD45+ (p-value= 0.4358) and Ly-6G+ (0.5330).H) Bar graphs depicting CD45+ (p-value= 0.6573), Ly-6G (0.2672) and RBC (0.3153) count in BALF. Statistical tests for F-G: Unpaired t test, two-tailed. I) Cytokine measurements in BALF, statistical tests, two-way ANOVA (comparison between transfused groups, p-value= 0.0005), with post-hoc Šídák's multiple comparisons test; data is also depicted in Fig 7M.

1. Nicolai, L.*, et al.* Single platelet and megakaryocyte morpho-dynamics uncovered by multicolor reporter mouse strains in vitro and in vivo. *Haematologica* (2021).
2. Tyanova, S., Temu, T. & Cox, J. The MaxQuant computational platform for mass spectrometry-based shotgun proteomics. *Nature Protocols* **11**, 2301-2319 (2016).
3. Tyanova, S*., et al.* The Perseus computational platform for comprehensive analysis of (prote)omics data. *Nature Methods* **13**, 731-740 (2016).

Suppl. Figure 1: Pulse-labelling method do not have a depleting effect on platelets and do not stain megakaryocyte

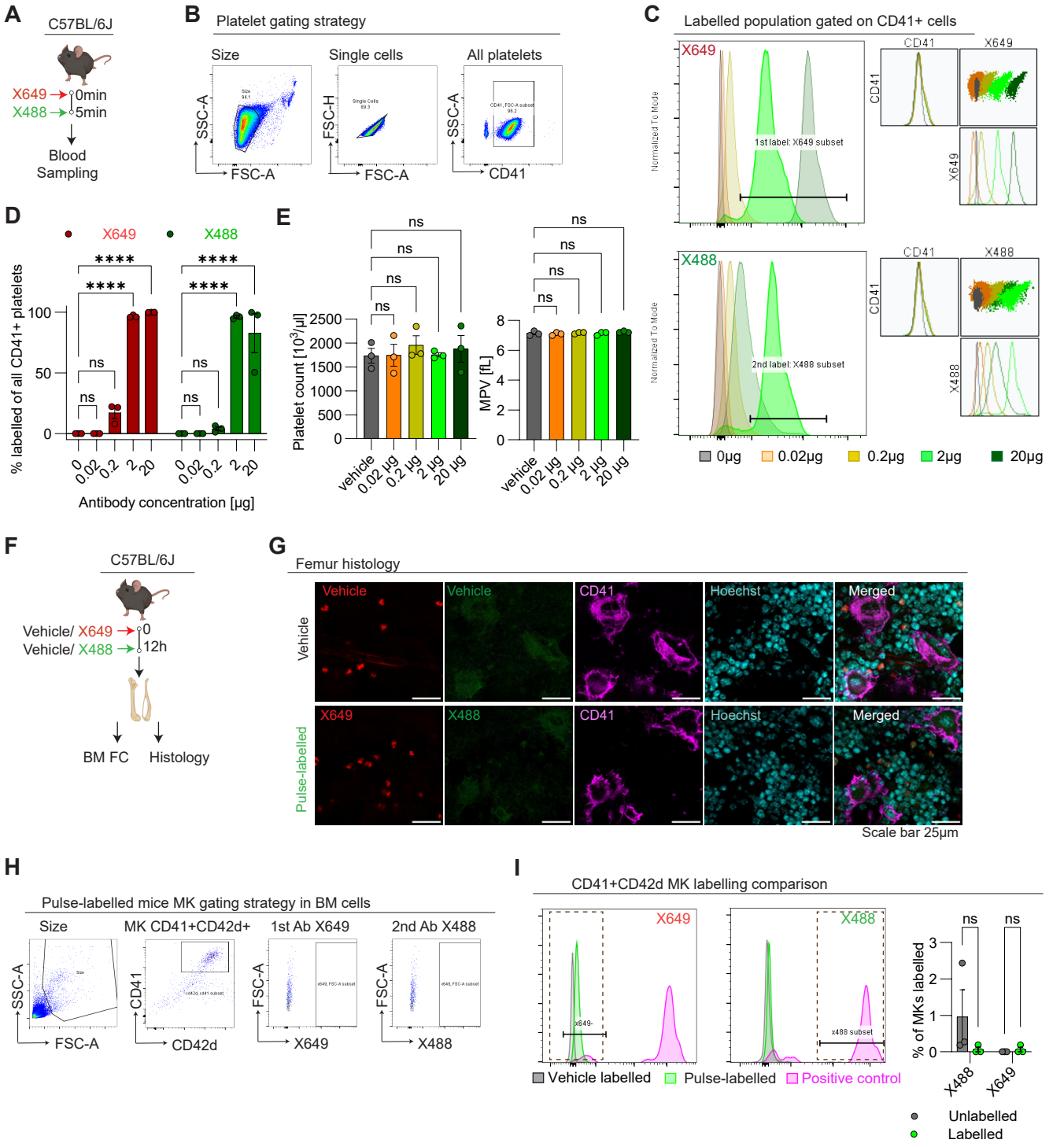

Suppl. Figure 2 Pulse labelling method validation

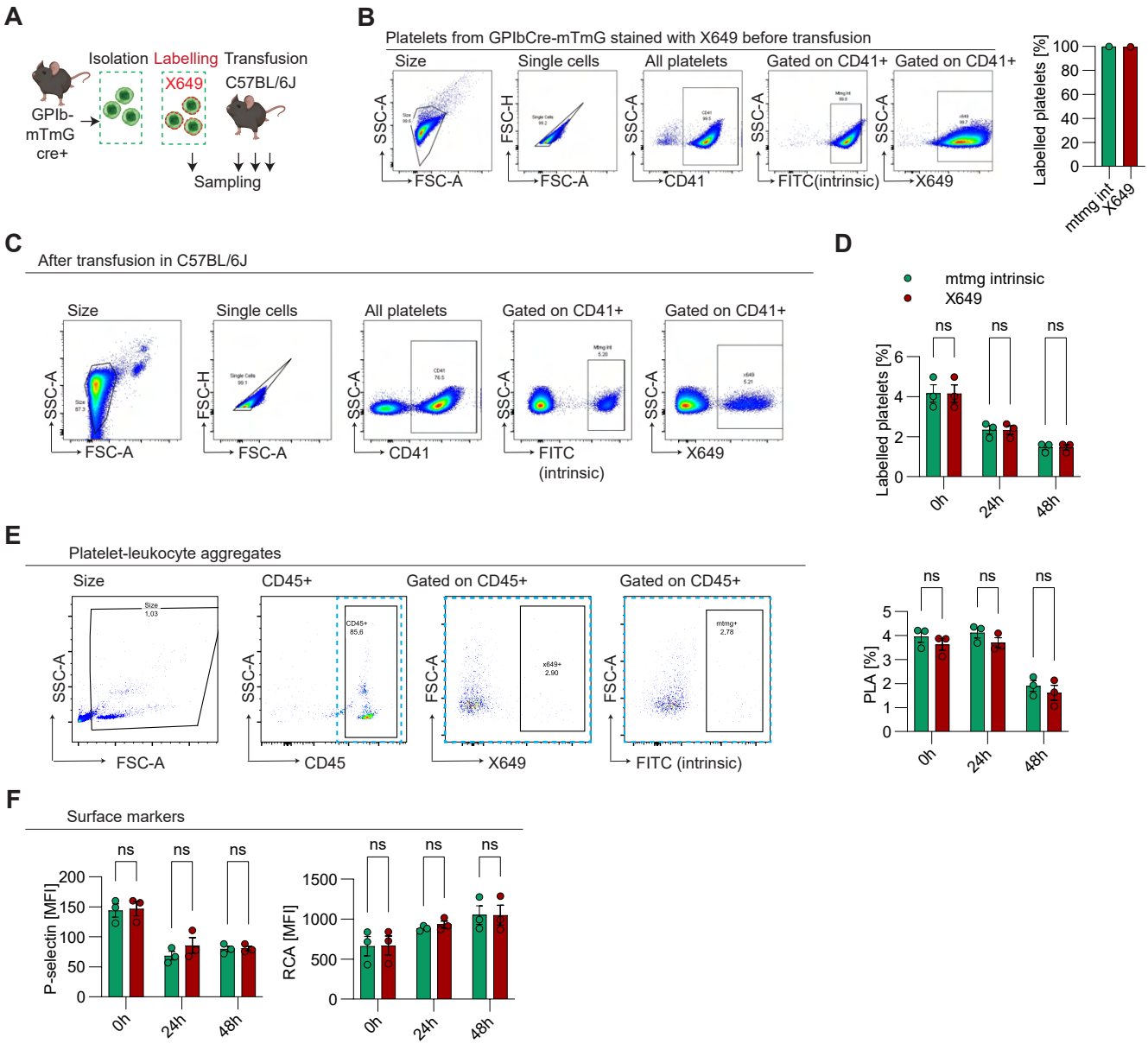

Suppl. Figure 3: Young platelets show increased activation and mitochondrial potential

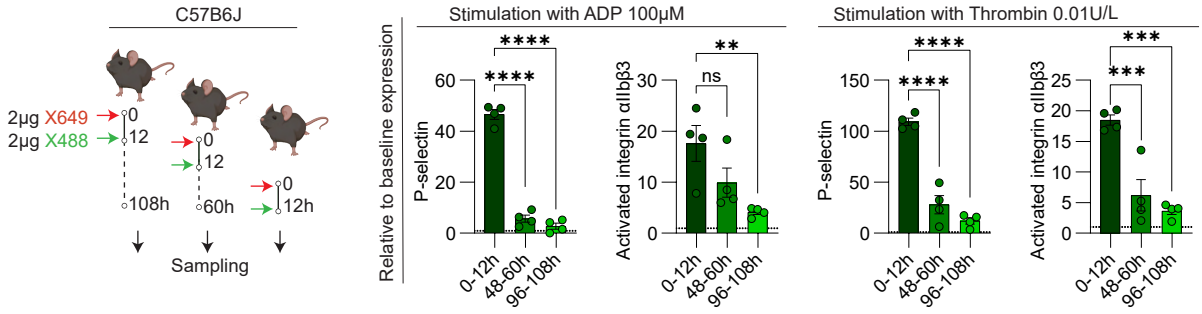

Suppl. Figure 4: PS exposure in Aged platelets and gating strategy of PLA and PNA

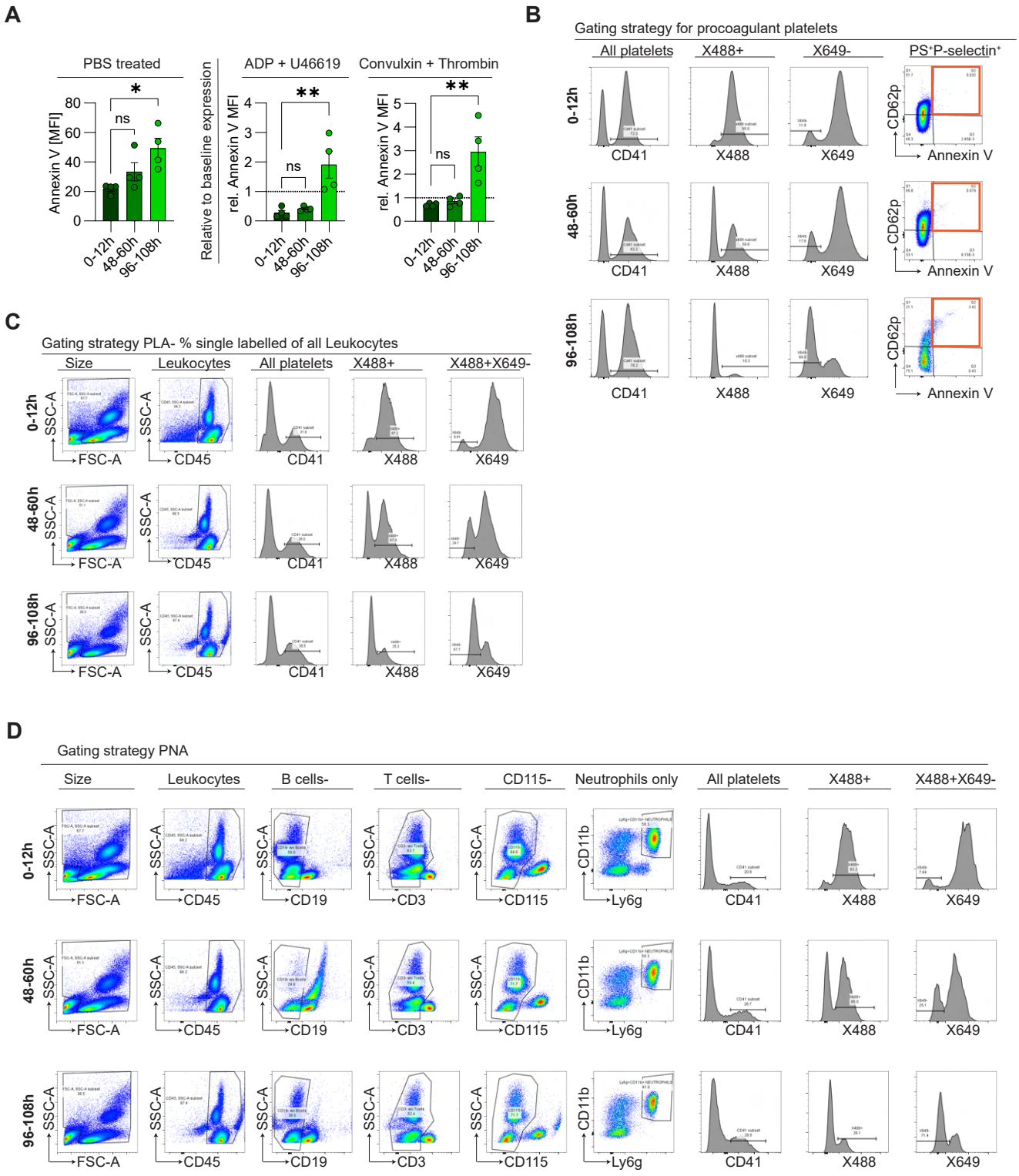

Suppl. Figure 5: Disrupting procoagulant platelet activation by genetic ablation of mitochondrial cyclophilin D (CypD) does not affect PNA formation in aged platelet cohort.

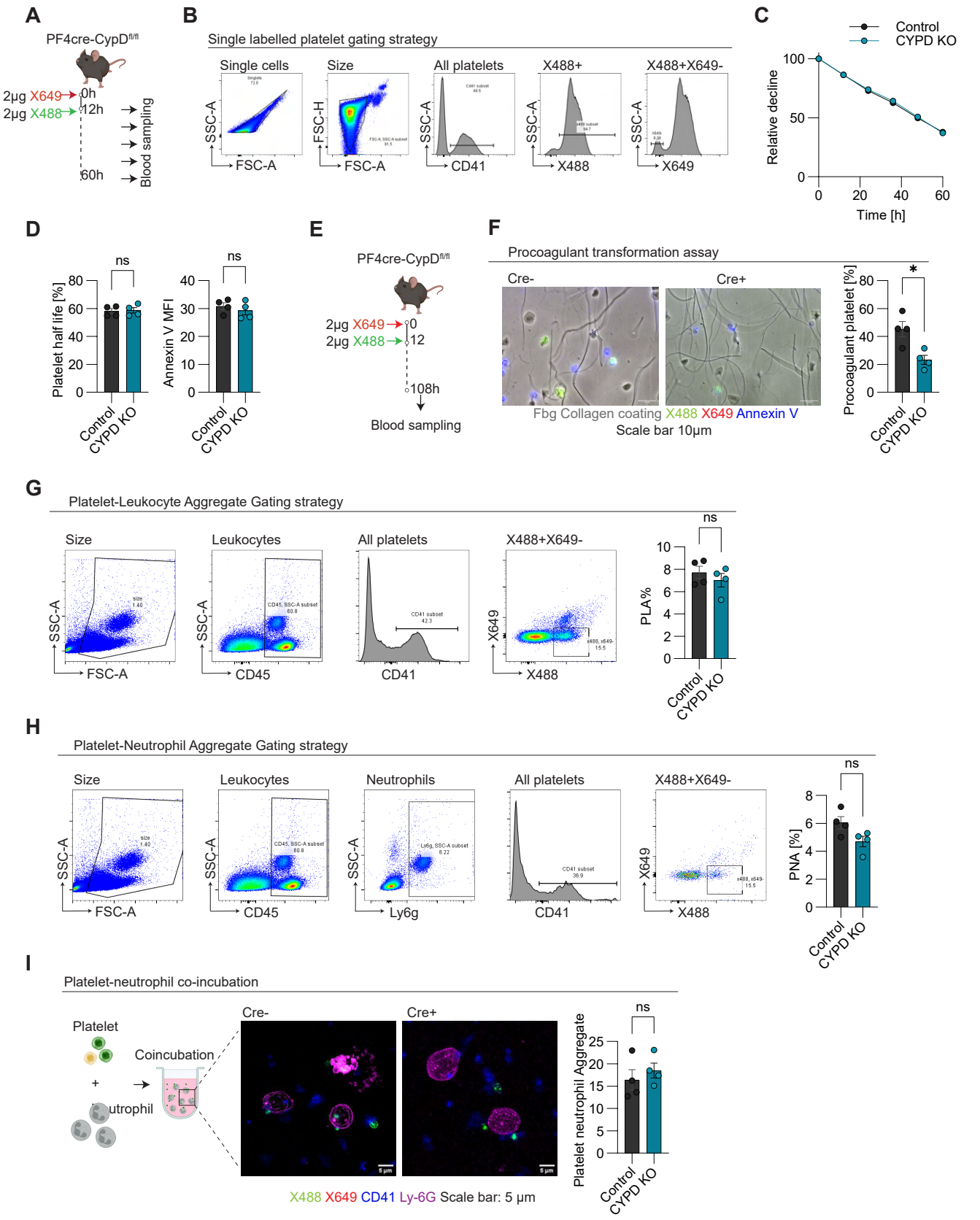

Suppl. Figure 6: Aged platelets show increased propensity to aggregate and kill MSSA

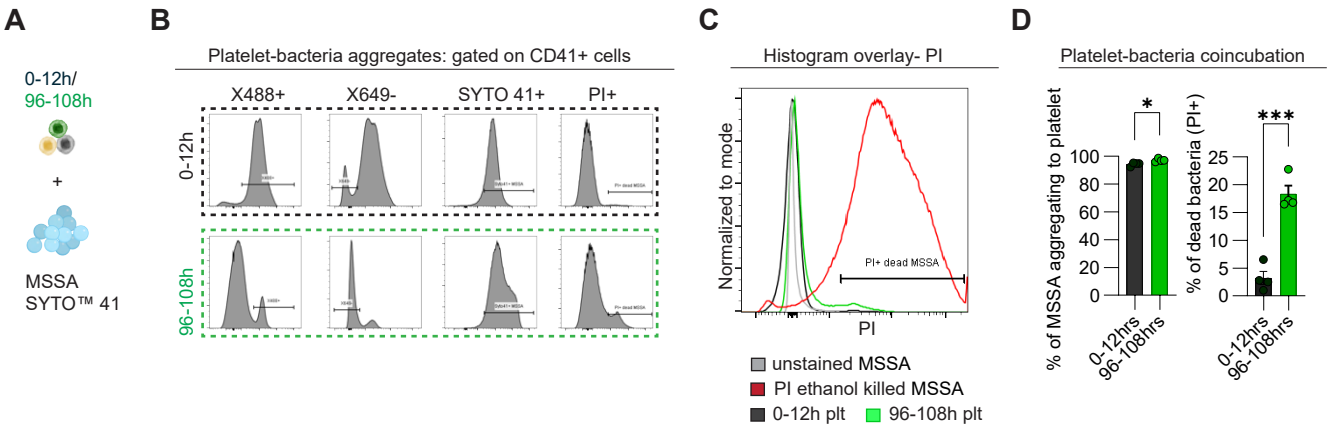

Suppl. Figure 7. Generation of functional young platelets in recovery phase post MK ablation

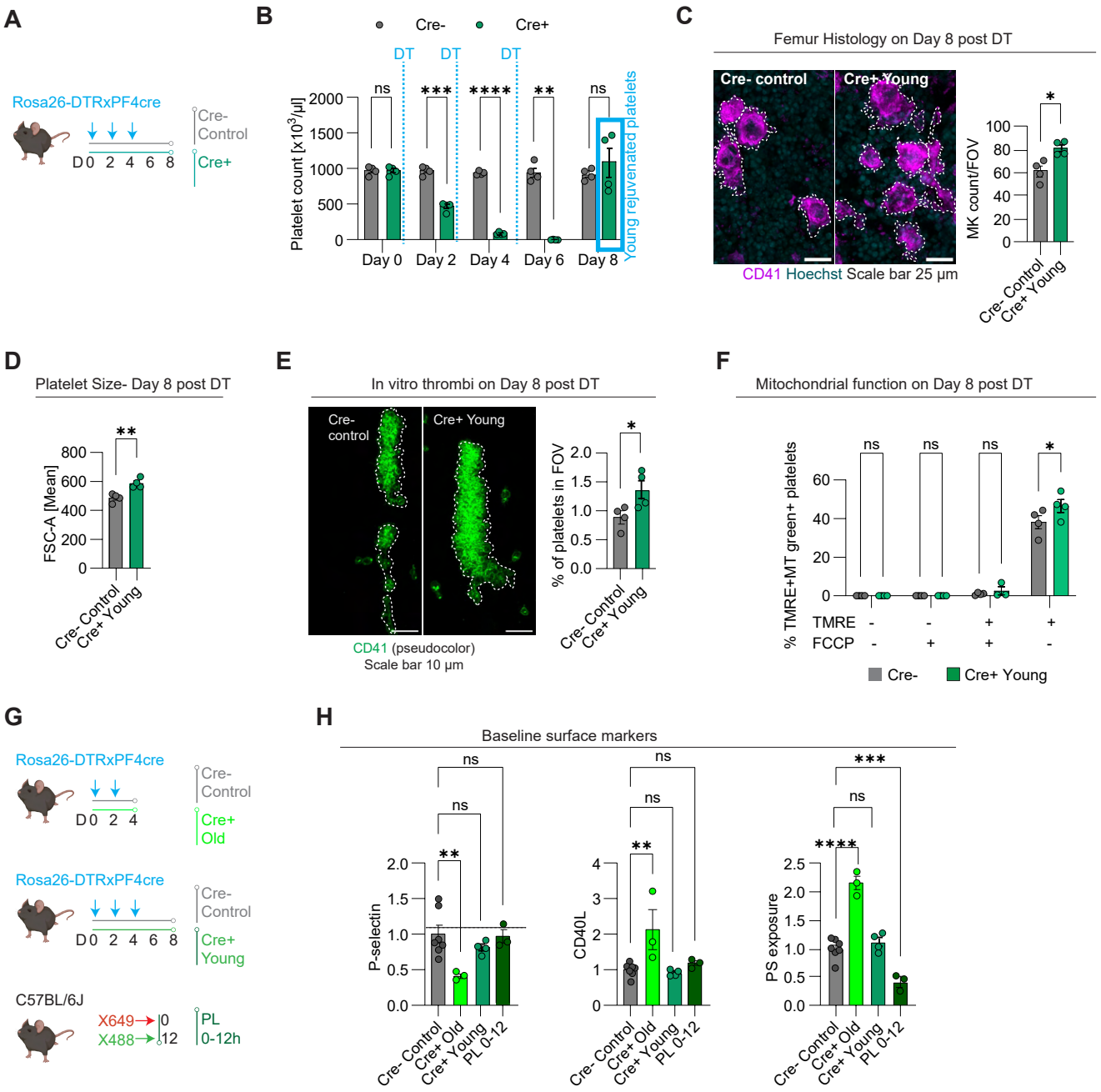

Suppl. Figure 8: Platelet aging proteomics.

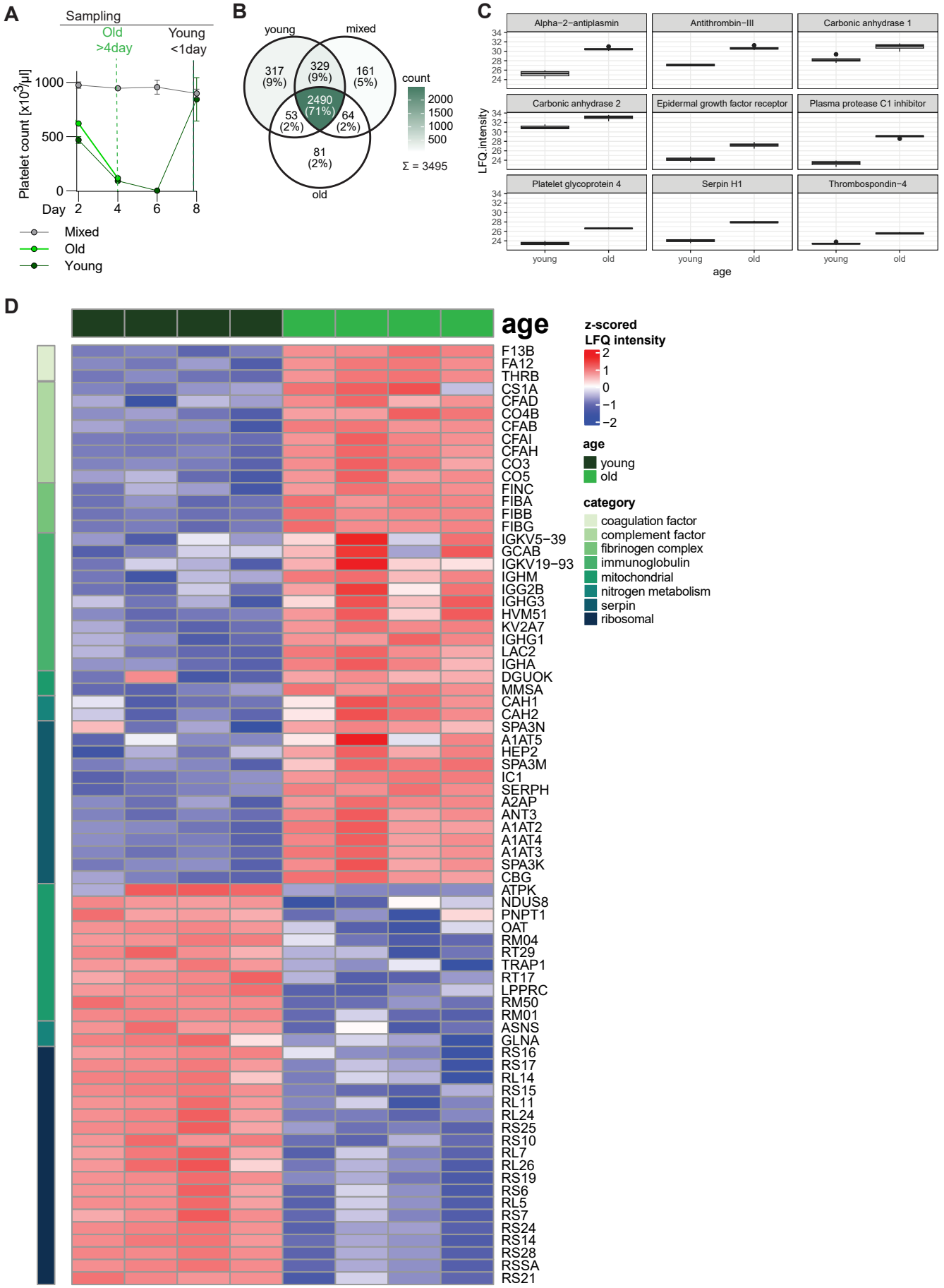

Suppl. Figure 9: Elevated cytokines in the lung of mice with constitutively aged platelets.

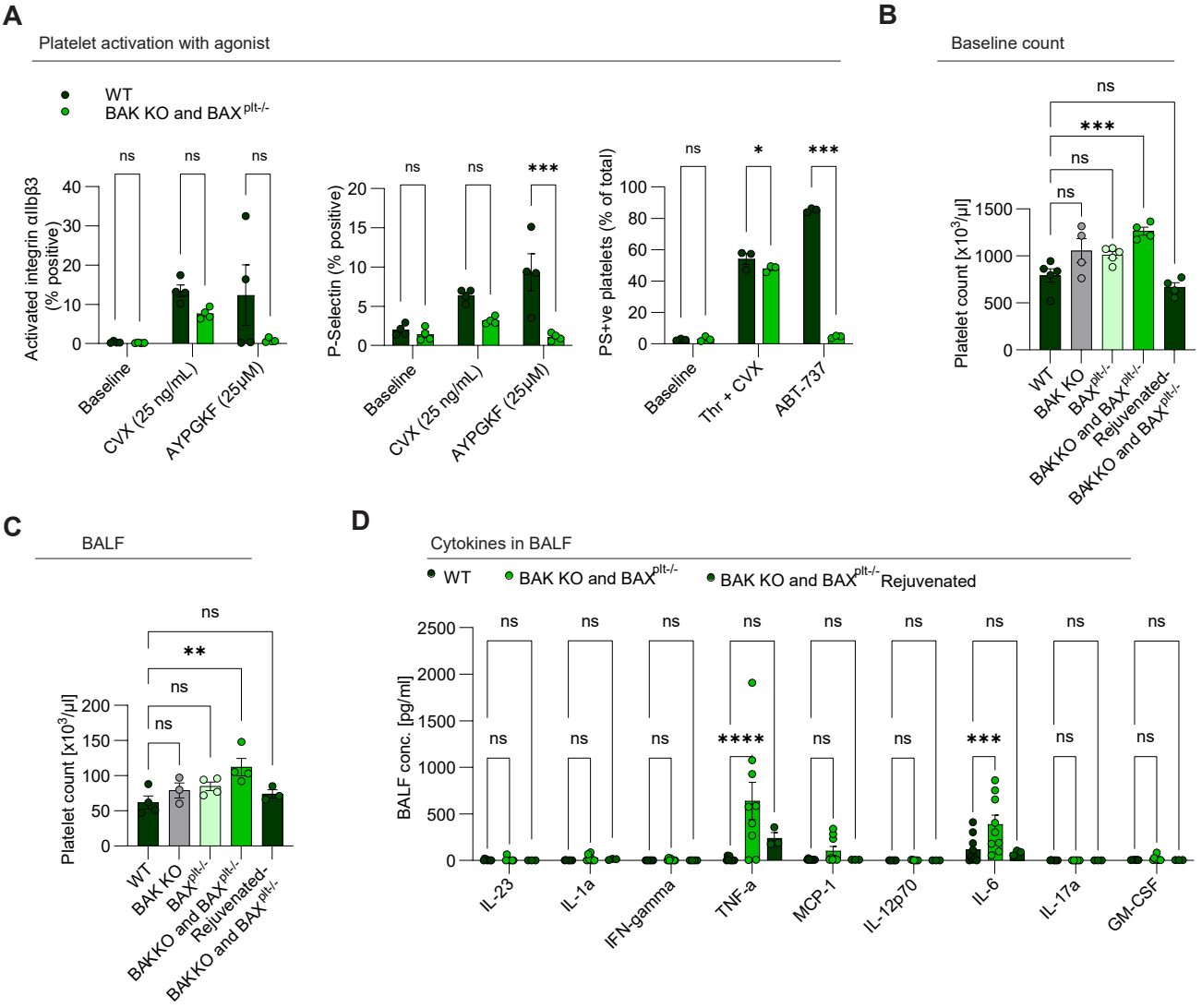

Suppl. Figure 10: Proinflammatory effect of human platelet concentrates depends on platelet age

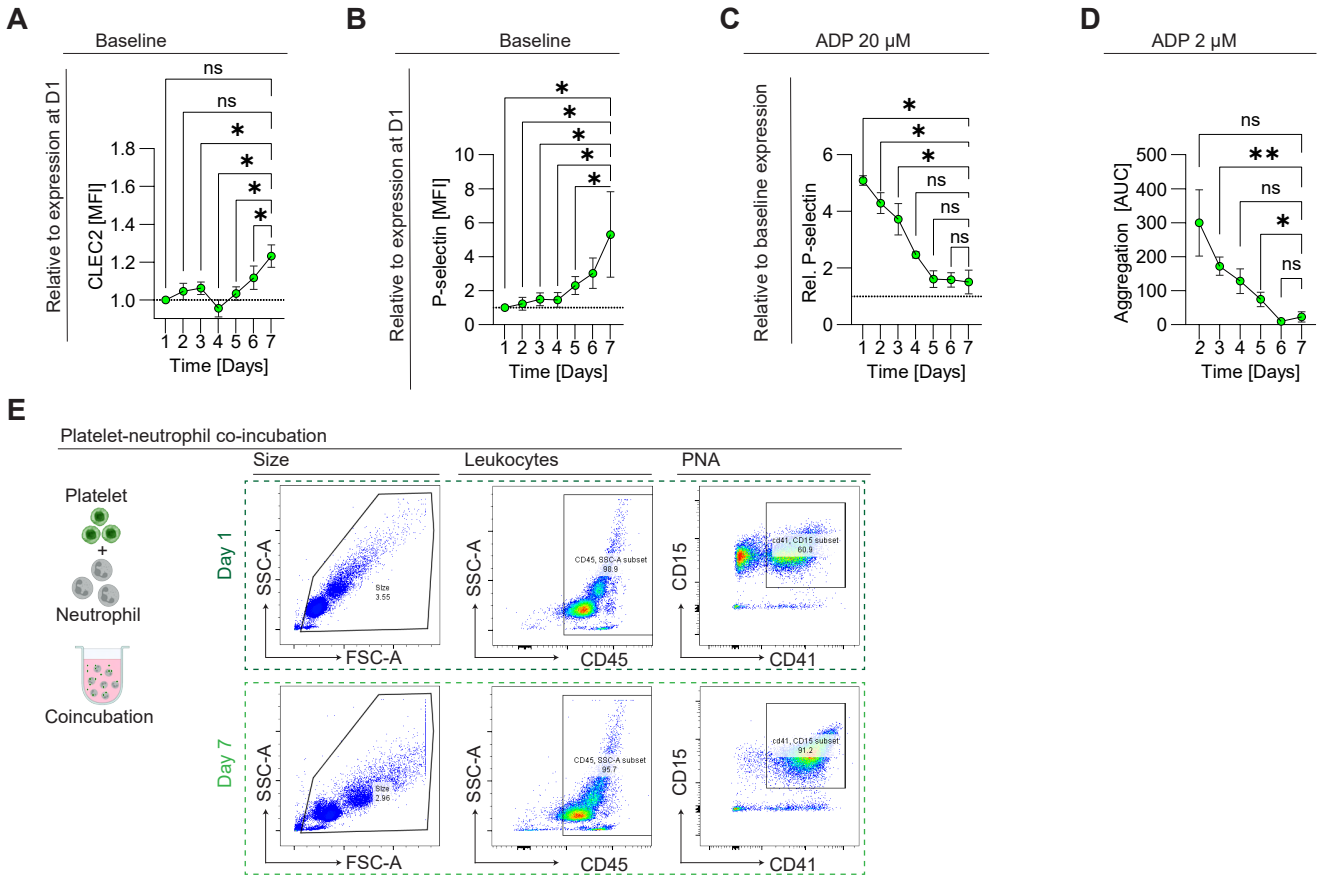

Suppl. Figure 11: Proinflammatory effect of in vitro aged murine platelets

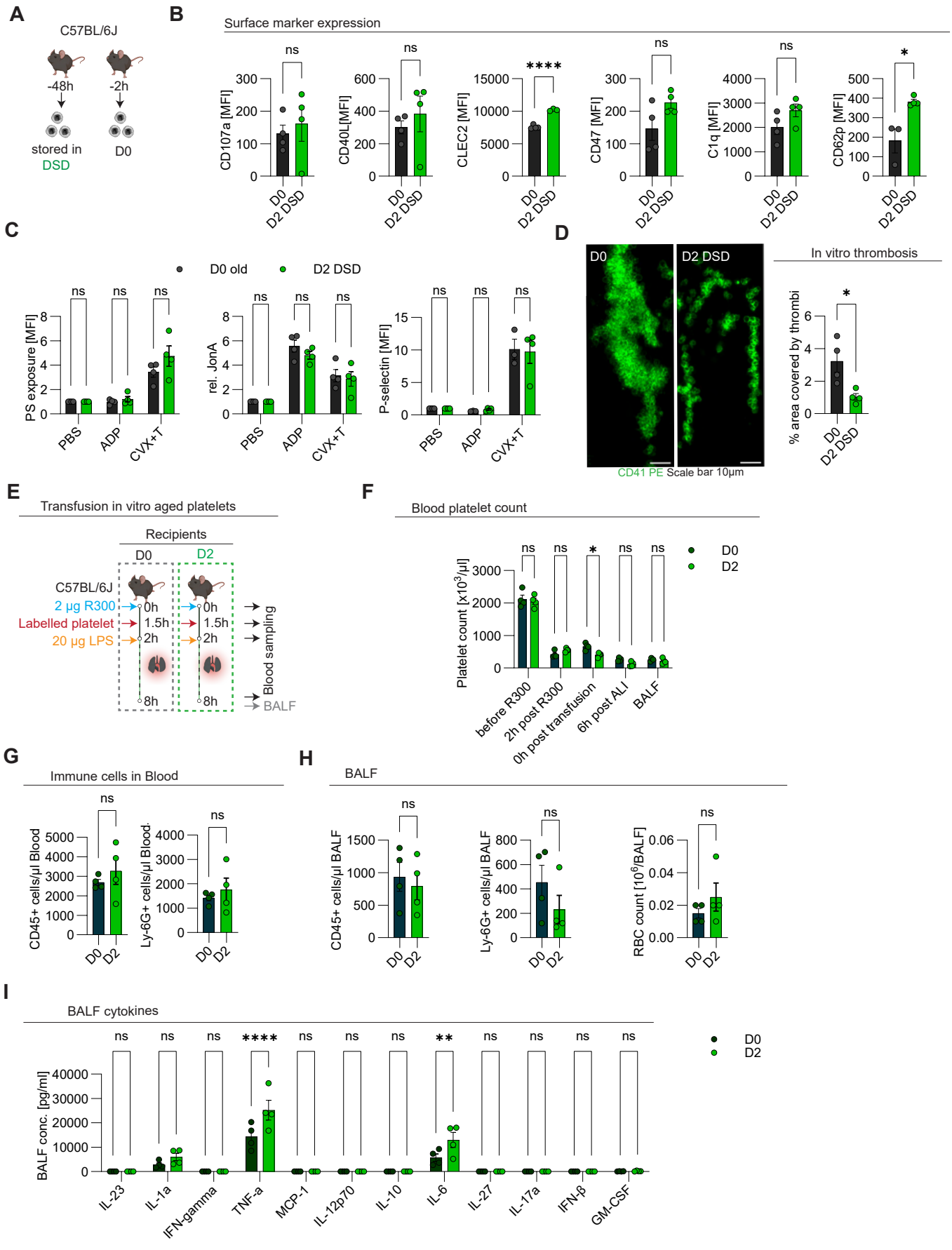

Part VI

Paper II

blood®
Regular Article

PLATELETS AND THROMBOPOIESIS

Procoagulant platelet sentinels prevent inflammatory bleeding through GPIIBIIIA and GPVI

Rainer Kaiser,[1,2] Raphael Escaig,[1,2] Jan Kranich,[3] Marie-Louise Hoffknecht,[1] Afra Anjum,[1,2] Vivien Polewka,[1] Magdalena Mader,[1,2] Wenbo Hu,[3] Larissa Belz,[1] Christoph Gold,[1,2] Anna Titova,[1] Michael Lorenz,[1] Kami Pekayvaz,[1,2] Stefan Kääb,[1,2] Florian Gaertner,[1,2] Konstantin Stark,[1,2] Thomas Brocker,[3] Steffen Massberg,[1,2] and Leo Nicolai[1,2]

[1]Medizinische Klinik und Poliklinik I, University Hospital, Ludwig-Maximilian University, Munich, Germany; [2]DZHK (German Center for Cardiovascular Research), partner site Munich Heart Alliance, Munich, Germany; and [3]Institute for Immunology, Biomedical Center, Medical Faculty, Ludwig-Maximilian University, Munich, Planegg-Martinsried, Germany

KEY POINTS

- **In inflammation, migrating platelets become procoagulant to recruit the coagulation cascade and prevent pulmonary inflammatory bleeding.**
- **Mechanosensitive GPIIBIIIA/Gα13 and GPVI signaling initiate CypD- and TMEM16F-dependent procoagulant activation of migrating platelets.**

Impairment of vascular integrity is a hallmark of inflammatory diseases. We recently reported that single immune-responsive platelets migrate and reposition themselves to sites of vascular injury to prevent bleeding. However, it remains unclear how single platelets preserve vascular integrity once encountering endothelial breaches. Here we demonstrate by intravital microscopy combined with genetic mouse models that procoagulant activation (PA) of single platelets and subsequent recruitment of the coagulation cascade are crucial for the prevention of inflammatory bleeding. Using a novel lactadherin-based compound, we detect phosphatidylserine (PS)-positive procoagulant platelets in the inflamed vasculature. We identify exposed collagen as the central trigger arresting platelets and initiating subsequent PA in a CypD- and TMEM16F-dependent manner both in vivo and in vitro. Platelet PA promotes binding of the prothrombinase complex to the platelet membrane, greatly enhancing thrombin activity and resulting in fibrin formation. PA of migrating platelets is initiated by costimulation via integrin αIIbβ3 (GPIIBIIIA)/$G\alpha_{13}$-mediated outside-in signaling and glycoprotein VI signaling, leading to an above-threshold intracellular calcium release. This effectively targets the coagulation cascade to breaches of vascular integrity identified by patrolling platelets. Platelet-specific genetic loss of either CypD or TMEM16F as well as combined blockade of platelet GPIIBIIIA and glycoprotein VI reduce platelet PA in vivo and aggravate pulmonary inflammatory hemorrhage. Our findings illustrate a novel role of procoagulant platelets in the prevention of inflammatory bleeding and provide evidence that PA of patrolling platelet sentinels effectively targets and confines activation of coagulation to breaches of vascular integrity.

Introduction

Platelets, the second most abundant cell type in peripheral blood, preserve integrity of the injured vessel wall by forming hemostatic clots but also contribute to occlusive thrombus formation, causing ischemia and organ damage.[1] Evidence has emerged that platelets are important beyond classical thrombosis and hemostasis and are uniquely positioned at the nexus of the vascular immune response.[2-4] Platelets exert a plethora of important functions in inflammatory conditions, including the recruitment and activation of blood leukocytes into inflamed tissue,[5-7] the scavenging and killing of microorganisms to prevent pathogen spreading,[8-10] and antigen presentation to adaptive immune cells.[11-13] Upon systemic dysregulation of the inflammatory response, platelet response and activating potential may, however, be detrimental to the host. Recent work has established platelets as prothrombotic and proinflammatory drivers of COVID-19, promoting disseminated clot formation through degranulation as well as neutrophil recruitment, hyperactivation, and neutrophil extracellular trap formation in severely affected patients.[14-16] Interestingly, platelets recruited in inflammation use receptors, pathways, and effector functions that are at least in part distinct from those operating during classical thrombosis and hemostasis, underlining the importance of understanding these processes in greater detail.[10]

One hallmark of inflammation is increased vessel permeability and predisposition for microbleeds. Inflammatory bleeding occurs in tissues that possess a vast network of microcirculation, such as the skin, gastrointestinal mucosa, and lung,[17] and most frequently affects critically ill patients who require intensive care treatment.[18-20] Interestingly, inflammatory bleeding is mainly attributed to neutrophil transmigration through inflamed endothelium, subsequent generation of microvascular defects, and ensuing leakage of plasma contents and red blood cells (RBCs).[17,21-24] Recently, we showed that immune-responsive platelets use cytoskeletal

protrusions to sense and migrate along adhesive gradients.[8] Platelets use their migratory capacity to reposition themselves to sites of vascular injury and leukocyte diapedesis, where they prevent neutrophil-induced microbleeds and bacterial dissemination alike.[8] We provided evidence that loss of the ability to migrate aggravated both pulmonary and microvascular hemorrhage in models of lipopolysaccharide (LPS)-induced inflammation. However, the mechanisms by which single platelets plug the endothelial holes left behind by transmigrating neutrophils remain insufficiently understood.[17] Studies have revealed considerable heterogeneity as well as redundancy in platelet receptors necessary to prevent inflammatory bleeding, with variety depending on both injury type and vascular bed.[22,25-28] Under specific inflammatory conditions, platelet secretion and release of angiopoetin-1 can enhance local vascular integrity.[27,29] However, the importance of plasmatic coagulation factors and the mechanisms that aid platelets in inflammatory hemostasis remain elusive.

Here, we show that blockade of plasmatic coagulation through factor II or X inhibition aggravates alveolar inflammatory bleeding. In the inflamed mesenteric vasculature, we detect fibrin(ogen)- and phosphatidylserine (PS)-positive platelets, a hallmark of platelet procoagulant activation (PA). These procoagulant platelets, which we visualize using a novel, highly sensitive PS-binding agent,[30] bind clotting factors to locally build up microthrombi that prevent inflammatory bleeding. Genetic ablation of procoagulant platelet activation by targeting mitochondrial cyclophilin D (CypD) or membrane scramblase TMEM16F exacerbates inflammatory hemorrhage in the lung without affecting leukocyte transmigration and, specifically, neutrophil recruitment. We show that encounter of subendothelial collagen triggers arrest of migrating platelets and initiates a procoagulant response both in vitro and in vivo. This effect involves costimulation via integrin αIIbβ3 (GPIIBIIIA)/$G\alpha_{13}$-mediated outside-in signaling and glycoprotein VI (GPVI) signaling, leading to an above-threshold intracellular calcium release. Targeting $G\alpha_{13}$ and blocking GPVI or GPVI-associated downstream kinases in migrating platelets reduce platelet calcium peaks and PA. Finally, we confirm that combined pharmacological targeting of GPIIBIIIA and GPVI reduces platelet PA in vivo and exacerbates alveolar hemorrhage.

Methods

Detailed methodology is provided in the supplemental Data (available on the *Blood* Web site).

Generation of fibrin(ogen), albumin, and collagen surfaces

Custom-made chambers for coating with fibrin(ogen), albumin, and collagen were generated as previously described.[8,9] In brief, coverslips (no. 1.5, D263T; Nexterion) were washed with 20% HNO_3, rinsed with clean H_2O for 1 hour each, subsequently air-dried and silanized with HMDS (Sigma) by spin coating for 30 seconds at 80 revolutions/sec. Ibidi sticky slide plastic channels ($VI^{0.4}$, #80608) were subsequently attached to the silanized coverslip. Coverslips were then coated with 37.5 μg/mL AF-conjugated or unconjugated fibrinogen, 0.2% human serum albumin, and/or Horm collagen I (25 μg/mL) solved in modified Tyrode's buffer (pH 7.2) for 15 minutes at room temperature. Fibrin surfaces were generated by addition of thrombin (1 U/mL), calcium (1 mM), and platelet-poor plasma. For some experiments, commercial flow chambers were coated with fibrinogen, collagen I, or a mixture without previous washing steps (Ibidi $VI^{0.4}$ ibitreat slides, #80606).

Acute lung injury model

Subacute lung injury models were performed as described previously.[8] In brief, mice were anesthetized, and 20 μg of *Escherichia coli*-derived LPS (O111:B4; Sigma) was applied intranasally. Anesthesia was antagonized immediately. In some experiments, mice received anticoagulants or platelet inhibitors by intravenous or subcutaneous injection: GPIIBIIIA inhibitor tirofiban (0.5 mg/kg body weight [BW]), factor Xa inhibitors rivaroxaban (3 mg/kg BW), and enoxaparin (10 mg/kg BW subcutaneously) or factor IIa inhibitor argatroban (5 mg/kg BW). For compounds with a short half-life, injections were repeated 4 and 8 hours after LPS application. Twenty-four hours after LPS treatment, mice were euthanized by cervical dislocation. Bronchoalveolar lavage (BAL) fluid was collected by intratracheal flushing with 2 × 1 mL 1% BSA containing 2 mM EDTA. Subsequently, aliquots of BAL fluids (BALF) were stained with antibodies and analyzed by flow cytometry or sonicated to assess hemoglobin content by fluorescence absorption using a Tecan Infinite F200 plate reader (405 nm). Buffer-only containing wells were used to normalize samples against background absorbance. BALF was only included in the analysis if at least half of the applied volume was recovered (>1 mL). In some animals, instead collecting BALF, lungs and abdominal organs were surgically removed, fixated in 4% PFA for 1 hour, dehydrated in 30% sucrose overnight, and cryoembedded. Histopathological staining and analyses are described in the supplemental Data.

Mesentery live imaging

Animals were injected with 1 mg/kg BW of LPS intraperitoneally. After 2 hours, mice were anesthetized, and antibodies against Gp1b on platelets (X488 or X649, emfret, 20 μg) or Ly6G on neutrophils (Ly6G, clone 1A8, 4 μg; Biolegend) as well as Annexin V-AF649 or Annexin V-FITC (50-80 μL corresponding to approximately 10-15 μg [batch-dependent concentration], Biolegend) or C1 multimer-AF649 (15 μL corresponding to 7 μg; mC1 multimers are commercially available through Biolegend as Apotracker Tetra reagents) were injected via the tail vein. In some experiments, 80 μg of fibrinogen-AF546 conjugate was injected intravenously. After ensuring adequate analgesia, laparotomy was performed, and the bowel was exteriorized and placed on a prewarmed glass cover slip. Mesenteric vessels were subsequently exposed on the coverslip. Tissue paper prewet with 37°C warm phosphate-buffered saline was used to fixate the exposed bowel in place. Imaging was performed using a Zeiss LSM 880 confocal microscope in either AiryScan Fast mode or AiryScan Superresolution mode.

Results

Both thrombocytopenia and anticoagulation aggravate inflammatory bleeding

Platelets are crucial for preventing leukocyte diapedesis-inflicted microbleeding in inflammation. Pulmonary LPS challenge induced alveolar neutrophil recruitment and subsequent hemorrhage, resulting in a proinflammatory cytokine signature in the lung (supplemental Figure 1A-D). Confirming previous findings,[24] antibody-induced thrombocytopenia aggravated pulmonary bleeding in our model of LPS-induced lung injury (Figure 1A-B). Alveolar hemorrhage in thrombocytopenic animals was severe

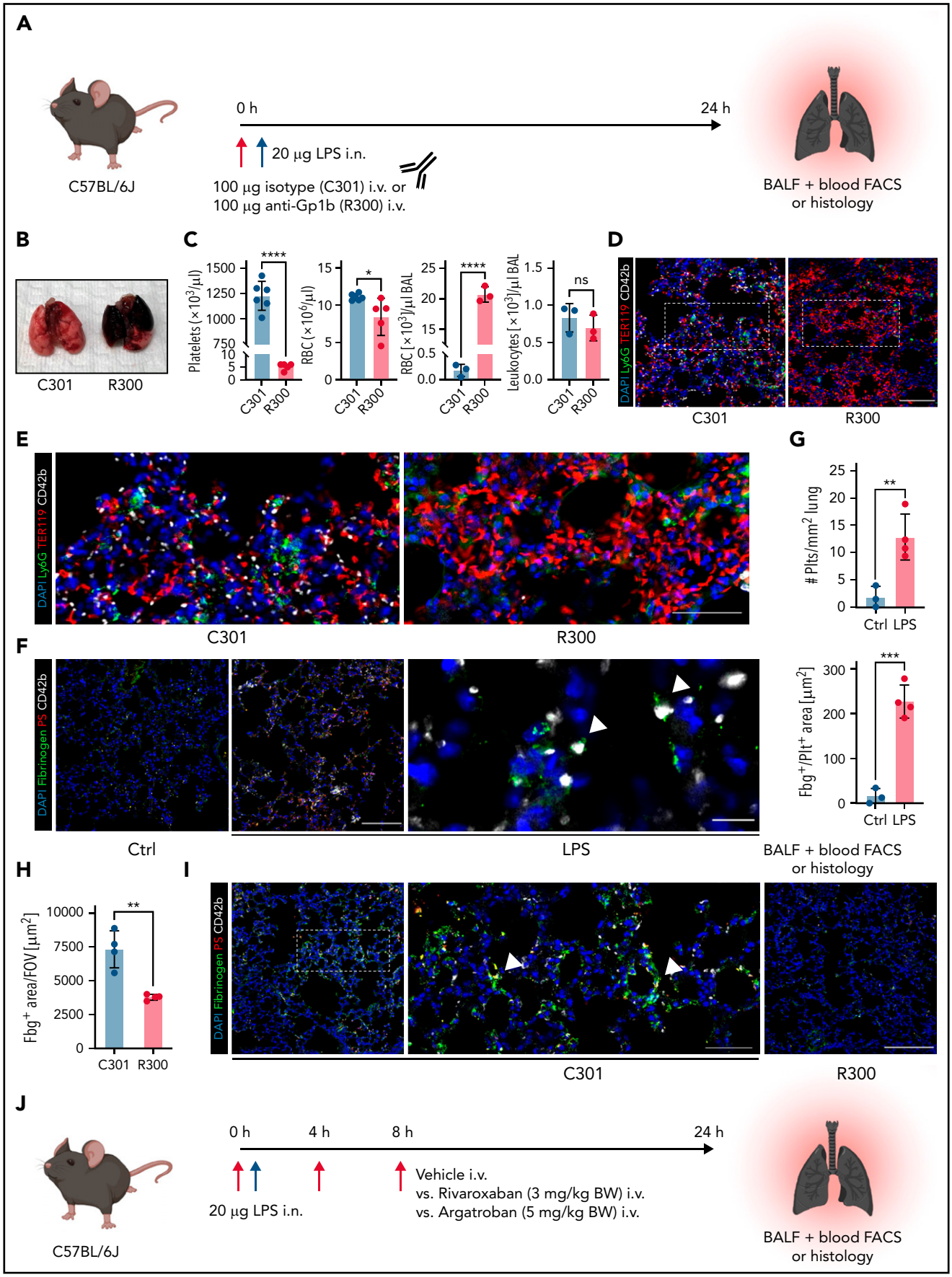

Figure 1.

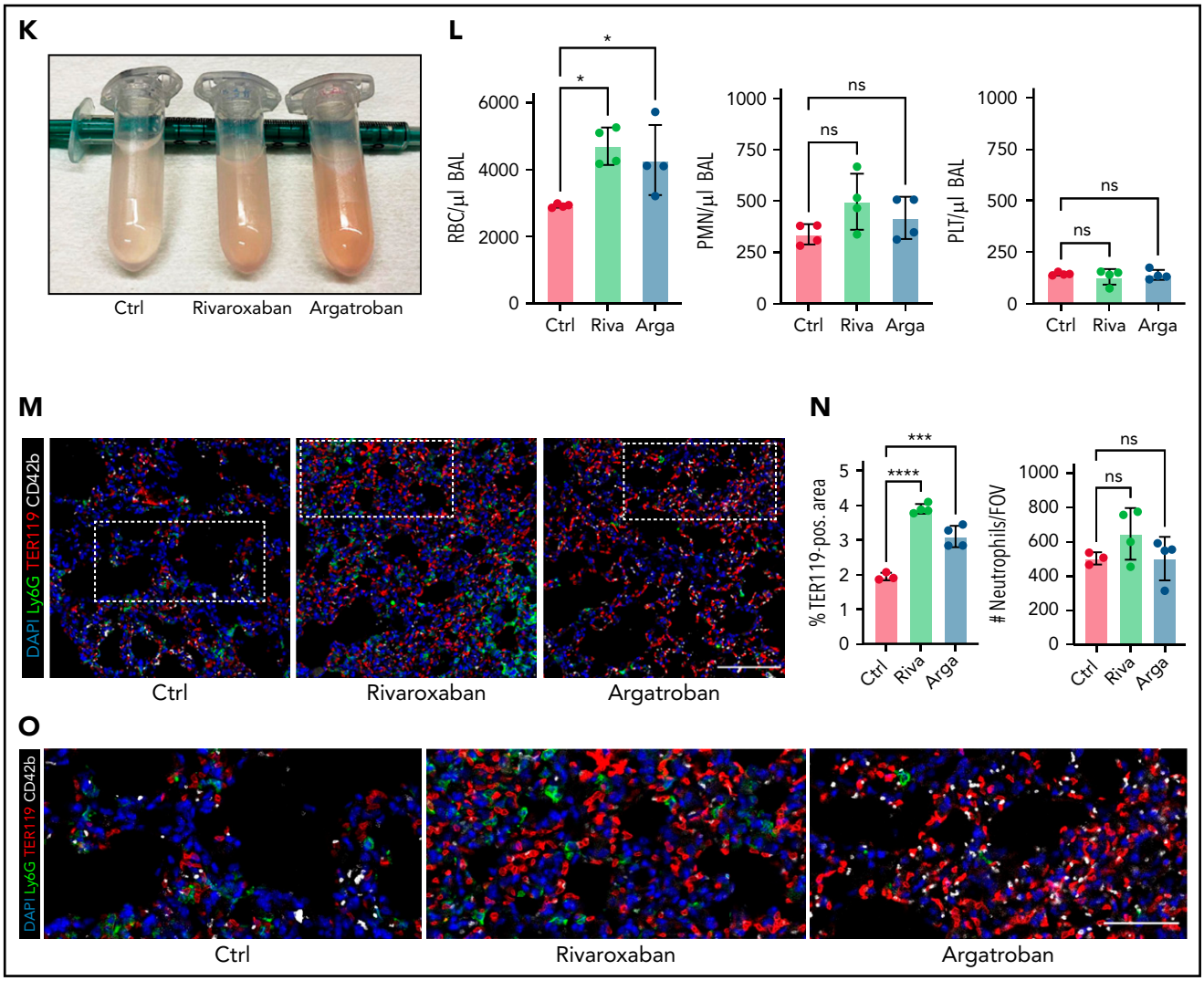

Figure 1 (continued) Both thrombocytopenia and anticoagulation aggravate inflammatory bleeding. (A) Experimental scheme of subacute lung injury model with or without antibody-mediated platelet depletion. The red arrow indicates antibody administration; the blue arrow indicates intranasal LPS administration. (B) Representative macroscopic images of lungs from control (C301) and thrombocytopenic animals (R300 treatment) 24 hours after LPS challenge. (C) Flow cytometric analysis of peripheral blood (platelet and RBC count) and BALF (RBC and leukocyte count/µL BALF). Student's *t* test, two-tailed, unpaired. (D) Representative micrographs of immunofluorescence stainings of alveolar hemorrhage in control (C301) and thrombocytopenic animals (R300). Bar represents 100 µm. (E) Magnified excerpts of representative micrographs, corresponding to white rectangles in Figure 1D. Bar represents 50 µm. (F) Representative images of immunofluorescence stainings of lungs from control (Ctrl) or septic animals (*E. coli*–derived LPS 1 mg/kg BW intraperitoneally). Bar represents 100 µm (left and mid panel) and 20 µm (right panel). White arrowheads indicate fibrin(ogen)-positive platelets. Red: anti-PS antibody (Merck). (G) Quantification of fibrinogen deposition and overlap of fibrinogen/platelet positive areas. n = 3 to 4 mice per group. Student's *t* test, two-tailed, unpaired. (H) Quantification of fibrinogen deposition in lungs from septic control (C301) and platelet-depleted animals (R300) per field of view (FOV). n = 4 mice per group. Student's *t* test, two-tailed, unpaired. (I) Representative micrographs of control (C301) and platelet-depleted mice (R300), referring to (H). Bar represents 200 µm (left and right panels). Magnified excerpt (middle; bar represents 20 µm) corresponds to the white rectangle of the left panel. Red: anti-PS antibody (Merck). (J) Experimental scheme of (sub)acute lung injury. Bl6 mice were treated with 20 µg of LPS intranasally (blue arrow) and intravenously injected with vehicle or rivaroxaban (3 mg/kg BW) right before and 8 hours after challenge or argatroban (5 mg/kg BW) right before and 4 and 8 hours after challenge; rivaroxaban-treated animals received vehicle injections at 4 hours after challenge (red arrows indicate timing of intravenous injections). (K) Representative macroscopic image of BALF derived from 1 simultaneously performed set of experimental groups, collected in 2 mL Eppendorf tubes. The right tube corresponds to the maximum bleeding observed in argatroban-treated animals. (L) Flow-cytometric assessment of BALF (RBC, polymorphonuclear, and PLT counts/µL BALF). One-way analysis of variance (ANOVA) with Holm-Šídák's multiple comparisons test compared with control groups. (M) Representative images of immunofluorescence stainings of lung slices from different experimental groups. Bar represents 100 µm. (N) Quantification of alveolar hemorrhage ($TER119^+$ area) and neutrophil recruitment. n = 3 to 4 mice/group. One-way ANOVA with Holm-Šídák's multiple comparisons test compared with control groups. (O) Magnified excerpts of representative micrographs, corresponding to white rectangles in Figure 1M. Bar represents 50 µm.

enough to cause anemia in some animals (Figure 1C) but did not cause alterations in pulmonary leukocyte recruitment (Figure 1C-E; supplemental Figure 1E).

We and others have shown that single platelets promote vascular homeostasis in the setting of inflammation, ensuring the effective sealing of transendothelial migration sites.[8,17,21,22,31] Recently, we demonstrated that migration and haptotaxis are essential for vasculoprotective effects of single platelets in microvascular inflammation of both the lung and skeletal muscles.[8] To understand how platelets prevent inflammatory bleeding once positioned at extravasation sites, we studied platelets in the inflamed lung using high-resolution immunofluorescence-based imaging of lung slices (Figure 1F). Recruited

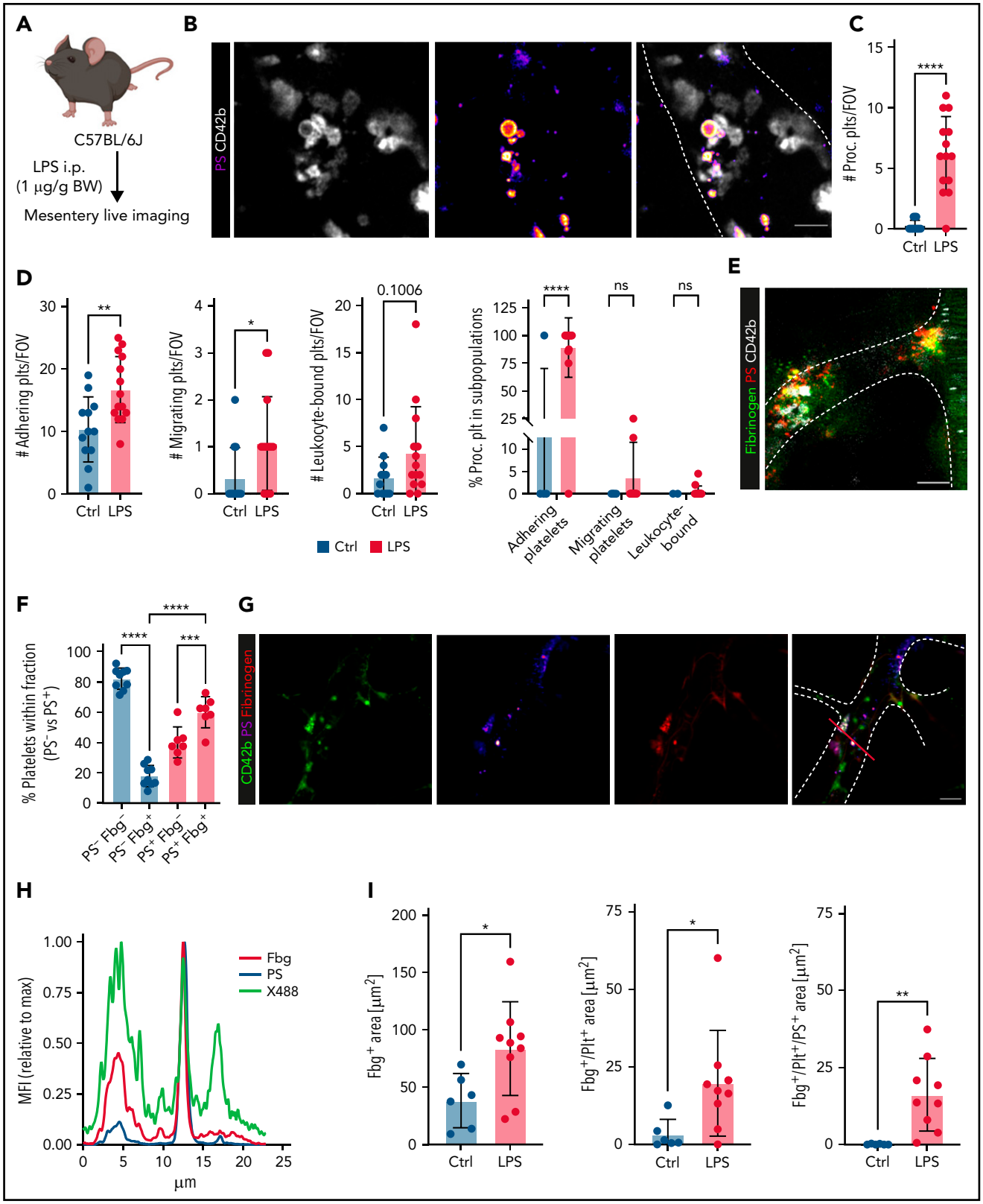

Figure 2. Procoagulant platelets are induced by inflammation in vivo. (A) Experimental scheme of peritoneal sepsis and mesenteric live imaging. (B) Representative images derived from 4-dimensional (4D) live microscopy of mesentery venules. Dotted lines indicate vessel walls. Bar represents 5 µm. PS staining agent: mC1. (C) Quantification of procoagulant platelets in mesenteric venules of sham- or LPS-treated Bl6 mice. Student's *t* test, two-tailed, unpaired. (D) Analysis of motility patterns and quantification of procoagulant platelet content in different motility subgroups in sham- or LPS-treated animals. Student's *t* test, two-tailed, unpaired. (E) Example image derived from 4D live microscopy of mesentery venules. Yellow signal indicates overlap between phosphatidylserine (PS, mC1) and fibrinogen. Dotted lines indicate vessel walls. Bar represents 10 µm. (F) Quantification of fibrinogen-binding behavior of non-procoagulant (PS^-, blue) and procoagulant platelets (PS^+, red) from live imaging data (n = 4 LPS-treated mice; n = 2-3 videos per mouse). Data are shown as % of all platelets of the respective subset. One-way ANOVA. (G-H) Example image derived from 4D live microscopy of mesentery venules revealing PS^+, fibrinogen-binding adherent platelets. Dotted lines indicate vessel walls. The red line corresponds to the plot profiles for expression of fibrinogen, PS and CD42b (X488) as shown in (H). PS staining agent: mC1. Bar represents 20 µm. (I) Absolute quantification of the area of Fbg, Fbg/CD42b, and Fbg/CD42b/PS overlap in sham- or LPS-injected mice (n = 3-4 mice per condition; n = 2-3 videos per mouse). Student's *t* test, two-tailed, unpaired.

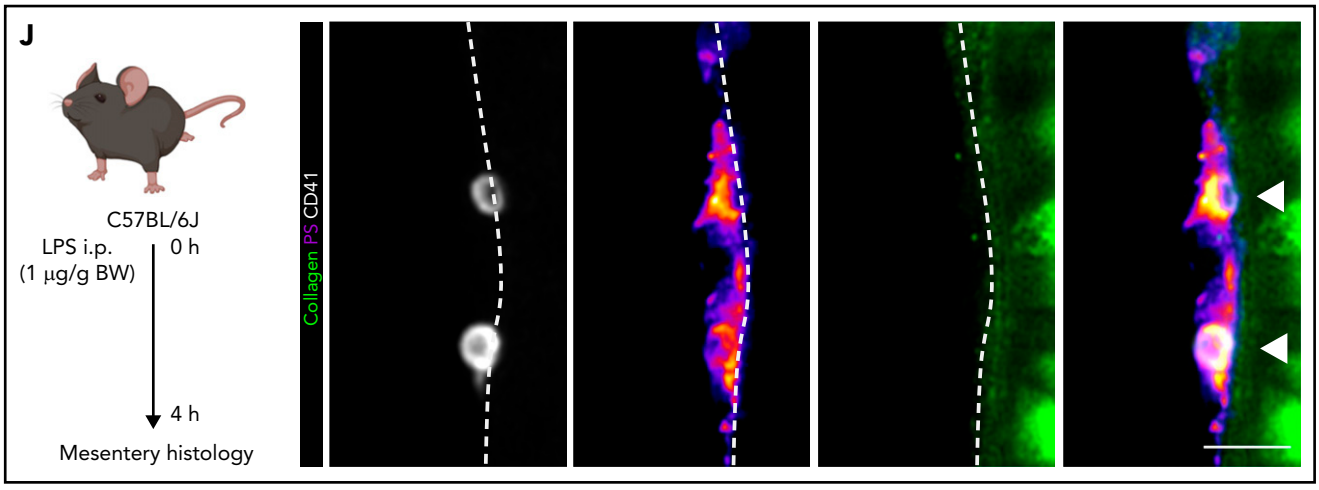

Figure 2 (continued) (J) Experimental scheme and representative immunofluorescence images of mesenteric venules after 4 hours of LPS intraperitoneal injection. White arrowheads indicate procoagulant platelets (CD41/GPIIBIIIA-positive, PS-positive) in close proximity to antibody-stained collagen fibers (green). Bar represents 5 µm. PS staining agent: anti-PS antibody. Refer to supplemental Figure 2N for overview images.

platelets stained positive for fibrin(ogen), with evidence of fibrin fibers associated with platelets (Figure 1F). Accordingly, platelet recruitment and platelet fibrin(ogen) association were enhanced under inflammatory conditions (Figure 1F-G). Fibrin(ogen) deposition in the inflamed lung was markedly reduced in platelet-depleted septic animals (Figure 1H-I), suggesting close interplay of platelets and coagulation.

To assess whether plasmatic coagulation cascades and downstream fibrin formation contribute to prevention of inflammatory bleeding, we treated Bl6 mice with the clinically approved factor IIa or factor Xa antagonists argatroban, enoxaparin, or rivaroxaban, respectively, and subsequently challenged them with LPS intranasally (Figure 1J; supplemental Figure 1F-J). Treatment with both factor IIa and Xa inhibitors aggravated alveolar hemorrhage, as assessed by flow cytometry of bronchoalveolar lavage (BAL) fluid (Figure 1K-L; supplemental Figure 1F-I). Notably, peripheral platelet and leukocyte counts as well as platelet-neutrophil aggregate (PNA) formation were not affected by treatment (supplemental Figure 1J). Histopathological analysis of LPS-challenged lungs confirmed a significant increase in alveolar hemorrhage in mice that had received argatroban, enoxaparin, or rivaroxaban (Figure 1M-O; supplemental Figure 1K-M). In contrast, alveolar leukocyte recruitment did not differ between treatment groups, suggesting that anticoagulation does not interfere with transendothelial migration and that the observed effect was not due to increased neutrophil diapedesis (Figure 1L-O; supplemental Figure 1K-M). Treatment of isolated platelets with either inhibitor did not affect their ability to migrate in vitro, emphasizing that the observed increase in bleeding was not due to loss of migratory capacity (supplemental Figure 1N-O). These findings suggest an essential, possibly platelet-dependent role for plasmatic coagulation in preventing inflammatory bleeding in the lung.

Inflammation induces single procoagulant platelets that form fibrin(ogen)-positive microthrombi in vivo

Platelets promote coagulation by turning procoagulant through exposure of PS and by binding of prothrombinase complex on their membranes, boosting local thrombin generation.[32,33] Procoagulant platelet activation occurs upon dual stimulation with strong agonists and can be augmented by mechanical stress such as locally increased shear,[32-36] but the impact of systemic factors and inflammation are unknown. We have recently described the generation of a novel, lactadherin-based compound for the detection of PS, the key marker for procoagulant platelets.[30] Here, we used biotinylated murine lactadherin C1 domains multimerized using Streptavidin (C1) and found that this compound sensitively and accurately detected PS^+ platelets at lower concentrations than annexin V (supplemental Figure 2A-E) in vitro.[30] To investigate whether local procoagulant platelet activation occurs under inflammatory conditions in vivo, we performed 4-dimensional live imaging of mesenteric postcapillary venules after intraperitoneal LPS injection (Figure 2A). Intravenous injection of C1 or Annexin V revealed hardly any PS^+ platelets in control mice, but readily detected PS^+ platelet balloons bound to the inflamed vessel wall of mesenteric venules in septic animals (Figure 2B-C; supplemental Video 1; supplemental Figure 2F).

Analysis of motility patterns of platelets in sham- vs LPS-treated animals revealed significant increases in adhering, migrating, and, specifically, procoagulant platelets (Figure 2C-D). Migrating platelets remained stationary once they turned procoagulant (Figure 2D; supplemental Video 1; supplemental Figure 2F). Most adherent, stationary procoagulant platelets were found to be fibrin(ogen)-positive (Figure 2E-F). In line, inflammation-associated deposition of fibrin(ogen) along the endothelial lumen was pronounced in regions were procoagulant platelets were binding (Figure 2G-I). Confirming these observations, most fibrin(ogen)-positive platelets in the inflamed lung were found to be procoagulant (supplemental Figure 2G).

Previous studies have established that the peritoneum is not a major site of inflammatory bleeding, even though thrombocytopenia does increase vascular permeability in peritonitis.[22,37] In thrombocytopenic animals, we found that LPS-induced peritonitis was associated with abdominal microbleeding (supplemental Figure 2H-M). Notably, thrombocytopenia also reduced intraperitoneal neutrophil recruitment, possibly explaining the relatively modest bleeding phenotype in platelet-depleted mice, which

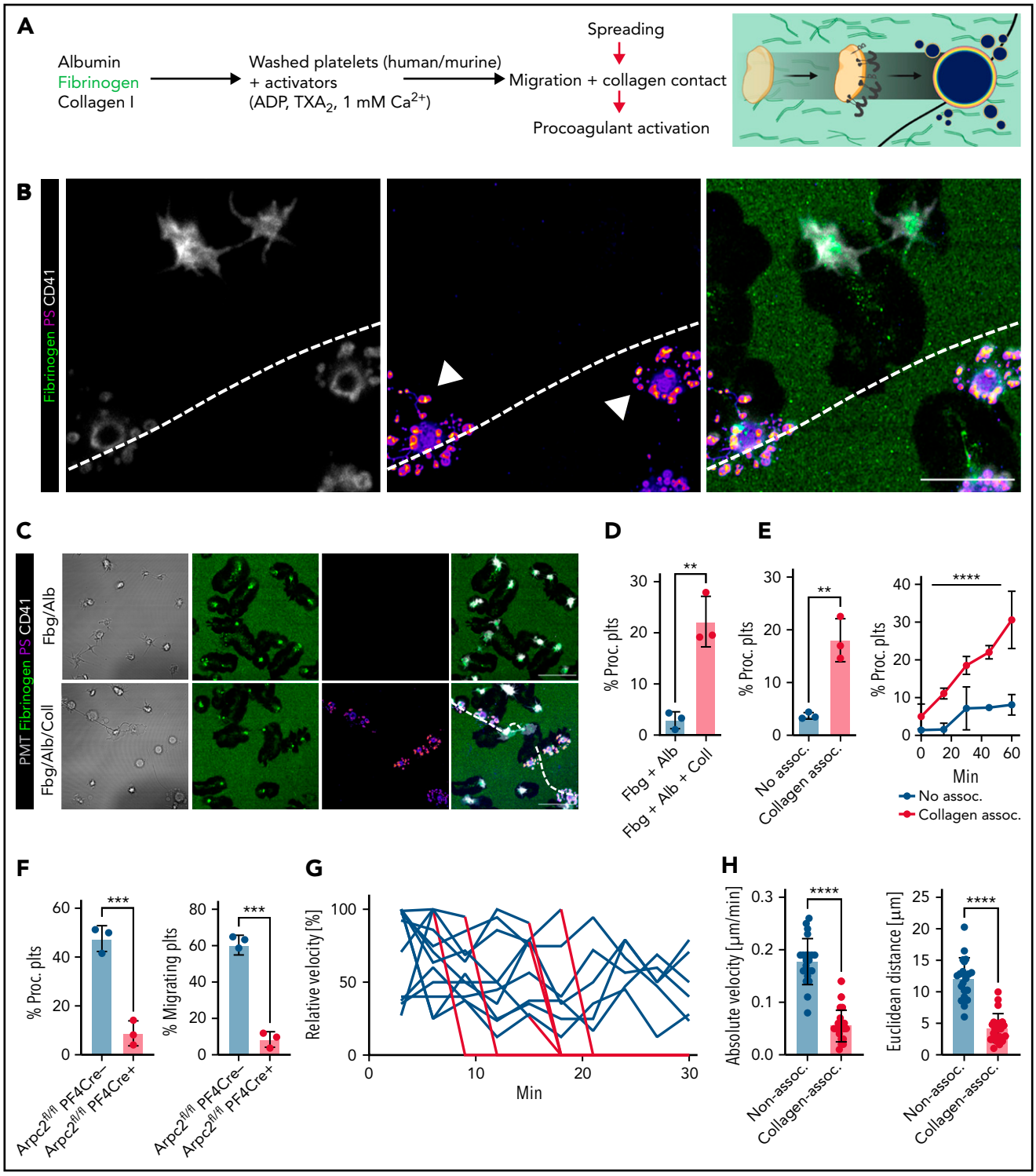

Figure 3. Migrating platelets turn procoagulant upon sensing collagen. (A) Experimental setup of hybrid matrices mimicking the inflamed endothelium, with black lines corresponding to collagen fibers. (B) Representative confocal micrograph of human migrating platelets (CD41, white) with or without contact to collagen fibers. White arrowheads indicate procoagulant platelet formation with PS positivity (mC1) and secretion of microvesicles after sensing collagen; dashed white lines indicate collagen fibers. Bar represents 10 µm. (C-E) Representative micrographs of human platelets migrating on an albumin/fibrinogen matrix (upper panel) or a hybrid matrix containing albumin, fibrinogen, and collagen I (lower panel, dashed white lines). Quantification of procoagulant platelet activation on the respective matrix of freely migrating vs collagen-sensing platelets after 45 minutes (fixed time point) or over a period of 1 hour (time course experiment). PS staining agent: mC1. Bar represents 10 µm. Student's *t* test, two-tailed, unpaired; one-way ANOVA with Holm-Šídák's multiple comparisons test compared with t = 0 minutes for time course experiment (right panel, E). (F) Quantification of procoagulant platelet activation and migrating platelets of PF4cre-Arpc2$^{fl/fl}$ Cre-positive mice and Cre-negative littermates. Student's *t* test, two-tailed, unpaired. (G) Relative velocity plots of tracked human platelets from live-imaging data. Absolute velocities were normalized to peak velocity to allow for interplatelet comparisons. Blue lines indicate the onset of procoagulant platelet activation. (H) Quantification of absolute velocity and Euclidean distance of migrating human platelets from live-imaging data. Individual dots represent n = 3 individuals per experimental group, with n > 30 individual platelets analyzed per n. Student's *t* test, two-tailed, unpaired.

was not significantly affected by neutrophil depletion (supplemental Figure 2H-K).[22]

The factors that induce platelet PA in inflammation are unknown. When staining mesenteric vessels for procoagulant platelets, we frequently found single PS^+ and fibrin(ogen)$^+$ procoagulant platelets in close association with the collagen-positive subendothelial matrix in septic mice (Figure 2J; supplemental Figure 2N). This was in part dependent on immune cell recruitment because neutrophil-depleted LPS-treated animals exhibited reduced intravascular fibrin(ogen) depositions (supplemental Figure 2M). We therefore hypothesized that exposure of subendothelial matrix proteins upon transendothelial leukocyte migration and inflammation-mediated vascular injury would lead to procoagulant activation and arrest of migrating platelets.

Migrating platelets turn procoagulant upon sensing collagen

To reconstruct the inflammatory microenvironment in vitro, we designed a hybrid substrate consisting of albumin, fibrinogen, and collagen I fibers, mimicking exposure to extracellular matrix proteins observed in severe inflammatory endotheliopathy (Figure 3A).[17] When encountering collagen fibers, the characteristic half moon–like shape of migrating platelets was rapidly replaced by a balloon-like morphology with extensive microvesicle formation and PS exposure (Figure 3B), known hallmarks of procoagulant platelets.[32,33] PA of migrating platelets was specific to sensing collagen fibers because migrating platelets that did not encounter collagen fibers barely adopted a procoagulant phenotype (Figure 3C-E). In line, actin-related protein 2/3 complex subunit 2 (Arpc2)-deficient platelets, which are unable to migrate,[8,9] showed significantly lower PA levels compared with platelets from Cre-negative littermates when adhering to the hybrid substrate. However, they retained their procoagulant potential when exposed to purified collagen fibers or soluble agonists (Figure 3F; supplemental Figure 3A-C). In addition to morphological changes, relative and absolute velocity as well as migration distance of human platelets that had become procoagulant decreased significantly, essentially arresting them at the site of collagen encounter (Figure 3G-H). Exposure of mouse platelets to collagen fibers in solution did not provoke procoagulant activity or fibrin(ogen) binding, underlining a role for mechanosensing (supplemental Figure 3D-F). In contrast to published assays using platelets in suspension, procoagulant function of migrating platelets was independent of the presence of soluble agonists in our assay.[38,39] Clinically used antiplatelet drugs such as terutroban, cangrelor, and vorapaxar, which inhibit thromboxane, ADP receptor P2Y12, and protease-activated receptor 1 (PAR1), respectively, did not affect migratory capacity or platelet PA in vitro (supplemental Figure 3G). Likewise, inhibition of PAR4, previously shown to affect platelet PA during human thrombus formation,[40] or simultaneous inhibition of PAR1 and PAR4 had no effect (supplemental Figure 3H). Given the proximity of procoagulant platelets and both intravascular and pulmonary fibrin(ogen) observed in vivo, we investigated the contribution of PA-associated secretion of fibrin(ogen)-containing α-granules. In vitro, we did not observe substantial endogenous fibrin(ogen) secretion around migrating or procoagulant platelets, suggesting that deposited fibrin(ogen) originates from other sources (supplemental Figure 3I-J).

Cyclophilin D (CypD) and transmembrane protein 16F (TMEM16F) are central drivers of platelet PA. While CypD promotes mitochondrial depolarization and supramaximal intracellular calcium bursts, TMEM16F mediates platelet PS exposure.[33,35,38,41-46] To genetically ablate procoagulant platelet activation, we generated transgenic mice with platelet- and megakaryocyte-specific knockouts of CypD (PF4cre-CypD$^{fl/fl}$) and TMEM16F (PF4cre-TMEM16F$^{fl/fl}$). Animal weight, peripheral platelet, RBCs, and leukocyte counts at baseline as well as expression of several key platelet receptors did not differ between Cre-positive and negative animals of either mouse line (supplemental Figure 4A-F). Tail bleeding experiments revealed no significant differences in bleeding time in either PF4cre-CypD$^{fl/fl}$ or -TMEM16F$^{fl/fl}$ animals, with TMEM16F-deficient mice exhibiting a nonsignificant trend toward longer time to hemostasis (supplemental Figure 4G-H). Arterial thrombus formation was impaired in both mouse lines when we injured the carotid endothelium using ferric chloride, confirming previous observations (supplemental Figure 4I-L).[39,47]

Combined exposure of isolated CypD- or TMEM16F-knockout platelets to strong agonists such as PAR agonist thrombin and GPVI agonist convulxin yielded significantly lower PS expression levels, consistent with reduced procoagulant potential in suspension for both mouse lines (Figure 4A-B; supplemental Figure 4C,F). Despite reduced PA, both CypD- and TMEM16F-deficient platelets retained migratory capacity (Figure 4C-D). As reported earlier,[47] CypD$^{-/-}$ and TMEM16F$^{-/-}$ platelets exerted intact degranulation and integrin activation, as measured by P-selectin and activated GPIIBIIIA expression, respectively (supplemental Figure 4B-C,E-F). When encountering collagen fibers, migrating TMEM16F knockout platelets exhibited a characteristic morphological phenotype with formation of string-like filopodia but were unable to form PS^+ balloons (Figure 4D; supplemental Figure 4M-N). In line with previous findings,[42] TMEM16F$^{-/-}$ platelets were incapable of releasing microvesicles (supplemental Figure 4M-N).

Pharmacological inhibition of CypD and TMEM16F using cyclosporin A and niflumic acid, respectively, significantly reduced PA of migrating mouse platelets without affecting migratory capacity (Figure 4E-F). We reproduced this observation when we inhibited CypD and TMEM16F in human platelets (Figure 4G). PS^+ platelets predominantly stained caspase-negative, pointing toward a procoagulant, not apoptotic phenotype (supplemental Figure 4O-P). However, we also observed single platelets positive for phosphatidylserine with signs of caspase activation, and treatment of migrating platelets with the pan-caspase inhibitor Q-VD-OPh reduced PA to some extent (supplemental Figure 4Q).[32,38,48]

To confirm that genetic ablation of either CypD or TMEM16F led not only to a decrease in platelet PA and PS exposure but also to a functional decline in procoagulant function, we incubated wild-type and knockout platelets with a fluorescent probe indicating thrombin turnover (Figure 4H). Loss of either protein led to decreased platelet PA and a significant decrease in thrombin turnover (Figure 4H-I; supplemental Figure 4R). We observed a reduced fraction of thrombin-positive procoagulant platelets specifically in procoagulant platelets derived from PF4cre-TMEM16F$^{fl/fl}$ mice, indicating that the inability to flip PS to the outer membrane layer also functionally reduces binding of coagulation factors (Figure 4I; supplemental Figure 4R). In summary, we show that immune-responsive platelets become procoagulant independent of soluble agonist stimulation upon

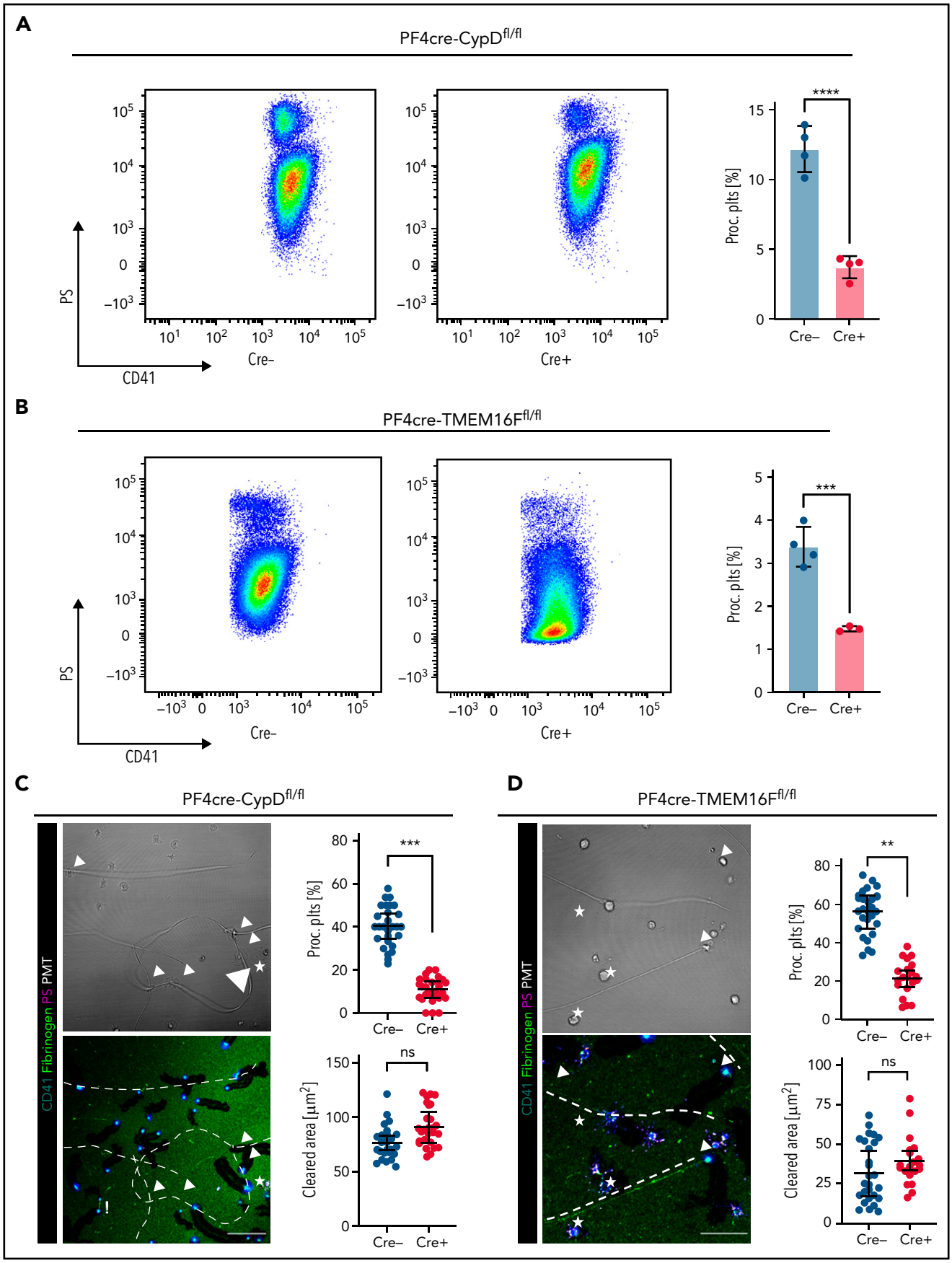

Figure 4. Genetic or pharmacological targeting of CypD and TMEM16F reduces procoagulant platelet activation without impairing migratory capacity. (A-B) Representative scatter plots and analyses derived from flow cytometric measurements of stimulated platelets from CypD- (A) or TMEM16F-knockout mice (B) (n = 3-4 mice per group). PS staining agent: mC1. Platelets were stimulated with thrombin (0.1 U/L) and convulxin (0.1 µg/mL) for 30 minutes at room temperature.

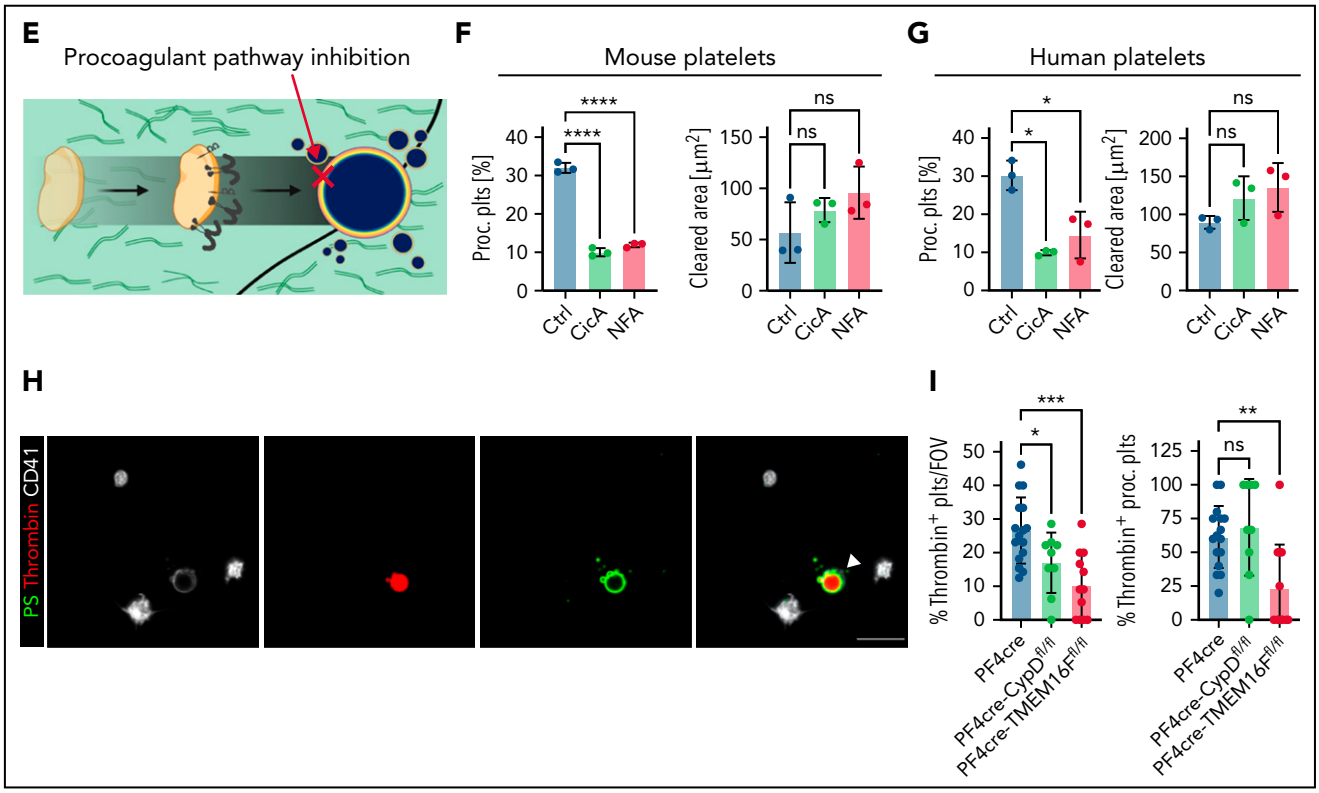

Figure 4 (continued) Student's *t* test, two-tailed, unpaired. (C-D) Representative micrographs of isolated murine platelets from platelet-specific CypD- (C) or TMEM16F- (D) knockout mice migrating on an albumin/fibrinogen/collagen I hybrid matrix. Quantification of platelet procoagulant activity and cleared area (as a surrogate for migration length) depicted as SuperPlots, with individual circles indicating individual images and the error bars corresponding to the mean data of 6 images of n = 3 to 4 mice per Cre-positive or -negative group. White dashed lines indicate collagen fibers. White arrowheads indicate migrating platelets with collagen contact but without procoagulant activity. White stars indicate procoagulant platelets. Bar represents 25 (left panel) and 15 µm (right panel). PS staining agent: mC1. Student's *t* test, two-tailed, unpaired. (E) Experimental scheme of migration assay on hybrid matrix with targeting of platelet PA-promoting pathways. (F-G) Quantification of procoagulant platelets and cleared area by murine (F) and human platelets (G) treated with inhibitors of CypD (cyclosporine A, CicA, 2 µM) or TMEM16F (niflumic acid [NFA] 10 µM). One-way ANOVA with Holm-Šídák's multiple comparisons test compared with control groups. (H) Representative images of migrating human platelets stained for CD41 and PS (mC1) and incubated with an internally quenched 5-FAM/QXL 520 FRET substrate indicating thrombin activity. White arrowhead indicates a procoagulant, thrombin-positive platelet. Bar represents 10 µm. See supplemental Figure 4R for detailed images. (I) Cell-based quantification of thrombin-positive cells/FOV and the fraction of thrombin-positive cells as percentage of procoagulant platelets. Per condition, >100 cells from at least n = 2 animals were analyzed. One-way ANOVA with Holm-Šídák's multiple comparisons test compared with control groups.

encountering collagen in vitro and the subendothelial matrix of inflamed vessels in vivo.

Genetic ablation of platelet PA aggravates inflammatory bleeding

Next, we hypothesized that platelets serve as motile sentinels targeting the coagulation cascade to sites of inflammatory injury, thereby preventing microbleeds. To study this, we performed acute lung injury experiments on both PF4cre-CypD$^{fl/fl}$ and PF4cre-TMEM16F$^{fl/fl}$ mouse lines. Platelet-specific genetic ablation of CypD aggravated alveolar hemorrhage 24 hours after LPS exposure (Figure 5A-C). This increase in pulmonary bleeding was not due to blunt vascular trauma, as shown by the low counts of single, non–leukocyte-bound platelets in bronchoalveolar lavage fluid (Figure 5C; supplemental Figure 5A-B). Neither peripheral platelet nor leukocyte counts were significantly altered after acute lung injury, excluding thrombocytopenia or leukocytosis as possible causes of increased pulmonary bleeding; the number of infiltrating neutrophils did not differ either (supplemental Figure 5A-B). Immunofluorescence stainings of LPS-challenged lungs confirmed a significant increase in alveolar hemorrhage in mice with CypD-deficient platelets, whereas neither pulmonary platelet nor neutrophil recruitment differed between genotypes (Figure 5D-F).

Pulmonary LPS exposure of PF4cre-TMEM16F$^{-/-}$ animals phenocopied the effects observed in CypD-deficient mice. Both flow cytometric and histological analysis of alveolar hemorrhage showed marked increases in pulmonary bleeding (Figure 5G-L). Free-floating platelets were hardly detected in BALF, whereas most infiltrating neutrophils were platelet-coated (Figure 5I; supplemental Figure 5C). In accordance with results derived from CypD-deficient mice, neither platelet and neutrophil recruitment to the lung nor peripheral platelet and leukocyte counts in platelet-specific TMEM16F-knockout animals revealed any differences 24 hours after LPS exposure (Figure 5I,K; supplemental Figure 5D). These data suggest that platelet PA is an important effector function of platelets in inflammation, aiding in the prevention of transmigration-associated pulmonary hemorrhage.

Impact of genetic targeting of PA pathways on platelet calcium oscillations

We next sought to elucidate cellular pathways triggering procoagulant function in inflammation. PA depends on the ability of

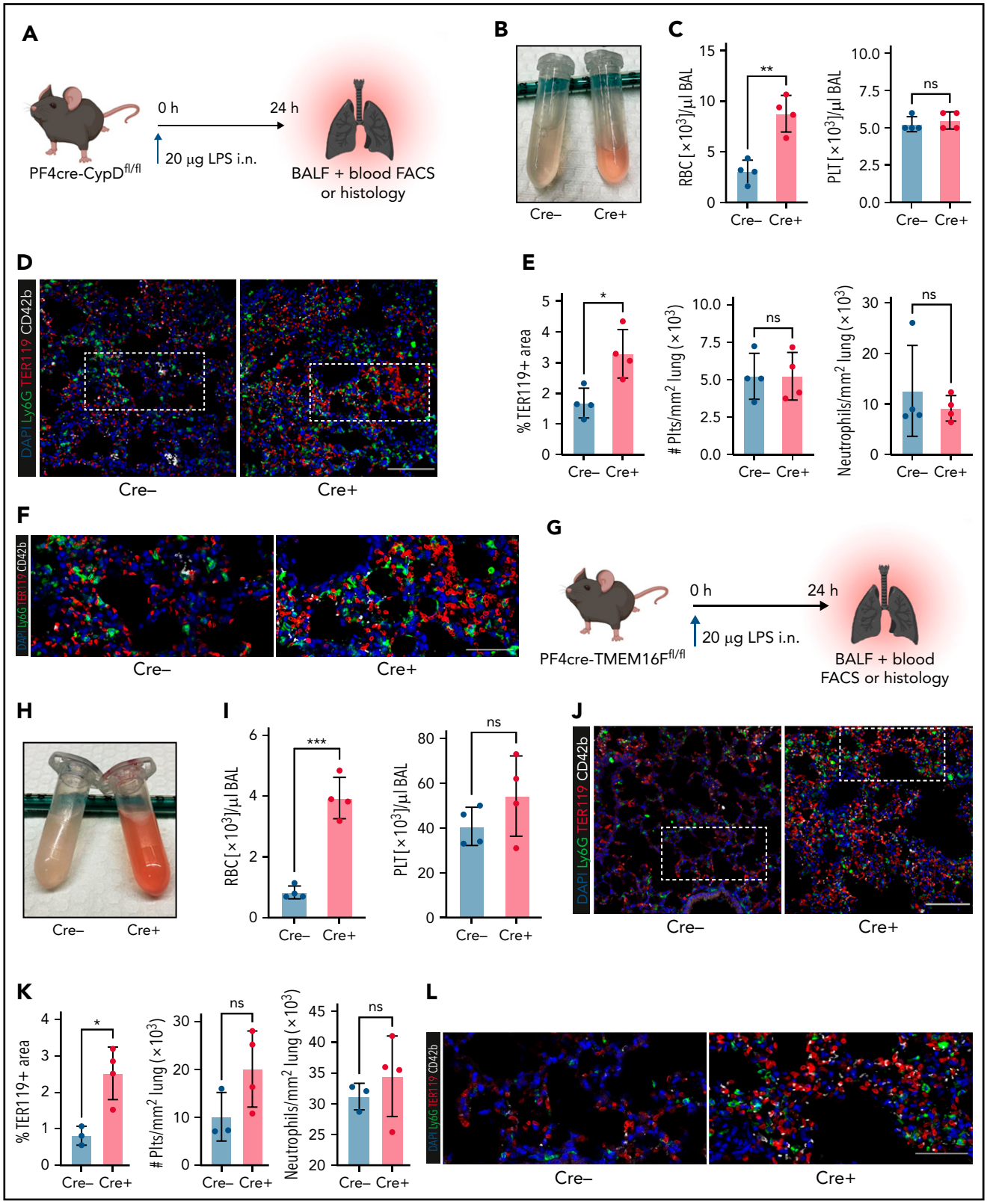

Figure 5. Genetic ablation of platelet PA aggravates inflammatory bleeding. (A) Experimental scheme for acute lung injury in platelet-specific CypD-knockout mice. (B) Representative image of BALF from platelet-specific CypD-knockout mice and Cre-negative littermates. (C) Flow cytometric analysis of RBC and platelet counts in BALF. Student's *t* test, two-tailed, unpaired. (D) Representative micrograph of immunofluorescence-stained lung slices from CypD-knockout mice and Cre-negative control animals. Bar represents 100 µm. (E) Histological quantification of alveolar hemorrhage (TER119$^+$ area) as well as pulmonary neutrophil and platelet recruitment. Student's *t* test, two-tailed, unpaired. (F) Magnified excerpts of representative micrographs, corresponding to white rectangle in Figure 5D. Bar represents 50 µm. (G) Experimental scheme for acute lung injury in TMEM16F-knockout mice. (H) Representative image of BALF from platelet-specific TMEM16F-knockout mice and Cre-negative littermates. (I) Flow cytometric analysis of RBC and platelet counts in BALF. Student's *t* test, two-tailed, unpaired. (J) Representative micrograph of immunofluorescence-stained lung slices from TMEM16F-knockout mice and Cre-negative littermates. Bar represents 100 µm. (K) Histopathological quantification of alveolar hemorrhage (TER119$^+$ area) as well as pulmonary neutrophil and platelet recruitment. Student's *t* test, two-tailed, unpaired. (L) Magnified excerpts of representative micrographs, corresponding to white rectangle in Figure 5J. Bar represents 50 µm.

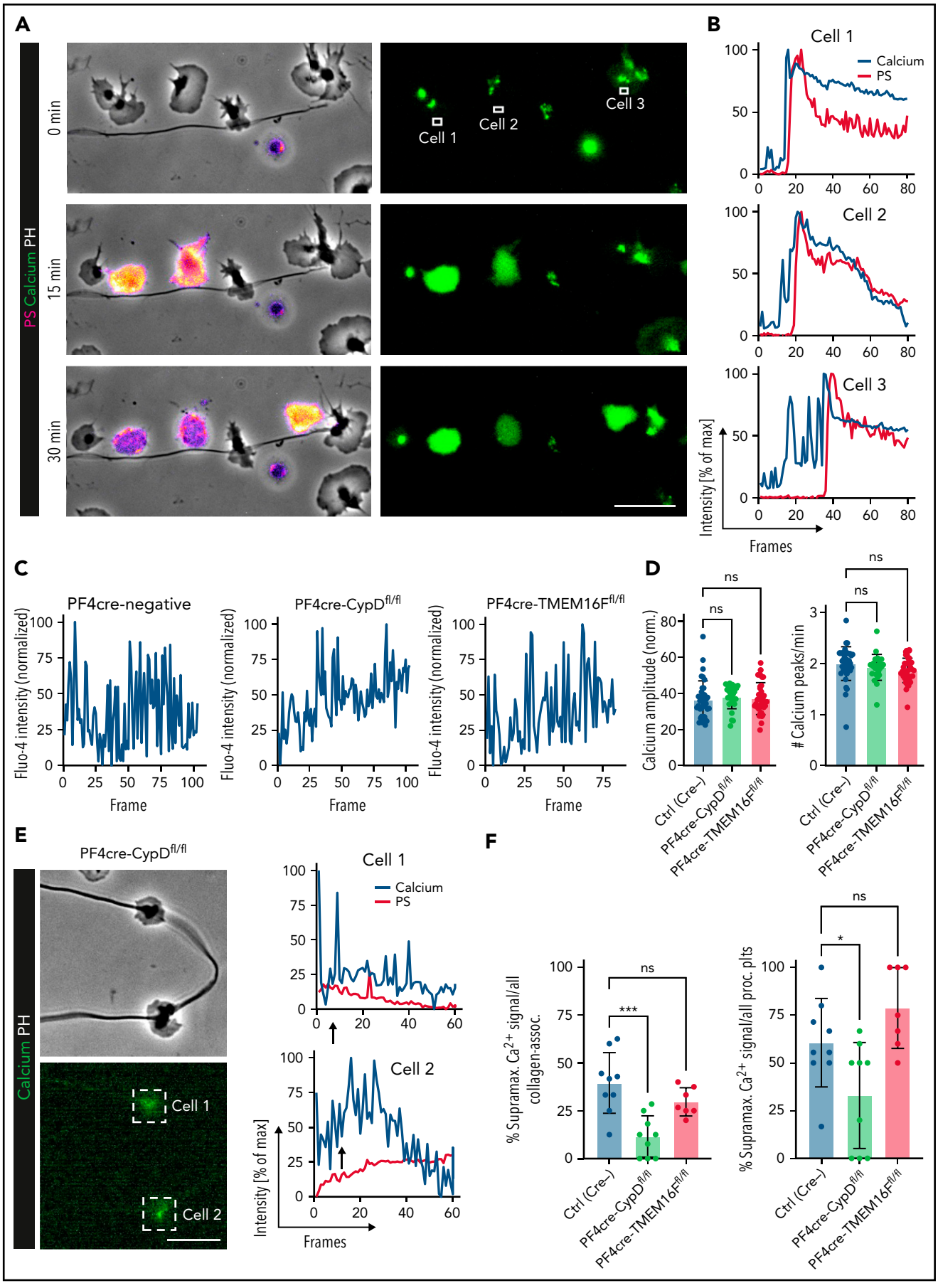

Figure 6.

the individual platelet to rapidly increase cytosolic calcium levels, with a recent study describing "supramaximal calcium bursts"[44] within the range of 100 μM, exceeding normal intracellular levels by far. In migrating platelets, we observed rhythmic calcium oscillations throughout the course of migration on fibrinogen and albumin matrices (supplemental Figure 6A). When migrating platelets hit collagen fibers, instant intracellular calcium bursts occurred (Figure 6A-B; supplemental Video 2). These calcium bursts preceded both morphological changes (ballooning and microvesiculation) and the exposure of phosphatidylserine, which was exteriorized following maximum calcium bursts (Figure 6A-B; supplemental Video 2).

To investigate the impact of CypD- and TMEM16F-deficiency on calcium currents of migrating platelets, we performed additional live imaging experiments. Migrating platelets from both wild-type and CypD- or TMEM16F-deficient mice exhibited similar baseline calcium oscillation profiles (Figure 6C). Both calcium oscillation frequency and mean oscillation amplitudes did not differ between genotypes (Figure 6D). However, in contrast to both control and TMEM16F-deficient platelets, migrating CypD-deficient platelets continued to show rhythmic calcium oscillations despite ongoing physical interaction with collagen (Figure 6E-F; supplemental Figure 6B-E). Consequently, we hardly detected supramaximal calcium bursts in CypD-deficient platelets in contact with collagen fibers, confirming CypD-dependent mitochondrial depolarization to be crucial for PA of migrating platelets without affecting baseline oscillations necessary for migratory capacity (Figure 6F). The few CypD-deficient platelets mounting a procoagulant activation response took longer to achieve supramaximal calcium peaks (supplemental Figure 6C-E), suggesting compensatory calcium currents in the absence of the CypD-dependent mitochondrial permeability transition pore formation[43] (supplemental Figure 6F-G). In contrast to CypD-deficient platelets, TMEM16F-deficient platelets turning procoagulant also exhibited supramaximal calcium currents, confirming that calcium peaks precede scramblase activity (Figure 6F; supplemental Figure 6D-E).[46,49] Notably, single inhibition of calcium currents such as store-operated, mitochondrial, or extracellular calcium entry[44] reduced PA without affecting migratory capacity, which was only attenuated when all 3 sources of calcium were blocked simultaneously. This suggests functional redundancy of the individual calcium currents in maintaining migratory capacity (supplemental Figure 6F-G).

Pharmacological inhibition of platelet PA by combined GPIIBIIIA and GPVI blockade aggravates inflammatory bleeding in vivo

Next, we investigated which platelet activation pathways and receptors are crucially involved in platelet PA upon migration and collagen sensing. We have previously shown that platelet migration depends on GPIIBIIIA activation (supplemental Figure 7A-B) as well as actin-myosin networks.[8,9] In line, downstream inhibition of Rho kinase, phospholipase Cγ, myosin light chain, and Rac1,[1,50] inhibited platelet migration reduced the likelihood of encountering collagen fibers and, consequently, reduced platelet PA (supplemental Figure 7C-D). Because platelets in solution showed no procoagulant function in the presence of fibrinogen and collagen (compare supplemental Figure 3D-F), we hypothesized that GPIIBIIIA-dependent mechanosensing might influence PA.[34,51] Indeed, when we partially inhibited mechanosensitive GPIIBIIIA outside-in signaling by targeting $G\alpha_{13}$, platelet PA was effectively inhibited while platelet migration remained intact despite characteristic morphological changes[51,52] (Figure 7A-B; supplemental Figure 7E-F). The significant increase in migration was likely due to reduced PA on collagen-coated matrices because mP6-treated platelets moving on fibrinogen/albumin matrices did not migrate farther than their respective controls (supplemental Figure 7G).

Seminal studies have established that fibrin(ogen) is also bound by collagen receptor GPVI and that platelet activation and subsequent thrombin turnover are increased upon GPVI-mediated fibrin(ogen) sensing.[53-56] The impact of GPVI on PA of migrating platelets, however, remains elusive. Inhibition of GPVI signaling using either an anti-GPVI antibody or the novel Syk kinase inhibitor BI-1002494 diminished mouse platelet PA (Figure 7A-B). Interestingly, migratory capacity of murine platelets decreased only when using higher doses of BI-1002494, whereas increasing concentrations of GPVI-blocking JAQ1 had no such effect (supplemental Figure 7H-I). This indicates that GPVI-mediated fibrinogen binding is dispensable for platelet migration in vitro. Modulating GPIIBIIIA-$G\alpha_{13}$ signaling or GPVI signaling in human platelets also attenuated PA without affecting migration (Figure 7C). In contrast, treatment of human platelets with the small molecule antagonist TC-I15, which inhibits the collagen receptor integrin $\alpha2\beta1$, had no effect on PA, indicating that collagen sensing through this receptor is not required for PA of migrating platelets (supplemental Figure 7J).

Time-lapse microscopy of platelets treated with low-dose GPIIBIIIA outside-in signaling inhibitors or GPVI antagonists revealed no alterations in amplitude and frequency of calcium oscillations but showed that treated platelets that encountered collagen fibers did not mount supramaximal calcium bursts (Figure 7D-E; supplemental Figure 7K-L; supplemental Video 3). This finding highlights that co-engagement of GPVI and GPIIBIIIA outside-in signaling triggers supramaximal calcium release and, in turn, platelet PA. Strikingly, inhibition of both pathways resulted in additive suppression of procoagulant function, whereas migratory capacity was retained (supplemental Figure 8A-B).

Figure 6. Impact of genetic and pharmacological targeting of PA pathways on platelet calcium oscillations. (A) Representative images of time-lapse microscopy of migrating human platelets and respective calcium oscillations (green) and PS exposure (annexin V, pink). PH, phase contrast. Bar represents 10 μm. White boxes indicate the area of measurement analyzed in (B). See supplemental Video 2 for corresponding live imaging. (B) Intensity projection for calcium (blue) and PS signal intensity (red) over time as % of maximum intensity for cells 1 to 3. (C) Representative calcium oscillation profiles of migrating platelets from CypD- or TMEM16F-deficient compared with platelets from PF4cre-negative animals. (D) Quantification of mean normalized calcium amplitudes and calcium peak frequency measured from mouse platelets across genotypes. n = 103 individual platelets. One-way ANOVA with Holm-Šídák's multiple comparison test. (E) Representative micrographs and calcium (blue) and PS intensity profiles (mC1, red) derived from live imaging of the 2 CypD-deficient mouse platelets indicated by white boxes. Bar represents 10 μm. Arrows indicate the beginning of contact to collagen fibers. (F) Relative quantification of percentage of supramaximal calcium peaks of all collagen-associated mouse platelets as well as relative quantification of supramaximal calcium peak-positive procoagulant platelets. Individual dots represent percentages derived from individual time-lapse microscopy videos. Platelets were isolated from n = 2 to 3 mice/group. PS staining agent: mC1. One-way ANOVA with Holm-Šídák's multiple comparisons test.

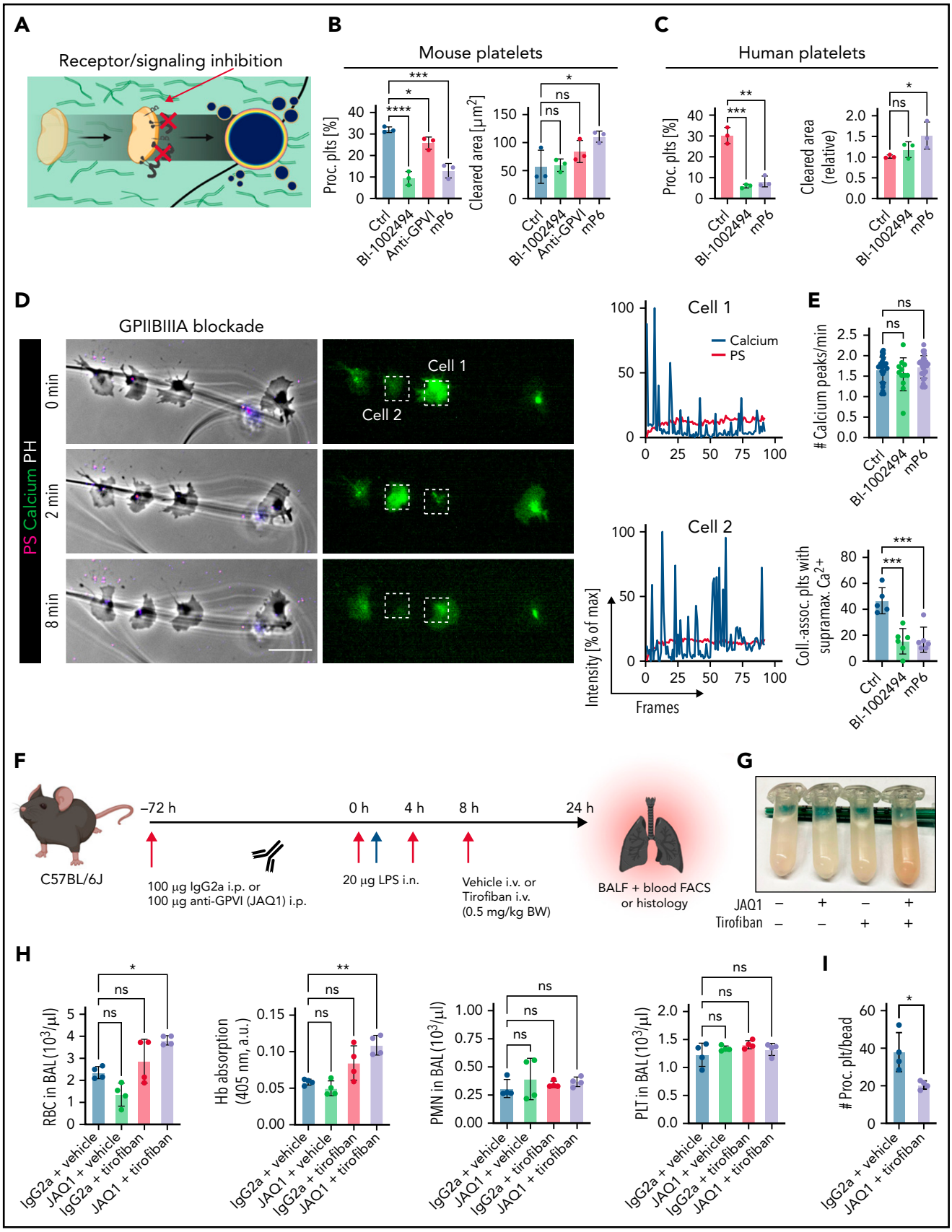

Figure 7. Pharmacological ablation of platelet PA through simultaneous GPIIBIIIA and GPVI inhibition aggravates inflammatory bleeding. (A) Experimental scheme of migration assay on hybrid matrix with targeting of platelet receptors and signaling cascades. (B-C) Quantification of procoagulant platelets and cleared area by murine (B) and human platelets (C) treated with inhibitors of GPVI signaling (BI-1002494 = Syk inhibitor, 5 µM; JAQ1 = GPVI-blocking antibody, 10 µg/mL) or GPIIBIIIA

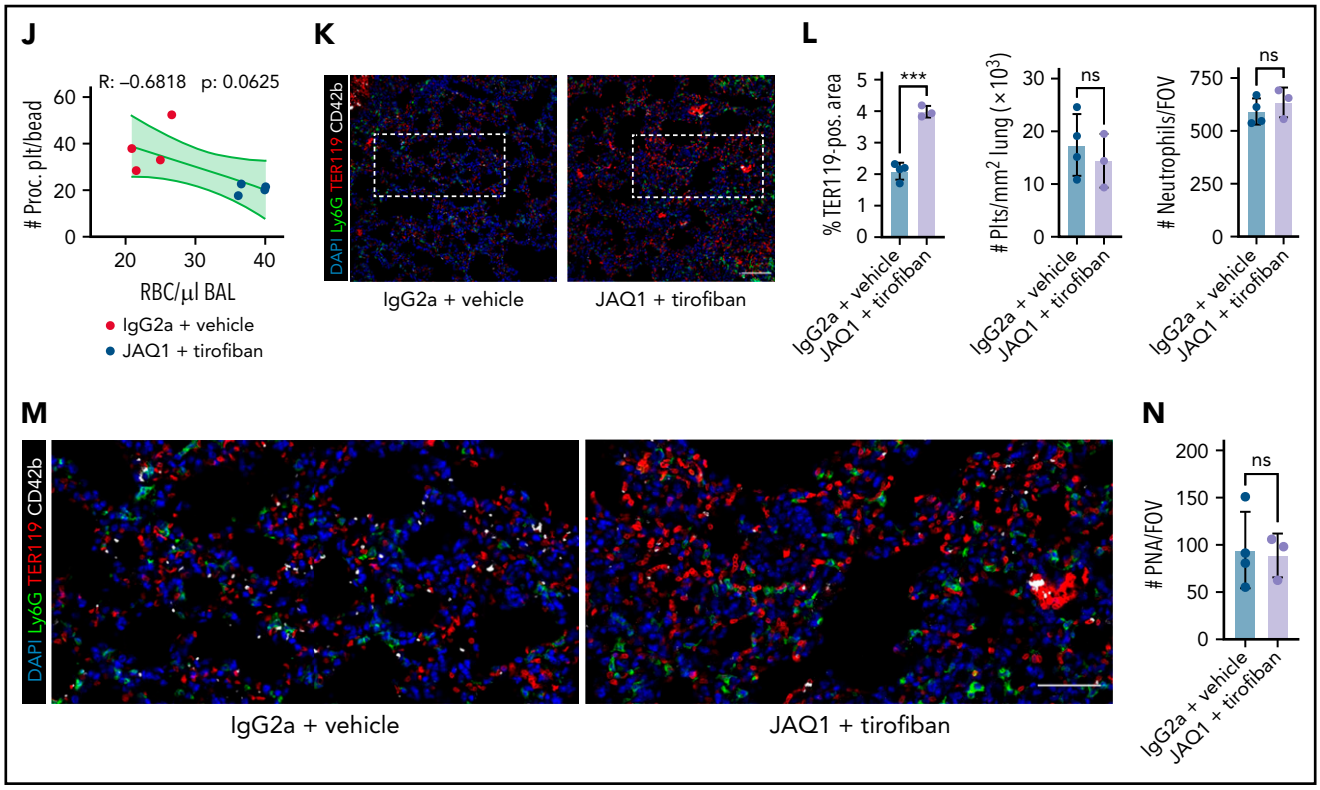

Figure 7 (continued) outside-in signaling (mP6 = $G\alpha_{13}$ inhibitor, 20 µM). One-way ANOVA with Holm-Šídák's multiple comparisons test. (D) Representative images of time-lapse microscopy of migrating human platelets and respective calcium oscillations (blue) and PS exposure (red) recorded after 0, 2, and 8 minutes of migration. Bar represents 10 µm. White boxes indicate the area of measurement depicted next to micrographs. See supplemental Video 3 for corresponding live imaging. (E) Upper panel: Quantification of calcium peaks of migrating human platelets treated with vehicle, mP6 (20 µM) or BI-1002494 (2.5 µM). Lower panel: Relative quantification (%) of migrating, collagen-associated platelets treated with vehicle, mP6, or BI-1002494 that express supramaximal calcium peaks upon collagen contact (n = 5-6 videos from n = 2-3 mice per condition with a total of >100 platelets were analyzed). One-way ANOVA with Holm-Šídák's multiple comparisons test. (F) Experimental scheme for acute lung injury in Bl6 mice treated with JAQ1, a GPVI-blocking antibody, or isotype (red arrow) 72 hours prior to LPS challenge (blue arrow) and vehicle or tirofiban injections (red arrows) at 0, 4, and 8 hours after LPS challenge. (G) Representative image of BALF collected from different experimental groups. (H) Assessment of Hb absorption and flow cytometric analysis of RBC, polymorphonuclear, and platelet counts in BALF (n = 4 mice per group). One-way ANOVA with Holm-Šídák's multiple comparisons test compared with control groups. (I) Flow cytometric measurement of circulating procoagulant platelets in peripheral blood, normalized to counting beads. Student's *t* test, two-tailed, unpaired. (J) Linear regression analysis of the correlation of circulating procoagulant platelets and inflammatory bleeding severity as assessed by RBC count/µL BALF. (K) Representative micrograph of immunofluorescence-stained lung slices from IgG2a and vehicle vs JAQ1 and tirofiban-treated animals. Bar represents 100 µm. (L) Quantification of alveolar hemorrhage ($TER119^+$ area) as well as pulmonary platelet and neutrophil recruitment. PS staining agent for all experiments shown in Figure 7: mC1. n = 4 mice per group. Student's *t* test, two-tailed, unpaired. (M) Magnified excerpts of representative immunofluorescence stainings, corresponding to white rectangles in Figure 7K. Bar represents 50 µm. (N) Histopathological quantification of pulmonary PNAs per FOV 24 hours after LPS challenge. Student's *t* test, two-tailed, unpaired.

Finally, we sought to confirm the identified pathways in vivo. We first evaluated the effective blockade of GPIIBIIIA and depletion of GPVI in mice by using the clinically available integrin antagonist tirofiban[57] and a GPVI-depleting antibody (JAQ1), respectively[58] (Figure 7F; supplemental Figure 8C-G). While intraperitoneal injection of JAQ1 reduced the surface expression of GPVI (supplemental Figure 8C-D), tirofiban treatment effectively blocked integrin activation in thrombin- and convulxin-activated mouse platelets (supplemental Figure 8E-F). Tirofiban did not affect murine or human platelet migration in vitro at the indicated concentrations but reduced procoagulant potential; this effect was further enhanced upon dual blockade with both tirofiban and JAQ1 (supplemental Figure 8A-B,G).

When we performed acute lung injury experiments on Bl6 mice treated with JAQ1, tirofiban, or both, only simultaneous blockade of GPIIBIIIA and GPVI aggravated alveolar hemorrhage 24 hours after LPS challenge (Figure 7F-H). Alveolar neutrophil recruitment did not differ (Figure 7H). Although most neutrophils were coated with platelets, we detected few free-floating platelets in BALF, excluding BAL contamination by traumatic vessel leakage (Figure 7H). Flow cytometry of blood samples revealed a significant decrease in circulating procoagulant platelets only in mice receiving dual treatment (Figure 7I). Circulating procoagulant platelet counts negatively correlated with excessive alveolar hemorrhage (Figure 7J). Apart from GPVI expression, we detected no differences in platelet receptor surface expression and PNA formation across treatment groups, and clinical status remained similar between treatment conditions (supplemental Figure 8H-K). Histologically, we confirmed increased alveolar hemorrhage upon dual inhibition but did not detect any differences in pulmonary neutrophil and platelet recruitment or PNA formation (Figure 7K-N). We also depleted GPIIBIIIA and GPVI and challenged mice with intraperitoneal LPS injections (supplemental Figure 8L-R). PA of both circulating and adherent platelets was effectively reduced, and we detected an increase in mesenteric microbleeding in our model, suggesting that platelet PA may be involved in maintaining vascular homeostasis in mesenteric inflammation (supplemental Figure 8M-R).

In summary, pharmacological inhibition of procoagulant platelet activation by dual targeting of GPIIBIIIA and GPVI reduced platelet PA in vivo and exacerbated inflammatory microbleeding in both lung and mesentery.

Discussion

Platelets are uniquely positioned to be vascular first responders due to their short reaction time and abundancy in peripheral blood. Recent work has revealed that platelets recruited to sites of inflammation behave differently using a distinct set of receptors and signaling pathways. In contrast to classical thrombus formation, single platelets are recruited to the vascular endothelium under inflammatory conditions.[8,22] These platelets crucially maintain vascular integrity because severe thrombocytopenia exacerbates endothelial leakage and inflammatory hemorrhage.[24,31,59,60] However, it remains insufficiently understood how platelets effectively seal endothelial defects in the absence of clot formation.[17]

Here, we describe a novel effector function of immune-responsive platelets (procoagulant activity) that recruits the coagulation cascade and has a critical role in maintaining local vascular integrity without triggering diffuse intravascular clotting. We show that platelets migrate at sites of vascular injury and fibrin(ogen) deposition, constantly scanning their microenvironment. Upon encountering vascular breaches with exposure of subendothelial collagen, migrating platelets engage GPVI, which triggers intracellular calcium release and PS exposure. This arrests platelets at the injury site and allows binding of the prothrombinase complex on the platelet membrane, greatly enhancing thrombin activity resulting in fibrin formation.[32] Importantly, our study does not address the origin of fibrin(ogen) deposits, leaving the question of whether local fibrin(ogen) accumulation derives from plasma or platelet-intrinsic storage pools. Previous studies provide evidence that α-granule secretion is dispensable for inflammatory hemostasis,[27,61] and we have found no evidence of substantial fibrinogen secretion by procoagulant platelets in vitro.

The identified mechanism effectively targets the coagulation cascade to breaches identified by patrolling platelets and might therefore circumvent widespread coagulation activation. In line with this, blocking GPVI and GPIIBIIIA reduced procoagulant platelets in vivo and enhanced hemorrhage in lung and mesentery alike following LPS exposure. These findings highlight glycoprotein redundancy in inflammatory platelet signaling in vivo as observed by other groups: GPVI was previously thought to be entirely dispensable for the prevention of bleeding in the lung, as shown using GPVI-knockout animals.[17,22,28,62] In our hands, antibody-mediated blockade of GPVI alone confirmed this observation and resulted in no aggravation of inflammatory bleeding. Moreover, our study may reconcile previously dichotomous findings regarding the role of GPIIBIIIA in the inflammatory hemostasis in the lung: While some studies found no significant effect of pharmacological inhibition of GPIIBIIIA using direct inhibitors like integrillin or a GPIIBIIIA-targeted antibody on inflammatory bleeding, plasma leakage, and alveolar neutrophil recruitment,[28,63] we have previously shown that genetic ablation of GPIIBIIIA using bone marrow chimeric mice aggravates LPS-induced pulmonary hemorrhage.[8] The bleeding phenotype reported in our recent study may be attributable to the loss of migratory capacity that is observed in GPIIBIIIA-deficient platelets but not in pharmacological inhibition.[9] In the current study, we only observed a significant increase in inflammatory hemorrhage upon dual inhibition of GPVI and GPIIBIIIA while providing evidence that neither single nor dual inhibition of either receptor impaired migratory capacity in vitro (supplemental Figure 8A). Additional factors such as extracellular vesicle formation, which is affected by GPIIBIIIA blockade through tirofiban[64] and can itself impact on hemostasis,[65] were not investigated in this study and may also contribute to the observed bleeding phenotype. Specific pharmacological inhibition of platelet PA and thus reduction of procoagulant PS expression, as mediated through maintaining flippase activity in procoagulant platelets,[66] may specifically address these remaining aspects.

Preventing procoagulant activity by genetic ablation of either CypD-dependent mitochondrial permeability transition pore formation or TMEM16F scramblase-dependent phosphatidylserine exposure exacerbated inflammatory bleeding while having a negligible effect on classical hemostasis assessed by tail bleeding assay.[42] Although we describe a protective local effect of procoagulant activity, circulating procoagulant platelets have been associated with both local and remote organ injury as well as disseminated intravascular coagulation.[41,67] Denorme et al.[41] highlighted a detrimental role for PS-positive PNAs in ischemic stroke, which aggravated brain damage and vascular obstruction. In COVID-19, the level of antibody-induced circulating procoagulant platelets correlated with D-dimer levels and an increased incidence of systemic thromboembolism.[68] Considering these data, it is tempting to speculate that even though local induction of procoagulant platelets may be crucial to maintain vascular integrity in inflammation, systemic and dysregulated procoagulant platelet activation could be one of the drivers of systemic coagulation activation.[32,67,69,70] Further studies are needed to define factors that trigger systemic platelet PS exposure and investigate the role of platelet procoagulant activity in other conditions with increased vascular permeability, as observed in cancer.[10] In inflammatory bleeding, the involvement of specific platelet signaling pathways and receptors as well as degranulation has been shown to be highly dependent on the mode of injury and the respective vascular bed.[17,21,23,24,27,61] Therefore, further studies need to define platelet-coagulation interplay in distinct inflammatory contexts. Finally, it remains unclear whether other platelet receptors such as CLEC-2, which is known to attenuate acute lung injury through podoplanin-mediated interplay with alveolar macrophages[71] but does not affect inflammatory bleeding severity,[28] and the GPIb-IX-V complex that play a role in the prevention of inflammatory bleeding can also trigger platelet procoagulant activity.[27] In particular, combined inhibition of other platelet glycoproteins may yield additional insights into potential functional redundancies in the context of inflammatory bleeding.[72]

Limitations of this study include the lack of generalizability of platelet PA as a platelet-inherent protective function in other models of inflammatory hemorrhage, particularly neutrophil-driven ischemic-reperfusion injury of the brain, sterile injury of the skin microvasculature, and tumor-associated bleeding.[17,22,26,27] We also note that compared with the severe bleeding phenotype observed in thrombocytopenic animals, the increase in pulmonary hemorrhage upon pharmacological or genetic interference with platelet PA was not as severe, suggesting compensatory

mechanisms beyond PA that may mask its intrinsic contribution to inflammatory hemostasis (supplemental Table 2). Although we observed no effect on neutrophil and leukocyte recruitment to the lungs of CypD- and TMEM16F-deficient mice, the lack of platelet PA may influence the inflammatory microenvironment and promote endothelial dysfunction beyond aggravating inflammatory hemorrhage. Thus, future studies need to elucidate the functional role of procoagulant platelets in both local and systemic inflammatory responses.

In summary, we describe an essential function of procoagulant platelets in promoting vascular integrity in inflammation, adding to the pivotal role of platelets across the inflammatory spectrum and the complex pathophysiology of inflammatory hemorrhage.

Acknowledgments

The authors thank all laboratory members for technical support.

This study was supported by the Deutsche Herzstiftung e.V., Frankfurt a.M. (R.K. and L.N.), Deutsche Forschungsgemeinschaft (DFG) SFB 914 (S.M. [B02 and Z01] and K.S. [B02]), the DFG Project-ID 210592381 – SFB 1054 (T.B. [B03 and Z01]), the DFG SFB 1123 (S.M. [B06] and K.S. [A07]), the DFG FOR 2033 (S.M.), the German Center for Cardiovascular Research (DZHK) (Clinician Scientist Program [L.N.], Start-Up Grant [L.N.] 1.4VD [S.M.], the DFG Clinician Scientist Program PRIME (413635475, R.K. and K.P.) and the FP7 program (project 260309, PRESTIGE [S.M.]). This work was also supported by the European Research Council (ERC-2018-ADG "IMMUNOTHROMBOSIS" [S.M.] and ERC "T-MEMORE" [K.S.]).

Authorship

Contribution: L.N. initiated the study; R.K. and L.N. conceptualized the study; R.K., R.E., and L.N. created the methodology; R.K., R.E., J.K., M.-L.H., A.A., V.P., M.M., W.H., L.B., C.G., A.T., M.L., and L.N. conducted the investigation; R.K., K.P., S.K., F.G, K.S., T.B., S.M., and L.N. collected the resources; R.K., R.E., and L.N. conducted formal analysis; R.K. and L.N. wrote the original draft; all authors edited the draft; R.K., R.E., and L.N. handled data curation and software; R.K. visualized the study; R.K., J.K., K.P., K.S., T.B., S.M., and L.N. provided supervision and project administration; and R.K., K.S., S.M., and L.N. administered the funding.

Conflict-of-interest disclosure: T.B. and J.K. have an exclusive licensing agreement with BioLegend, Inc. for the commercialization of mC1-multimer. The remaining authors declare no competing financial interests.

ORCID profiles: R.K., 0000-0003-1750-3395; J.K., 0000-0002-9928-4132; M.-L.H., 0000-0002-5894-0308; A.A., 0000-0002-1976-4102; K.P., 0000-0003-4040-650X; S.K., 0000-0001-8824-3581; F.G., 0000-0001-6120-3723; T.B., 0000-0001-7060-5433; L.N., 0000-0003-0776-5885.

Correspondence: Rainer Kaiser, Medizinische Klinik und Poliklinik I, University Hospital, Ludwig-Maximilian University Munich, Marchioninistr 15, 81377 Munich, Germany; e-mail: rainer.kaiser@med.uni-muenchen.de; and Leo Nicolai, Medizinische Klinik und Poliklinik I, University Hospital, Ludwig-Maximilian University Munich, Marchioninistr 15, 81377 Munich, Germany; e-mail: leo.nicolai@med.uni-muenchen.de.

Footnotes

Submitted 15 December 2021; accepted 12 April 2022; prepublished online on *Blood* First Edition 26 April 2022. DOI 10.1182/blood.2021014914.

Data sharing is available upon request from the corresponding authors.

The online version of this article contains a data supplement.

There is a *Blood* Commentary on this article in this issue.

The publication costs of this article were defrayed in part by page charge payment. Therefore, and solely to indicate this fact, this article is hereby marked "advertisement" in accordance with 18 USC section 1734.

REFERENCES

1. Van der Meijden PEJ, Heemskerk JWM. Platelet biology and functions: new concepts and clinical perspectives. *Nat Rev Cardiol*. 2019;16(3):166-179.
2. Nicolai L, Gaertner F, Massberg S. Platelets in host defense: experimental and clinical insights. *Trends Immunol*. 2019;40(10):922-938.
3. Stark K, Massberg S. Interplay between inflammation and thrombosis in cardiovascular pathology. *Nat Rev Cardiol*. 2021;18(9):666-682.
4. Yeaman MR. Platelets: at the nexus of antimicrobial defence. *Nat Rev Microbiol*. 2014;12(6):426-437.
5. Sreeramkumar V, Adrover JM, Ballesteros I, et al. Neutrophils scan for activated platelets to initiate inflammation. *Science*. 2014; 346(6214):1234-1238.
6. Semple JW, Italiano JE Jr, Freedman J. Platelets and the immune continuum. *Nat Rev Immunol*. 2011;11(4):264-274.
7. Kaiser R, Escaig R, Erber J, Nicolai L. Neutrophil-platelet interactions as novel treatment targets in cardiovascular disease. *Front Cardiovasc Med*. 2022;8:824112.
8. Nicolai L, Schiefelbein K, Lipsky S, et al. Vascular surveillance by haptotactic blood platelets in inflammation and infection. *Nat Commun*. 2020;11(1):5778.
9. Gaertner F, Ahmad Z, Rosenberger G, et al. Migrating platelets are mechano-scavengers that collect and bundle bacteria. *Cell*. 2017; 171(6):1368-1382.e23.
10. Gaertner F, Massberg S. Patrolling the vascular borders: platelets in immunity to infection and cancer. *Nat Rev Immunol*. 2019;19(12):747-760.
11. Verschoor A, Neuenhahn M, Navarini AA, et al. A platelet-mediated system for shuttling blood-borne bacteria to CD8α^+ dendritic cells depends on glycoprotein GPIb and complement C3. *Nat Immunol*. 2011; 12(12):1194-1201.
12. Elzey BD, Schmidt NW, Crist SA, et al. Platelet-derived CD154 enables T-cell priming and protection against Listeria monocytogenes challenge. *Blood*. 2008;111(7): 3684-3691.
13. Guo L, Shen S, Rowley JW, et al. Platelet MHC class I mediates CD8$^+$ T-cell suppression during sepsis. *Blood*. 2021;138(5): 401-416.
14. Middleton EA, He XY, Denorme F, et al. Neutrophil extracellular traps contribute to immunothrombosis in COVID-19 acute respiratory distress syndrome. *Blood*. 2020; 136(10):1169-1179.
15. Nicolai L, Leunig A, Brambs S, et al. Immunothrombotic dysregulation in COVID-19 pneumonia is associated with respiratory failure and coagulopathy. *Circulation*. 2020;142(12): 1176-1189.
16. Zuo Y, Yalavarthi S, Shi H, et al. Neutrophil extracellular traps in COVID-19. *JCI Insight*. 2020;5(11):138999.
17. Ho-Tin-Noé B, Boulaftali Y, Camerer E. Platelets and vascular integrity: how platelets prevent bleeding in inflammation. *Blood*. 2018;131(3):277-288.
18. Al-Samkari H, Karp Leaf RS, Dzik WH, et al. COVID-19 and coagulation: bleeding and thrombotic manifestations of SARS-CoV-2 infection. *Blood*. 2020;136(4):489-500.
19. Thomas J, Kostousov V, Teruya J. Bleeding and thrombotic complications in the use of extracorporeal membrane oxygenation. *Semin Thromb Hemost*. 2018;44(1):20-29.
20. Lara AR, Schwarz MI. Diffuse alveolar hemorrhage. *Chest*. 2010;137(5):1164-1171.
21. Hillgruber C, Pöppelmann B, Weishaupt C, et al. Blocking neutrophil diapedesis prevents hemorrhage during thrombocytopenia. *J Exp Med*. 2015;212(8):1255-1266.

22. Gros A, Syvannarath V, Lamrani L, et al. Single platelets seal neutrophil-induced vascular breaches via GPVI during immune-complex-mediated inflammation in mice. *Blood.* 2015;126(8):1017-1026.

23. Ho-Tin-Noé B, Carbo C, Demers M, Cifuni SM, Goerge T, Wagner DD. Innate immune cells induce hemorrhage in tumors during thrombocytopenia. *Am J Pathol.* 2009; 175(4):1699-1708.

24. Goerge T, Ho-Tin-Noe B, Carbo C, et al. Inflammation induces hemorrhage in thrombocytopenia. *Blood.* 2008;111(10): 4958-4964.

25. Boulaftali Y, Mawhin MA, Jandrot-Perrus M, Ho-Tin-Noé B. Glycoprotein VI in securing vascular integrity in inflamed vessels. *Res Pract Thromb Haemost.* 2018;2(2):228-239.

26. Volz J, Mammadova-Bach E, Gil-Pulido J, et al. Inhibition of platelet GPVI induces intratumor hemorrhage and increases efficacy of chemotherapy in mice. *Blood.* 2019;133(25):2696-2706.

27. Deppermann C, Kraft P, Volz J, et al. Platelet secretion is crucial to prevent bleeding in the ischemic brain but not in the inflamed skin or lung in mice. *Blood.* 2017;129(12): 1702-1706.

28. Rayes J, Jadoui S, Lax S, et al. The contribution of platelet glycoprotein receptors to inflammatory bleeding prevention is stimulus and organ dependent. *Haematologica.* 2018;103(6):e256-e258.

29. Braun LJ, Stegmeyer RI, Schäfer K, et al. Platelets docking to VWF prevent leaks during leukocyte extravasation by stimulating Tie-2. *Blood.* 2020;136(5): 627-639.

30. Rausch L, Lutz K, Schifferer M, et al. Binding of phosphatidylserine-positive microparticles by PBMCs classifies disease severity in COVID-19 patients. *J Extracell Vesicles.* 2021;10(14):e12173.

31. Ho-Tin-Noé B, Demers M, Wagner DD. How platelets safeguard vascular integrity. *J Thromb Haemost.* 2011;9(suppl 1):56-65.

32. Agbani EO, Poole AW. Procoagulant platelets: generation, function, and therapeutic targeting in thrombosis. *Blood.* 2017;130(20):2171-2179.

33. Agbani EO, van den Bosch MT, Brown E, et al. Coordinated membrane ballooning and procoagulant spreading in human platelets. *Circulation.* 2015;132(15): 1414-1424.

34. Pang A, Cui Y, Chen Y, et al. Shear-induced integrin signaling in platelet phosphatidylserine exposure, microvesicle release, and coagulation. *Blood.* 2018; 132(5):533-543.

35. Van Kruchten R, Mattheij NJ, Saunders C, et al. Both TMEM16F-dependent and TMEM16F-independent pathways contribute to phosphatidylserine exposure in platelet apoptosis and platelet activation. *Blood.* 2013;121(10):1850-1857.

36. Delaney MK, Liu J, Kim K, et al. Agonist-induced platelet procoagulant activity requires shear and a Rac1-dependent signaling mechanism. *Blood.* 2014;124(12): 1957-1967.

37. Petri B, Broermann A, Li H, et al. von Willebrand factor promotes leukocyte extravasation. *Blood.* 2010;116(22): 4712-4719.

38. Schoenwaelder SM, Yuan Y, Josefsson EC, et al. Two distinct pathways regulate platelet phosphatidylserine exposure and procoagulant function. *Blood.* 2009;114(3): 663-666.

39. Hua VM, Abeynaike L, Glaros E, et al. Necrotic platelets provide a procoagulant surface during thrombosis. *Blood.* 2015; 126(26):2852-2862.

40. French SL, Arthur JF, Lee H, et al. Inhibition of protease-activated receptor 4 impairs platelet procoagulant activity during thrombus formation in human blood. *J Thromb Haemost.* 2016;14(8):1642-1654.

41. Denorme F, Manne BK, Portier I, et al. Platelet necrosis mediates ischemic stroke outcome in mice. *Blood.* 2020;135(6): 429-440.

42. Fujii T, Sakata A, Nishimura S, Eto K, Nagata S. TMEM16F is required for phosphatidylserine exposure and microparticle release in activated mouse platelets. *Proc Natl Acad Sci USA.* 2015; 112(41):12800-12805.

43. Jobe SM, Wilson KM, Leo L, et al. Critical role for the mitochondrial permeability transition pore and cyclophilin D in platelet activation and thrombosis. *Blood.* 2008; 111(3):1257-1265.

44. Abbasian N, Millington-Burgess SL, Chabra S, Malcor JD, Harper MT. Supramaximal calcium signaling triggers procoagulant platelet formation. *Blood Adv.* 2020;4(1): 154-164.

45. Millington-Burgess SL, Harper MT. Gene of the issue: *ANO6* and Scott syndrome. *Platelets.* 2020;31(7):964-967.

46. Suzuki J, Umeda M, Sims PJ, Nagata S. Calcium-dependent phospholipid scrambling by TMEM16F. *Nature.* 2010; 468(7325):834-838.

47. Baig AA, Haining EJ, uess E, et al. TMEM16F-mediated platelet membrane phospholipid scrambling is critical for hemostasis and thrombosis but not thromboinflammation in mice-brief report. *Arterioscler Thromb Vasc Biol.* 2016;36(11): 2152-2157.

48. Kholmukhamedov A, Jobe SM. Necrotic but not apoptotic platelets are functionally procoagulant. *Blood.* 2018;132(suppl 1): 2420.

49. Suzuki J, Fujii T, Imao T, Ishihara K, Kuba H, Nagata S. Calcium-dependent phospholipid scramblase activity of TMEM16 protein family members. *J Biol Chem.* 2013;288(19): 13305-13316.

50. Li Z, Delaney MK, O'Brien KA, Du X. Signaling during platelet adhesion and activation. *Arterioscler Thromb Vasc Biol.* 2010;30(12):2341-2349.

51. Durrant TN, van den Bosch MT, Hers I. Integrin $\alpha_{IIb}\beta_3$ outside-in signaling. *Blood.* 2017;130(14):1607-1619.

52. Gong H, Shen B, Flevaris P, et al. G protein subunit Galpha13 binds to integrin alphaIIbbeta3 and mediates integrin "outside-in" signaling. *Science.* 2010; 327(5963):340-343.

53. Xu RG, Gauer JS, Baker SR, et al. GPVI (glycoprotein VI) interaction with fibrinogen is mediated by avidity and the fibrinogen αC-region. *Arterioscler Thromb Vasc Biol.* 2021;41(3):1092-1104.

54. Slater A, Perrella G, Onselaer MB, et al. Does fibrin(ogen) bind to monomeric or dimeric GPVI, or not at all? *Platelets.* 2019; 30(3):281-289.

55. Alshehri OM, Hughes CE, Montague S, et al. Fibrin activates GPVI in human and mouse platelets. *Blood.* 2015;126(13):1601-1608.

56. Mammadova-Bach E, Ollivier V, Loyau S, et al. Platelet glycoprotein VI binds to polymerized fibrin and promotes thrombin generation. *Blood.* 2015;126(5):683-691.

57. Neumann FJ, Hochholzer W, Pogatsa-Murray G, Schömig A, Gawaz M. Antiplatelet effects of abciximab, tirofiban and eptifibatide in patients undergoing coronary stenting. *J Am Coll Cardiol.* 2001; 37(5):1323-1328.

58. Massberg S, Gawaz M, Grüner S, et al. A crucial role of glycoprotein VI for platelet recruitment to the injured arterial wall in vivo. *J Exp Med.* 2003;197(1): 41-49.

59. Ho-Tin-Noé B, Goerge T, Wagner DD. Platelets: guardians of tumor vasculature. *Cancer Res.* 2009;69(14):5623-5626.

60. Gupta S, Konradt C, Corken A, et al. Hemostasis vs. homeostasis: platelets are essential for preserving vascular barrier function in the absence of injury or inflammation. *Proc Natl Acad Sci USA.* 2020; 117(39):24316-24325.

61. Deppermann C. Platelets and vascular integrity. *Platelets.* 2018;29(6):549-555.

62. Claushuis TAM, de Vos AF, Nieswandt B, et al. Platelet glycoprotein VI aids in local immunity during pneumonia-derived sepsis caused by gram-negative bacteria. *Blood.* 2018;131(8):864-876.

63. Grommes J, Alard JE, Drechsler M, et al. Disruption of platelet-derived chemokine heteromers prevents neutrophil extravasation in acute lung injury. *Am J Respir Crit Care Med.* 2012;185(6):628-636.

64. Heinzmann ACA, Karel MFA, Coenen DM, et al. Complementary roles of platelet $\alpha_{IIb}\beta_3$ integrin, phosphatidylserine exposure and cytoskeletal rearrangement in the release of extracellular vesicles. *Atherosclerosis.* 2020;310:17-25.

65. Sekhon UDS, Swingle K, Girish A, et al. Platelet-mimicking procoagulant nanoparticles augment hemostasis in animal models of bleeding. *Sci Transl Med.* 2022; 14(629):eabb8975.

66. Millington-Burgess SL, Harper MT. Maintaining flippase activity in procoagulant platelets is a novel approach to reducing thrombin generation. *J Thromb Haemost.* 2022;20(4):989-995.

67. Yuan Y, Alwis I, Wu MCL, et al. Neutrophil macroaggregates promote widespread pulmonary thrombosis after gut ischemia. *Sci Transl Med.* 2017;9(409):eaam5861.

68. Althaus K, Marini I, Zlamal J, et al. Antibody-induced procoagulant platelets in severe COVID-19 infection. *Blood.* 2021;137(8):1061-1071.

69. Chen M, Yan R, Zhou K, et al. Akt-mediated platelet apoptosis and its therapeutic implications in immune thrombocytopenia. *Proc Natl Acad Sci USA.* 2018;115(45):E10682-E10691.

70. Agbani EO, Williams CM, Li Y, et al. Aquaporin-1 regulates platelet procoagulant membrane dynamics and in vivo thrombosis. *JCI Insight.* 2018;3(10):99062.

71. Lax S, Rayes J, Wichaiyo S, et al. Platelet CLEC-2 protects against lung injury via effects of its ligand podoplanin on inflammatory alveolar macrophages inthe mouse. *Am J Physiol Lung Cell Mol Physiol.* 2017;313(6):L1016-L1029.

72. Rayes J, Watson SP, Nieswandt B. Functional significance of the platelet immune receptors GPVI and CLEC-2. *J Clin Invest.* 2019;129(1):12-23.

Procoagulant platelet sentinels prevent inflammatory bleeding through GPIIBIIIA and GPVI – Supplementary Information.

Rainer Kaiser[1,2*], Raphael Escaig[1,2], Jan Kranich[3], Marie-Louise Hoffknecht[1], Afra Anjum[1,2], Vivien Polewka[1], Magdalena Mader[1,2], Wenbo Hu[3], Larissa Belz[1], Christoph Gold[1,2], Anna Titova[1], Michael Lorenz[1], Stefan Kääb[1,2], Kami Pekayvaz[1,2], Florian Gaertner[1,2], Konstantin Stark[1,2], Thomas Brocker[3], Steffen Massberg[1,2] and Leo Nicolai[1,2*]

[1]Medizinische Klinik und Poliklinik I University Hospital Ludwig-Maximilian University, Munich, Germany
[2]DZHK (German Centre for Cardiovascular Research), partner site Munich Heart Alliance, Germany
[3]Institute for Immunology, Biomedical Center, Medical Faculty, Ludwig-Maximilian University Munich, 82152 Planegg-Martinsried, Germany

*Correspondence to rainer.kaiser@med.uni-muenchen.de and leo.nicolai@med.uni-muenchen.de, Medizinische Klinik und Poliklinik I, University Hospital Ludwig-Maximilian-University Munich, Marchioninistr. 15 81377, Munich, Germany.

Table of contents

Supplementary Methods

Mouse strains

C57BL/6J (Stock No: 000664, labeled Bl6 or wild-type/WT), PF4cre[1] and CypD$^{fl/fl}$ (Ppif^{tm1Mmos}/J, Stock No: 005737) mice were purchased from The Jackson Laboratory and maintained at our animal facility. The TMEM16F$^{fl/fl}$ line was provided by the RIKEN BioResource Center (BRC) through the National BioResource Project of the Ministry of Education, Culture, Sports, Science and Technology (MEXT)/Agency for Medical Research and Development (Japan)[2,3]. Arpc2$^{fl/fl}$ were gifts from Rong Li and the Wellcome Trust Sanger Institute, respectively. All strains used in this study were backcrossed to C57BL/6J background. Mice of both sexes were used for *in vitro* studies and tail bleeding assays. For acute lung injury, intraperitoneal sepsis and mesentery live imaging models, female mice were used, while male mice were used for the arterial thrombosis model. Unless otherwise stated, mice were 8 to 14 weeks of age when entering experiments.

Mouse anesthesia

Anesthesia was performed by intraperitoneal injection of medetomidine (0.5 mg/kg body weight), midazolam (5 mg/kg body weight) and fentanyl (0.05 mg/kg body weight, MMF) after initial induction with isoflurane. Anesthetized mice were kept on heating pads, where depth of anesthesia was monitored by toe pinching reflexes and breathing patterns. To maintain narcosis, repeated s.c. injections of 25-50% of the induction dose was applied.

Intraperitoneal sepsis model and evaluation of peritoneal bleeding

Mice were injected with 1 mg/kg BW LPS intraperitoneally and clinically scored for four to six hours. Subsequently, mice were sacrificed, and blood and organs were collected for flow cytometric and histopathological analysis. To assess the impact of thrombocytopenia and neutrophil depletion on peritoneal hemorrhage, mice were injected with a platelet-depleting antibody (R300, emfret, 100 µg per mouse) intravenously, a neutrophil-depleting antibody (UltraLeaf anti-Ly6G, Biolegend, 100 µg per mouse) intraperitoneally 12 hours prior to NaCl or LPS administration. Depletion efficiency was analyzed by flow cytometry and automated cell counting. For assessment of inflammatory bleeding in the peritoneal cavity, mice were sacrificed and 8 ml of PBS containing 5% BSA and 0.25 mM EDTA were instilled using a 26G needle after careful incision of the abdominal skin. A 20G needle was used to collect as much peritoneal lavage fluid as possible. Inflammatory bleeding and leukocyte infiltration were subsequently assessed by flow cytometry and immunofluorescence staining.

Tail bleeding assay

Mice were anesthetized as described above. Hereafter, 5 mm of the distal tail was resected using a precision scissor (MST) and the tail was immediately placed in 40 ml PBS (room temperature). Bleeding and re-bleeding times were recorded for 20 min. Bleeding was further quantified by using an automated cell counter to assess hemoglobin content.

$FeCl_3$-induced arterial thrombosis (A. carotis)

Ferric chloride-induced arterial thrombosis was performed as previously described[4]. In brief, male mice were anaesthetized and a DyLight 488-conjugated Gp1b antibody (X488, emfret, 50 µl) was injected into the tail vein. Next, the right carotid artery was surgically exposed, and a small filter paper (0.5 mm^2) saturated with $FeCl_3$ solution (10%, Sigma Aldrich) was placed touching the proximal end of the exposed carotid proportion. The filter paper was removed after 3 min and the forming thrombus was visualized using a fluorescence microscope (AxioScope, Carl Zeiss), with images taken every 10 sec. After 30 min, the carotid containing the thrombus was retrieved for histological analysis.

GPVI depletion *in vivo*

For platelet-specific depletion and shedding of the collagen receptor GPVI, mice were injected with 100 µg of anti-GPVI antibody (clone JAQ1, emfret) i.p. Isotype-injected animals were used as controls. Subsequent experiments were initiated after 72 hours, when GPVI depletion remained sufficient and transient thrombocytopenia had resolved[5]. Efficacy of GPVI depletion was assessed by flow cytometric measurement of surface GPVI expression compared to isotype-treated animals as well as in platelet activation assays and flow cytometric measurement after stimulation with GPVI-specific agonist collagen and convulxin. Only animals with sufficient GPVI depletion were included in the respective experiments and analyses.

Platelet and neutrophil depletion *in vivo*

To deplete platelets, Bl6 mice were injected with 100 µg of an anti-Gp1b antibody (R300, emfret) i.v. immediately before or 12 hours prior to performing acute lung injury and peritoneal inflammation experiments, respectively. A non-immunogenic antibody mix (C301, emfret) was used as isotype control. For neutrophil depletion, 100 µg of an anti-Ly6G antibody (UltraLeaf anti-Ly6G, clone 1A8, Biolegend) were injected i.p. 12 hours prior to induction of LPS-mediated peritoneal inflammation; an isotype (UltraLeaf rat anti-mouse IgG2a, Biolegend, 100 µg) was used as control. Depletion efficiency of both platelets and neutrophils was assessed by flow cytometry.

Antibodies and fluorescence-coupled proteins for flow cytometry and histopathology

Antibodies and other fluorescent proteins or peptides are listed in Suppl. Table 1. Antibodies were used 1:100 for flow cytometric analysis unless otherwise stated. Secondary antibodies used for histopathology and immunofluorescence stainings were used 1:200. For previously unused antibodies in our lab, isotype control stainings were performed to ensure staining specificity. In addition to using fluorescence-coupled annexin V, Ca^{2+}-independent PS-staining reagent consisting of biotinylated C1 domains of murine lactadherin that have been multimerized using Strepatvidin. These C1 multimers (C1) were used for the detection of procoagulant platelets *in vitro* and *in vivo* and are commercially available through Biolegend (see above) and have been described by our group[6]. For the detection of caspase 3/7 activation in procoagulant platelets, the CellEvent kit (ThermoFisher, # C10423) was used (final concentration 20 µM). FITC: fluorescein isothiocyanate, PE: phycoerythrin, APC: allophycocyanin, AF: AlexaFluor, PB: pacific blue, BV: brilliant violet.

Multiplex cytokine measurements

Cytokine levels of murine plasma and BAL fluid sampled shown in Suppl. Figure 1D were assessed using the LEGENDplex™ Mouse Inflammation Panel (13-plex (Biolegend, #740446) according to the manufacturer's instructions. Samples were measured on a BD LSRFortessa flow cytometer and resulting MFIs were analyzed using the LEGENDplex™ Data Analysis Software Suite to assess approximate cytokine concentrations.

Human blood donors

Female and male volunteers aged 21 to 45 years served as donors for the isolation platelets, plasma samples or whole blood flow cytometry or thrombus formation experiments. All experiments involving human subjects are approved by a local ethical review board (LMU Munich), complying with any relevant regulation for experiments involving human samples.

Human and mouse platelet isolation

Human blood was drawn by venipuncture of the cubital into syringes containing acid-citrate dextrose (39 mM citric acid, 75 mM sodium citrate, 135 mM dextrose; ACD, 1/7 volumes) and immediately diluted 1:1 with modified Tyrode's buffer (137 mM NaCl, 2.8 mM KCl, 12 mM $NaHCO_3$, 5.5 mM sucrose, 10 mM HEPES, pH = 6.5). For mouse platelet isolation, all animals were anesthetized, and blood was subsequently collected by introduction of a glass capillary into the retroorbital vein plexus into 1/7 volumes of ACD followed by 1:1 dilution into Tyrode's buffer, pH 6.5. Both human and murine samples were subsequently centrifuged with 70g for 35 or 15 min, respectively, to generate platelet-rich plasma (PRP). To isolate platelets, PRP was diluted 1:2 in modified Tyrode's buffer supplemented with PGI_2 (0.1 mg/ml) and either albumin (0.1%) or casein (0.01%), and subsequently centrifuged for 5-10 min at 1000g. After

resuspending the pellet in Tyrode's buffer, platelet counts were assessed using a Sysmex XN-V Series XN-1000V cell counter. Platelet-poor plasma (PPP) was generated by centrifugation of PRP for 5 min at 14,000g.

Inhibitors and agonists

Cyclosporin A (#30024), niflumic acid (#N0630), Ru360 (#557440), Synta66 (SML1949), Thrombin (#T4648), E. coli-derived LPS O111:B4 (#L2630), adenosin diphosphate (ADP, #01905) and mP6 (#5098840001) were purchased from Sigma and MerckMillipore. The PAR4 inhibitor BMS-986120 was purchased from CaymanChem (#23497). All other inhibitors used and mentioned in Supplemental Data are described in detail by Nicolai et al.[4] The Syk inhibitor BI-1002494 and a control compound, BI-2492, were gifts from Boehringer Ingelheim. Clinical-grade tirofiban, enoxaparin and argatroban were purchased from ibigen, Sanofi-Aventis and Mitsubishi Pharma, respectively.

Chemicals

Horm collagen was purchased from Takeda (#1130630). Casein, human serum albumin, hexamethyldisilazane (HMDS), paraformaldehyde (PFA) and glutaraldehyde (GDA) were purchased from Sigma. Prostacycline (PGI_2) was ordered from abcam. Unconjugated and AF546- or AF488-conjugated fibrinogen as well as the calcium-binding compound Fluo-4 (#F14201) were acquired from ThermoFisher.

Migration and retraction assays

Isolated mouse and human platelets were diluted to a concentration of 150,000 – 200,000/µl. $4x10^6$ platelets were subsequently activated by the addition of 4 µM ADP, 2 µM U46619 and 1 mM calcium chloride, pipetted into pre-coated custom chambers and incubated for 15 min at 37°C. Hereafter, non-adherent cells were removed by three washing steps with cell-free wash buffer containing 1 mM calcium chloride and antibodies and/or compounds for detection of platelets and respective activation markers. After 30-60 min, cells were fixated with fixation mix containing 2% PFA and 0.005% GDA. Samples were imaged using either an epifluorescence (Olympus IX83 microscope) or a Zeiss LSM 880 confocal microscope. Per biological replicate, 5-6 random images were acquired. For live imaging of calcium oscillations, both murine and human isolated platelets were loaded with 1 µM Fluo-4 and allowed to seed for 15 min, washed three times and subsequently incubated for 10-15 minutes before imaging. Phase contrast, calcium oscillations and PS exposure were acquired every 10 seconds. In some instances, human PRP was loaded with 1 µM Fluo-4 for 20 min in the dark before centrifugation and isolation of washed platelets.

Live imaging of platelet migration, PS exposure and calcium signaling

Time-lapse video microscopy was performed using an inverted Olympus IX83 microscope with a 40x/1.0 or a 100x/1.4 oil-immersion objective and included recording of differential interference contrast (DIC), phase-contrast, and epifluorescence movies (5-20 s/frame). A pre-heated stage incubator (Tokai Hit) was used to mimic physiological conditions (humidified, 37°C). For live-imaging of calcium oscillations, human or murine PRP was loaded with 1 µM Fluo-4 (ThermoFisher) for 15 min at RT in the dark. Intensities of calcium oscillations and PS exposure were measured using Fiji ImageJ and quantified in a cell-based manner.

Thrombin turnover assay

Isolated mouse or human platelets were activated and left migrating on a collagen I/HSA/fibrinogen matrix as described above. After 15 min of migration, media were replaced by a solution containing PPP (20%) and a fluorescent thrombin substrate (13.3 µM final concentration, SensoLyte® 520 Thrombin Activity Assay Kit, Anaspec, #AS-72129) as well as an antibody against CD41 or CD42b and the C1 multimer to distinguish procoagulant from non-procoagulant platelets. Thrombin turnover was assessed by confocal imaging (Zeiss LSM 880). Thrombin positivity and procoagulant activation were assessed for at least 100 platelets from at least n = 2 individual mice and analyzed using Fiji ImageJ.

Pharmacological inhibition of platelet pathways and receptors

For testing of pathways involved in procoagulant activation of migrating and spreading platelets, inhibitors were added to the third and final washing step after platelets had adhered to the respective coating. Concentrations varied according to the compound used and are indicated in the respective figures and figure legends, with various concentrations being tested for all compounds (data not shown). In some cases (e. g. treatment with ciclosporine A), platelets were incubated with the respective compound or antibody for 15 min before being added to custom chambers. In case of dual receptor inhibition (e. g. GPIIBIIIA and GPVI), identical concentrations of individual compounds were used.

Platelet activation assay

Activation of platelets in suspension was performed as described previously[4]. In brief, isolated human or murine platelets suspended in modified Tyrode's buffer with 1 mM calcium chloride were incubated with fluorescent antibodies against platelet activation markers P-selectin, activated GPIIBIIIa and PS – among others – and activating agents targeting $P2Y_{12}$, thrombin receptors PAR2/4 (thrombin), GPVI (convulxin, collagen) and the thromboxane receptor TXA_2-R (U46119) for 30 min at RT or 37°C (concentrations indicated in the respective figures). Platelets were subsequently fixated with 1% PFA for 10 min in the dark, before being measured

on a BD LSRFortessa flow cytometer. Gating strategies are found in Suppl. Figure 9. Gating of subpopulations as well as MFI analyses were performed using FlowJo (v10).

Immunofluorescence staining

Platelets were fixated with fixation mix (PFA 2%, GDA 0.05%) for 10 min and subsequently stained using primary and secondary or primary-labelled antibodies in PBS containing 1% BSA for 1 h in the dark. In between primary and secondary antibodies as well as prior to imaging, platelets were washed three times with 1% BSA-containing PBS. Imaging was performed using a Zeiss LSM 880 confocal microscope in Airyscan mode (40/1.3 and 63/1.3 oil immersion objective).

Histopathological staining and analysis

For immunofluorescence and histopathological stainings, organs were first fixated in 4% PFA for 1 h at RT, dehydrated in 30% sucrose at 4°C overnight, cryoembedded and stored at either -80°C (long term storage) or -20°C (if processing was immediate). Organs were cut into 10 µm thick slices using a cryotome, fixated with 4% methylene-free PFA in PBS and subsequently permeabilized and blocked (10% goat serum, 0,5% saponin and 1% BSA in PBS). Samples were then stained using primary antibodies against TER119, Ly6G, CD42b, fibrinogen and phosphatidylserine as well as Hoechst dye to counterstain nuclei. Stained samples were imaged in Airyscan Super Resolution (SR) mode (20x/0.8 objective) on a Zeiss LSM 880 confocal microscope at 0.6x magnification. Random areas were acquired by focusing on nuclei without prior assessment of either bleeding or neutrophil infiltration to ensure objective measurement. Neutrophil and platelet recruitment were assessed using a custom-made macro in Fiji ImageJ, which uses a neutrophil- or platelet-specific size range to identify individual cells. Pulmonary hemorrhage as defined by extravascular TER119-positive areas was measured after thresholding and exclusion of intravascular erythrocytes from the image.

Data collection and visualization

Data from *in vivo* and *in vitro* live imaging experiments were collected using Fiji ImageJ[7]. For 4D *in vivo* timelapse microscopy, dimensions were reduced by maximum intensity projection. Assessment of motility patterns of platelets were defined as described by Nicolai *et al.*[4]. Migrating platelets from *in vitro* migration assays were tracked using the Fiji Manual tracking plugins, and were analyzed for directionality, velocity and acquired distance using the Chemotaxis Tool (ibidi) plugin. Shape analysis *in vitro* including platelet area, circularity and filopodia formation was performed described previously[4]. *In vivo*, motility patterns were defined as adherence, if platelets showed no distinguishable displacement over a duration of three acquired frames, leukocyte-dependent movement for platelets that showed movement while

in direct contact with CD45+ leukocytes and/or Ly6G+ neutrophils, respectively, and migration for movement of platelets along the vessel wall without contact to leukocytes and with displacement of at least one cell diameter during image acquisition. Procoagulant platelets were defined as CD42b-positive, balloon-like shapes that were platelet-like in size and stained positive for phosphatidylserine as assessed by Annexin V or mC1 multimer staining (see Figure 2B, C, Suppl. Figure 2A-E and Suppl. Video 1). Procoagulant platelets were counted as fibrinogen-positive if they exhibited an overlap between PS and fibrinogen channels (see Figure 2E, F, with yellow indicating channel overlap). In some cases, a line was manually drawn across a multi-channel image and MFIs of the respective fluorescence channels were analyzed and plotted using Fiji "plot profile" function. In *in vitro* migration assays that were imaged after fixation of cells, platelets were counted either in DIC/PH channels or a CD41 fluorescence channel. Platelets were defined as "migrating", if they had moved by at least one cell diameter as assessed by migration tracks in the fibrinogen channel. Procoagulant platelets were defined as having undergone morphological changes (ballooning, procoagulant spreading) and exposing PS as detected by Annexin V or C1 staining. In live imaging experiments, procoagulant platelets were considered positive for supramaximal calcium bursts if contact to collagen resulted in a calcium peak corresponding to at least 95% of the maximum fluorescence intensity. The cleared fibrinogen area, a surrogate for migration length, was analyzed by measuring the fibrinogen-negative area channel using Gaussian blur and thresholding in the fluorescent fibrinogen channel. Gaussian blurring, thresholding and area measurement were performed using a custom Fiji macro. For analysis of calcium oscillations of migrating platelets, measured Fluo-4 intensities and AnnV/C1 binding were normalized to 1) background fluorescence and 2) to % of maximum intensity to allow for comparison of live imaging videos collected at different days. In flow cytometry experiments, counting beads were used to normalize cell counts in both blood and BALF samples to counts per microliter of the respective sample. Individual graphs were generated using Prism v9 (Graphpad) and figures were generated using Illustrator 2021 (Adobe). Experimental schemes and the graphical abstract were designed using BioRender (www.biorender.com).

Statistical analysis

Data were analyzed using Prism v9 (Graphpad), Excel v16 (Microsoft) and FlowJo v10 (BD) and are visualized as mean ± standard deviation (SD); in selected graphs, data are depicted as SuperPlots[8], with single dots representing the single data points measured per replicate and error bars representing the SD of the mean from biological replicates. Unless otherwise stated, all data shown include at least three biological replicates, with at least 5-6 randomly taken, individual images underlying each biological replicate data point for imaging studies. Representative images or flow cytometry plots were chosen according to the mean value

represented in the respective data set. We estimated animal sample sizes according to power calculations performed when ethical approval of planned experiments was applied for. All experimental groups were matched according to age and sex of the respective mouse lines. Statistical differences between experimental groups were assessed using t-tests and analyses of variance (ANOVA) as stated in the respective figure legends. In experiments with uneven sample sizes across groups (e. g. due to death of animals in one experimental group), normality distribution of acquired data was ensured using Shaprio-Wilk tests prior to further statistical testing. Unless otherwise stated, experiments including more than two groups were tested using one-way ANOVA with post-hoc Holm-Šídák's multiple comparisons test compared to control groups. If different experimental conditions were assessed on the same biological replicate, paired t-tests were used; in all other cases unpaired t-testing was performed. All t-tests were two-sided. Across all statistical tests, a p-value of <0.05 was considered statistically significant; p-values were marked by asterisks as follows: * <0.05, ** <0.01, *** <0.005, **** <0.001, ns = non-significant. If no asterisks are indicated, there is no statistical difference between treatment groups.

Supplementary Tables

Suppl. Table 1: Antibodies and fluorescent proteins

Protein/epitope	Fluorophore	Target species	Manufacturer	Order #
act. CD42b (JonA)	PE	mouse	emfret	M023-2
Annexin V	FITC	-	Biolegend	640906
Annexin V	AF649	-	Biolegend	640912
Anti-mouse IgG	Cy3	mouse	Invitrogen	A10521
Anti-rabbit IgG	AF546	rabbit	Invitrogen	A11037
Anti-rabbit IgG	AF649	rabbit	Invitrogen	A21244
Anti-rat IgG	AF488	rat	Invitrogen	A21208
Anti-rat IgG	AF546	rat	Invitrogen	A11007
C301	-	mouse	emfret	C301
CD107a	BV785	mouse	Biolegend	328643
CD11b	BV605	human	Biolegend	101237
CD144	AF649	mouse	Biolegend	138006
CD15	APC	human	Biolegend	323008
CD31	AF649	mouse	Biolegend	102516
CD36	PE	mouse	Biolegend	102605
CD41	Pacific blue	human	Biolegend	303714
CD41	AF700	mouse	Biolegend	133926
CD42b	FITC	mouse	emfret	X488
CD42b	DyeLight-649	mouse	emfret	X649
CD42b	-	mouse	abcam	ab183345
CD44	AF700	mouse	Biolegend	103026
CD45	BV650	human	Biolegend	304044
CD45	PerCp-Cy5.5	mouse	Biolegend	103132
CD9	PE/Dazzle™ 594	mouse	Biolegend	124821
EpCAM	PE-Cy7	mouse	Biolegend	118216
Fibrinogen	-	-	BioRad	4440-8004
Fibrinogen	AF546	-	ThermoFisher	F13192
Fibrinogen	AF488	-	ThermoFisher	F13191
GPVI (JAQ1)	FITC	mouse	emfret	M011-0
Gr-1	AF488	mouse	Biolegend	108417
Hoechst Dye	-	-	ThermoFisher	H3570

Hoechst Dye	-	-	ThermoFisher	H3570
IgG2a (Ultra-LEAF™)	-	-	Biolegend	400565
Ly6G	PE	mouse	Biolegend	127608
Ly6G	PB	mouse	Biolegend	127612
Ly6G	BV711	mouse	Biolegend	127643
Ly6G (Ultra-LEAF™)	-	mouse	Biolegend	127649
mC1 multimer	Cy3	-	-	TBD
mC1 multimer	AF649	-	-	TBD
PAC-1	AF649	human	Biolegend	362806
P-selectin	BV421	human	Biolegend	304926
P-selectin	PE-Cy7	mouse	Biolegend	148310
P-selectin	PE	human	Biolegend	304905
Phosphatidylserine	-	-	Merck	05-719
R300	-	mouse	emfret	R300
Streptavidin	AF649	-	Biolegend	405237
Streptavidin	Cy3	-	Biolegend	405215
TER119	PE	mouse	Biolegend	116208
TER119	AF488	mouse	Biolegend	116215
Thrombin	5-FAM/QXL™ 520	-	Anaspec	AS-72129

Suppl. Table 2: Relative comparison of inflammatory bleeding severity

Mouse line/inhibitor	**Mean bleeding (% relative to LPS-treated control, ±SD)**
Platelet depletion (R300)	11093.89 ± 674.16
Argatroban (anti-FIIa)	160.76 ± 19.17
Rivaroxaban (anti-FXa)	146.69 ± 35.85
Enoxaparin (anti-FXa)	307.29 ± 70.21
PF4cre-CypD (Cre+)	287.30 ± 59.29
PF4cre-TMEM16F (Cre+)	473.21 ± 81.99
JAQ1 (anti-GPVI)	57.63 ± 22.19
Tirofiban (anti-GPIIBIIIA)	122.16 ± 42.24
JAQ1 + Tirofiban	162.39 ± 9.02
negative ctrl (NaCl i.n.)	5.90 ± 10.43

Supplementary Figure legends

Suppl. Figure 1: Anticoagulation aggravates inflammatory bleeding. | (A) Experimental scheme of subacute lung injury model, comparing intranasal LPS challenge (black arrow) with sham-treated animals. (B) Representative macroscopic image of BALF derived from experimental groups, collected in 2 ml Eppendorf tubes. (C) Flow-cytometric assessment of BALF RBC, neutrophil, platelet and platelet-neutrophil aggregate counts. n=4 animals per experimental group. Student's t-test, two-tailed, unpaired. (D) Quantification of cytokine measurements from plasma and BALF of sham- and LPS-treated animals collected 24 h hours after treatment. Two-way ANOVA with Holm-Šídák's multiple comparisons test. (E) Quantification of alveolar hemorrhage ($TER119^+$ area) and neutrophil recruitment in control (C301) and thrombocytopenic animals (R300) after LPS-induced lung injury, corresponding to Figure 1A-D. Student's t-test, two-tailed, unpaired. (F) Experimental scheme of subacute lung injury model with or without enoxaparin (ENOX)-mediated anticoagulation (s.c. injections of 10 mg/kg BW enoxaparin 0 and 6 hours (red arrows) after LPS challenge (black arrow)). (G) Representative macroscopic image of BAL fluid derived from experimental groups, collected in 2 ml Eppendorf tubes. (H) Flow-cytometric assessment of BALF RBC and leukocyte counts. Student's t-test, two-tailed, unpaired. (I) Clinical scores of individual animals for 24 h after LPS challenge treated with Rivaroxaban, Argatroban or vehicle. Sepsis scores contain appearance, activity, responsiveness and breathing patterns. One-way ANOVA with post-hoc Holm-Šídák's multiple comparisons test. (J) Flow-cytometric assessment of peripheral blood platelet and leukocyte counts as well as procoagulant platelets and platelet-neutrophil aggregates (PNA) post-treatment. One-way ANOVA with post-hoc Holm-Šídák's multiple comparisons test. (K) Quantification of platelet recruitment and platelet-neutrophil aggregate (PNA) formation per mm^2 lung, referring to Figure 1J-O. (L) Representative micrographs from immunofluorescence stainings of lung slices from mice treated with vehicle or 10 mg/kg BW enoxaparin. Scale bar 25 µm. (M) Quantification of alveolar hemorrhage ($TER119^+$ area), neutrophil and platelet recruitment. Student's t-test, two-tailed, unpaired. (N) Representative micrographs of migrating human platelets treated with vehicle, rivaroxaban (10 µg/ml) or argatroban (10 µg/ml). Scale bar 10 µm. (O) Quantification of % migrating platelets and the absolute cleared area per cell in $µm^2$ from n = 3 healthy individuals. One-way ANOVA with post-hoc Holm-Šídák's multiple comparisons test.

Suppl. Figure 2: The C1 multimer detects procoagulant platelets *in vitro* and *in vivo*. | (A) Representative micrograph of migrating human platelets stained with antibodies/compounds against CD42b (white) and phosphatidylserine (C1, red, and Annexin V, green). Scale bar 10 µm. (B) Quantification of PS staining positivity by C1 and Annexin V, n = 3 individual donors. Student's t-test, paired, two-tailed. (C) Quantification of % procoagulant

platelets (detected by C1 multimer) and AnnV MFI of human platelets after stimulation with indicated agonists. One-way ANOVA with with post-hoc Holm-Šídák's multiple comparisons test, compared to Ctrl. (D) Correlation of C1 MFI with AnnV MFI and CD41 MFI of human platelets from the same experiment. P-value of linear regression analyses indicates significantly non-zero. (E) Representative scatter plots of human platelets from the same experiment to identify procoagulant platelets in response to thrombin/convulxin dual stimulation with C1 (left panels) and AnnV (right panels), respectively. (F) Experimental scheme and micrographs of 4D live microscopy of an inflamed mesenteric venule, corresponding to Suppl. Video 1. Dashed lines indicate the vessel wall. PS staining: mC1. Scale bar 5 µm. (G) Representative micrograph and quantification of procoagulant platelet recruitment and overlap of fibrinogen/PS/platelet positive areas. n = 3-4 animals corresponding to Figure 1G, H. PS staining: anti-PS antibody (Merck). Student's t-test, two-tailed, unpaired. (H) Experimental scheme of peritoneal inflammation model with or without depletion of platelets and/or neutrophils through antibody injection (red arrow) 12 hours prior to NaCl or LPS injection i.p. (black arrow). (I) Representative image of peritoneal lavage fluid for indicated, LPS-treated experimental groups, contained in 15 ml collection tubes. (J) Flow cytometry-based quantification of peripheral platelet and neutrophil counts to confirm cell-specific depletion. One-way ANOVA with post-hoc Holm-Šídák's multiple comparisons test, compared to LPS-treated Isotype control group. (K) Flow cytometry-based quantification of peritoneal lavage RBC and leukocyte counts as well as % of neutrophils among peritoneal leukocytes. One-way ANOVA with post-hoc Holm-Šídák's multiple comparisons test, compared to LPS-treated Isotype control group. (L) Quantification of $TER119^{+}$ area in μm^2 and representative immunofluorescence images of mesenteric sections of thrombocytopenic mice i.p.-injected with NaCl (left panel) as well as LPS-challenged isotype- and R300-treated animals (center and right panels). White arrowheads indicate extravascular microbleeding. One-way ANOVA with post-hoc Holm-Šídák's multiple comparisons test, compared to LPS-treated Isotype control group. Scale bar 100 µm. (M) Quantification and representative immunofluorescence imaging of intravascular fibrin(ogen) deposition in mesenteric vessels of LPS-challenged animals treated with isotype or anti-Ly6G antibody. Student's t-test, two-tailed, unpaired. Scale bar 25 µm. (N) Representative micrograph of the mesenteric vasculature, corresponding to Figure 2J. Scale bar 20 µm.

Suppl. Figure 3: Supporting data migration assay (I). | (A) Representative images from migration assays of both Cre-positive and -negative murine platelets isolated from PF4cre-$Arpc2^{fl/fl}$ animals. White arrowheads indicate migrating platelets turning procoagulant. Scale bar 10. (B) Quantification of procoagulant activation from mouse platelets seeded on fibrinogen or collagen I mono-coatings. Student's t-test, unpaired, two-tailed. (C) Flow-cytometric

quantification of relative MFIs of P-selectin expression, GPIIBIIIA integrin activation and PS exposure (mC1) by both Cre-positive and -negative murine platelets isolated from PF4cre-Arpc2$^{fl/fl}$ animals after exposure to indicated agonists. Two-way ANOVA with post-hoc Holm-Šídák's multiple comparisons test, compared to PBS control group. (D) Representative scatter plots of flow cytometry experiments with isolated murine WT platelets incubated with PBS or collagen I; quantification of P-selectin-positive platelets and PS MFI (mC1) for platelets from n=4 mice. Student's t-test, unpaired, two-tailed. (E) Relative quantification of procoagulant platelet formation in the presence or absence of fibrinogen after stimulation with PBS, collagen I or convulxin and thrombin. Human platelets from n = 4 healthy donors. One-way ANOVA. (F) Relative quantification of fibrinogen-positive platelets and absolute quantification of mean fluorescence intensities (MFIs) of platelet-bound fibrinogen-AF488 after stimulation with PBS, collagen or convulxin and thrombin. Right panel: representative scatter plots. Human platelets from n = 4 healthy donors. One-way ANOVA with post-hoc Holm-Šídák's multiple comparisons test, compared to PBS control group. (G) Relative quantification of procoagulant platelet activation and cleared area from n=3 migration assays with human platelets incubated with PBS or a combination of Cangrelor (0.25 µM), Terutroban (1 µg/ml), and Vorapaxar (1 µM). Student's t-test, unpaired, two-tailed. (H) Quantification of procoagulant platelet activation and cleared area from n=4 migration assays with human platelets incubated with PBS, PAR1 inhibitor Vorapaxar (1 µM), PAR4 inibitor BMS-986120 (1 µM) or a combination of both inhibitors. One-way ANOVA with post-hoc Holm-Šídák's multiple comparisons test, compared to PBS control group. (I, J) Representative micrographs of migrating human platelets on a hybrid matrix. Red (anti-Fbg antibody, anti-Sheep secondary antibody coupled to AF649) indicates all fibrin(ogen), including endogenous (platelet-inherent) and exogenous (Fbg-AF488, used for coating) fibrin(ogen); yellow indicates overlap of both channels. The arrowhead indicates overlap of both stainings, the white star indicates red-only and thus endogenous fibrin(ogen) deposition next to a procoagulant platelet. PS-detecting agent: C1-Cy3. Scale bars 20 µm (I), 2 µm (J).

Suppl. Figure 4: Validation of PF4cre-CypD$^{fl/fl}$ and PF4cre-TMEM16F$^{fl/fl}$ mouse lines. | (A) Baseline quantification of body weight and peripheral platelet, RBC and leukocyte counts of PF4cre-CypD$^{fl/fl}$ mice, n=4 per Cre-positive/-negative animals. Student's t-test, unpaired, two-tailed. (B) Flow-cytometric analysis of baseline expression of several platelet receptors from isolated platelets. n=4 per Cre-positive/-negative animals of the PF4cre-CypD$^{fl/fl}$ mouse line. Two-way ANOVA. (C) Flow-cytometric quantification of absolute MFIs of P-selectin expression, GPIIBIIIA integrin activation and PS exposure (stained by C1) by both Cre-positive and -negative murine platelets isolated from PF4cre-CypD$^{fl/fl}$ animals after exposure to indicated agonists. n=4. Two-way ANOVA. (D) Baseline quantification of body weight and

peripheral platelet, RBC and leukocyte counts of PF4cre-TMEM16F$^{fl/fl}$ mice, n=3-4 per Cre-positive/-negative animals. Student's t-test, unpaired, two-tailed. (E) Flow-cytometric analysis of baseline expression of several platelet receptors from isolated platelets. n=4 per Cre-positive/-negative animals from PF4cre-TMEM16F$^{fl/fl}$ mice. Two-way ANOVA. (F) Flow-cytometric quantification of absolute MFIs of P-selectin expression and PS exposure (stained by C1) by both Cre-positive and -negative murine platelets isolated from PF4cre-TMEM16F$^{fl/fl}$ animals after exposure to indicated agonists. n=3-4. Two-way ANOVA. (G) Quantification of total bleeding time and time to first hemostasis of Cre-positive and -negative PF4cre-CypD$^{fl/fl}$ mice. n = 5-7 per group. Student's t-test, unpaired, two-tailed. (H) Quantification of total bleeding time and time to first hemostasis of Cre-positive and -negative PF4cre-TMEM16F$^{fl/fl}$ mice. n = 4-8 per group. Student's t-test, unpaired, two-tailed. (I) Analysis of arterial thrombosis experiments with PF4cre-CypD$^{fl/fl}$ mice (n = 7 for both Cre- and Cre+ mice) with quantification of time to first occlusion, % of vessel occlusion, maximum thrombus size as well as longitudinal assessment of % of occlusion-free vessels over time. (J) Representative images of carotid arteries from Cre+ and Cre- PF4cre-CypD$^{fl/fl}$ mice after 3 min of $FeCl_3$-induced injury at maximum thrombus size. Dashed lines represent vessel walls. Scale bar = 500 µm. (K) Analysis of arterial thrombosis experiments with PF4cre-TMEM16F$^{fl/fl}$ mice (n = 4-5 for both Cre- and Cre+ mice) with quantification of time to first occlusion, % of vessel occlusion, maximum thrombus size as well as longitudinal assessment of % of occlusion-free vessels over time. (L) Representative images of carotid arteries from Cre+ and Cre- PF4cre-TMEM16F$^{fl/fl}$ mice after 3 min of $FeCl_3$-induced injury at maximum thrombus size. Dashed lines represent vessel walls. Scale bar = 500 µm. (M) Representative micrographs of procoagulant activation of Cre-negative (left panels) and Cre-positive murine platelets (right panels) of PF4cre-TMEM16F$^{fl/fl}$ animals. PS staining: mC1. Scale bars 5 µm. (N) Cell-based quantification of the number of filopodia, number of released microvesicles and MFI of PS exposure of Cre-positive and -negative platelets isolated from PF4cre-TMEM16F$^{fl/fl}$ animals. Student's t-test, unpaired, two-tailed. (O) Representative micrograph of migrating and procoagulant mouse platelets that were co-stained for caspase activation using CellEvent™ Caspase-3/7 detection dye, showing caspase activation (red) in some procoagulant platelets. White arrowhead indicates a procoagulant, caspase-positive platelets, stars indicate migrating, caspase-negative platelets. Note that most procoagulant platelets are caspase-negative. Scale bar 20 µm. (P) Quantification of migrating and procoagulant mouse platelets for co-staining of PS (C1) and caspase activation. FOV-based quantification including 435 cells. One-way ANOVA with post-hoc Holm-Šídák's multiple comparisons test. (Q) Quantification of procoagulant activation and migratory capacity of platelets isolated from n = 3 WT mice with or without treatment with the pan-caspase inhibitor Q-VD-OPh (QVD, 50 µM). Student's t-test, unpaired, two-tailed. (R) Representative micrographs of migrating or procoagulant platelets:

migrating platelet from PF4cre mouse (Cre-positive, left panel), procoagulant platelet from PF4cre mouse (Cre-positive, center panel) and procoagulant platelet from PF4cre-TMEM16F$^{fl/fl}$ mouse (Cre-positive, left panel). PS staining: mC1. Scale bars 5 µm.

Suppl. Figure 5: Supporting data CypD/TMEM16F ALI experiments. | (A) BAL fluid neutrophil and platelet-neutrophil aggregate counts of PF4cre-CypD$^{fl/fl}$ animals 24 h after LPS challenge. Student's t-test, unpaired, two-tailed. (B) Peripheral platelet and leukocyte counts of PF4cre-CypD$^{fl/fl}$ animals 24 h after LPS challenge. Student's t-test, unpaired, two-tailed. (C) BAL fluid neutrophil and platelet-neutrophil aggregate counts of PF4cre-TMEM16F$^{fl/fl}$ animals 24 h after LPS challenge. Student's t-test, unpaired, two-tailed. (D) Peripheral platelet and leukocyte counts of PF4cre-TMEM16F$^{fl/fl}$ animals 24 h after LPS challenge. n = 4 animals per group. Student's t-test, unpaired, two-tailed.

Suppl. Figure 6: Supporting data mechanosensing and calcium imaging. | (A) Representative micrographs of isolated human platelets migrating on a fibrinogen/albumin matrix. Right panel: Representative calcium oscillations of migrating platelets. (B) Relative quantification of percentage of platelet procoagulant activation of all collagen-associated cells. Individual dots represent percentages derived from individual time-lapse microscopy videos. Platelets were isolated from n=2-3 mice per group. One-way ANOVA with post-hoc Holm-Šídák's multiple comparisons test. (C) Representative calcium (Fluo-4, green) and PS (mC1, pink) intensity profiles derived from live imaging of platelets from TMEM16F-deficient platelets. Arrows indicate the beginning of procoagulant activation after sensing collagen fibers, numbers indicate the time to supramaximal calcium plateau in seconds. (D) Quantification of time to calcium plateau for procoagulant platelets isolated from mice with indicated genotypes. n = 25 individual procoagulant platelets. One-way ANOVA with post-hoc Holm-Šídák's multiple comparisons test. (E) Representative micrographs of isolated platelets from CypD-deficient mice migrating on a fibrinogen/albumin/collagen I matrix, corresponding to Figure 6E. Scale bar 10 µm. (F) Quantification of procoagulant platelet activation and cleared area (as a proxy of migratory capacity) of human platelets treated with Synta66 (50 µM), Ru360 (50 µM) and BI-74932 (50 µM) to inhibit store-operated calcium entry (SOCE), mitochondrial calcium uniport and extracellular calcium influx, respectively. n = 3 healthy human donors. (G) Relative quantification of procoagulant platelet activation and cleared area per cell for human platelets (n=7) incubated with all the above calcium inhibitors (Synta66, Ru360 and BI-74932), normalized to untreated control platelets. Student's t-test, unpaired, two-tailed.

Suppl. Figure 7: Supporting data migration assay (II). | (A, B) Representative micrographs and quantification of migrating human platelets (n=3) on a hybrid collagen matrix with co-

staining of activated GPIIBIIIA by PAC-1 antibody. Arrowhead indicates migrating platelet with PAC-1 binding to the fibrin(ogen)-rich platelet's pseudonucleus. Note that only few procoagulant platelets bind PAC-1. Scale bar 20 µm. Student's t-test, unpaired, two-tailed. (C, D) Relative quantification of procoagulant platelets and cleared area from migration assays performed with human platelets from n = 3 healthy donors. Final concentrations for Ca^{2+} were 1 mM, unless calcium was depleted or not added to the assay. Inhibitor concentrations: PP2 20 µM, NSC27633 5 µM, U73122 10 µM, ML7 50 µM, Blebbistatin 1 µM. One-way ANOVA with post-hoc Holm-Šídák's multiple comparisons test compared to Ctrl group. (E) Representative micrographs of human platelets treated with the respective agonists/inhibitors, with the yellow outline indicative of the manual tracking of cell shape. Scale bar 3 µm. (F) Analysis of area, circularity and number of filopodia per platelet for n > 30 platelets per condition. One-way ANOVA with post-hoc Holm-Šídák's multiple comparisons test compared to control group. (G) Quantification of % migrating platelets and cleared area/platelet by murine platelets treated or not with 20 µM mP6. Student's t-test, unpaired, two-tailed. (H) Quantification of migrating platelets and cleared area/platelet by murine platelets treated or not with ascending concentrations of anti-GPVI antibody JAQ1. One-way ANOVA with post-hoc Holm-Šídák's multiple comparisons test compared to control group. (I) Quantification of migrating platelets and cleared area/platelet by murine platelets treated or not with ascending concentrations of Syk inhibitor BI-1002494. One-way ANOVA with post-hoc Holm-Šídák's multiple comparisons test compared to control group. (J) Quantification of migrating platelets, procoagulant activation and cleared area from migration assays with platelets from n = 3 human donors treated or not with the alpha2beta1 receptor inhibitor TC-I15 (10 µM). (K) Fluorescence microscopy image of migrating platelets, t = 16 min, corresponding to Figure 7D und Suppl. Video 3. PS staining: mC1. Scale bar = 10 µm. (L) Relative quantification of calcium amplitude of migrating platelets treated with vehicle, mP6 (20 µM) or BI-1002494 (2.5 µM). n=5-6 videos from n=2-3 mice per condition with a total of > 100 platelets were analyzed.

Suppl. Figure 8: Supporting *in vivo* and *in vitro* data for GPIIBIIIA and GPVI blockade. | (A) Representative confocal images of mouse platelets treated with isotype control and vehicle or JAQ1 (10 µg/ml) and tirofiban (1 µg/ml). PS staining: mC1. Scale bar = 10 µm. (B) Quantification of procoagulant platelet activation, migrating platelets and cleared area per platelet for indicated treatments. One-way ANOVA. (C) Representative scatter plots from flow cytometric measurements of isolated platelets from mice treated with the GPVI-blocking antibody JAQ1 or IgG2a isotype control (100 mg per animal injected i.p. 72 hours prior to platelet isolation). (D) MFIs for GPVI measured in platelets isolated from JAQ1- or IgG2a-treated Bl6 mice. Student's t-test, unpaired, two-tailed. (E) MFIs for PS (C1), P-selectin and activated GPIIBIIIA (JonA) after pre-incubation of human platelets with PBS or the GPIIBIIIA

antagonist tirofiban (1 µg/ml) and subsequent treatment with PBS or convulxin. One-way ANOVA. (F) Representative scatter plots from flow cytometric measurements of isolated human platelets after pre-treatment mit PBS or tirofiban and subsequent activation with convulxin. (G) Analysis of migrating platelets, procoagulant activation and cleared area of human platelets from n = 4 healthy human donors with or without tirofiban treatment (1 µg/ml). (H) Clinical scores of individual animals across treatment groups for 24 h after LPS challenge. Sepsis scores contain appearance, activity, responsiveness and breathing patterns. One-way ANOVA. (I) MFIs of several platelet receptors measured in whole blood of animals from treatment groups 24 h after LPS challenge. (J) MFI of GPVI in whole blood of mice from treatment groups 24 h after LPS challenge. One-way ANOVA. (K) Quantification of PNA formation in BAL fluid across treatment groups. One-way ANOVA. (L) Experimental scheme for peritoneal sepsis in Bl6 mice treated with JAQ1, a GPVI-blocking antibody, or isotype (red arrow) 72 hours prior to LPS challenge (black arrow) and vehicle or Tirofiban injections at 0 and 3 hours (red arrows) after LPS challenge. (M) Quantification of platelet GPVI expression, % procoagulant platelets and CD41 expression in whole blood across experimental groups (n=4). Student's t-test, two-tailed, unpaired. (N) Quantification of RBC and WBC counts as well as PNA formation in peritoneal lavage fluid (n=4). Student's t-test, two-tailed, unpaired. (O) Representative immunofluorescence stainings from mesenteric sections of control and JAQ1/tirofiban-treated animals, showing procoagulant (white arrowhead) and PS-negative platelets (white star) adherent to CD31-positive endothelium. Scale bar = 10 µm. (P) Quantification of platelet recruitment (number of all adherent vascular platelets) and % procoagulant platelets in mesenteric vessels of isotype/vehicle or JAQ1/tirofiban-treated animals after LPS administration (n=4). Student's t-test, two-tailed, unpaired. (Q) Representative immunofluorescence stainings from mesenteric sections of control and JAQ1/tirofiban-treated animals, revealing mesenteric microbleeding in dual blockade of GPVI and GPIIBIIIA (white arrowhead). Scale bar 50 µm. (R) Quantification of mesenteric microbleeding as assessed by extravascular RBC count per mm^2 mesentery. Student's t-test, two-tailed, unpaired. Holm-Šídák's multiple comparisons tests compared to control group were used for all one-way ANOVAs in this figure.

Suppl. Figure 9: Gating strategies for whole blood and BAL fluid. | (A) Representative scatter plots from whole blood with gating strategies for the identification of platelets, procoagulant platelets, leukocytes, neutrophils and neutrophil-platelet aggregates. MFIs were measured after gating for the respective population. (B, C) Representative scatter plots from BAL fluid with gating strategies for the identification of leukocytes, neutrophils and red blood cells. Peritoneal lavage samples (not shown) were gated according to the strategy shown in C.

Supplementary Video legends

Suppl. Video 1: Platelet procoagulant activation *in vivo*. 4D live microscopy of a mesentery venule. White: platelets, fire: PS exposure (mC1). Dotted lines indicate the vessel wall. Scale bar 10 µm.

Suppl. Video 2: Supramaximal calcium bursts prior to platelet ballooning and PS exposure of migrating platelets. Live microscopy of migrating human platelets on a hybrid albumin/fibrinogen/collagen I matrix. Phase contrast. Green: Fluo-4 (intracellular calcium oscillations), fire: PS exposure (AnnV). Scale bar 10 µm.

Suppl. Video 3: Calcium oscillations in migrating platelet pre-treated with mP6. Live microscopy of migrating human platelets on a hybrid albumin/fibrinogen/collagen I matrix. Phase contrast. Green: Fluo-4 (intracellular calcium oscillations), fire: PS exposure (mC1). Scale bar 10 µm.

Suppl. References

1. Tiedt R, Schomber T, Hao-Shen H, Skoda RC. Pf4-Cre transgenic mice allow the generation of lineage-restricted gene knockouts for studying megakaryocyte and platelet function in vivo. *Blood*. 2007;109(4):1503-1506.
2. Suzuki J, Fujii T, Imao T, Ishihara K, Kuba H, Nagata S. Calcium-dependent phospholipid scramblase activity of TMEM16 protein family members. *J Biol Chem*. 2013;288(19):13305-13316.
3. Fujii T, Sakata A, Nishimura S, Eto K, Nagata S. TMEM16F is required for phosphatidylserine exposure and microparticle release in activated mouse platelets. *Proc Natl Acad Sci U S A*. 2015;112(41):12800-12805.
4. Nicolai L, Schiefelbein K, Lipsky S, et al. Vascular surveillance by haptotactic blood platelets in inflammation and infection. *Nat Commun*. 2020;11(1):5778.
5. Schulte V, Rabie T, Prostredna M, Aktas B, Gruner S, Nieswandt B. Targeting of the collagen-binding site on glycoprotein VI is not essential for in vivo depletion of the receptor. *Blood*. 2003;101(10):3948-3952.
6. Rausch L, Lutz K, Schifferer M, et al. Binding of phosphatidylserine-positive microparticles by PBMCs classifies disease severity in COVID-19 patients. *J Extracell Vesicles*. 2021;10(14):e12173.
7. Schindelin J, Arganda-Carreras I, Frise E, et al. Fiji: an open-source platform for biological-image analysis. *Nat Methods*. 2012;9(7):676-682.
8. Lord SJ, Velle KB, Mullins RD, Fritz-Laylin LK. SuperPlots: Communicating reproducibility and variability in cell biology. *J Cell Biol*. 2020;219(6).

Suppl. Figure 1: Anticoagulation aggravates inflammatory bleeding

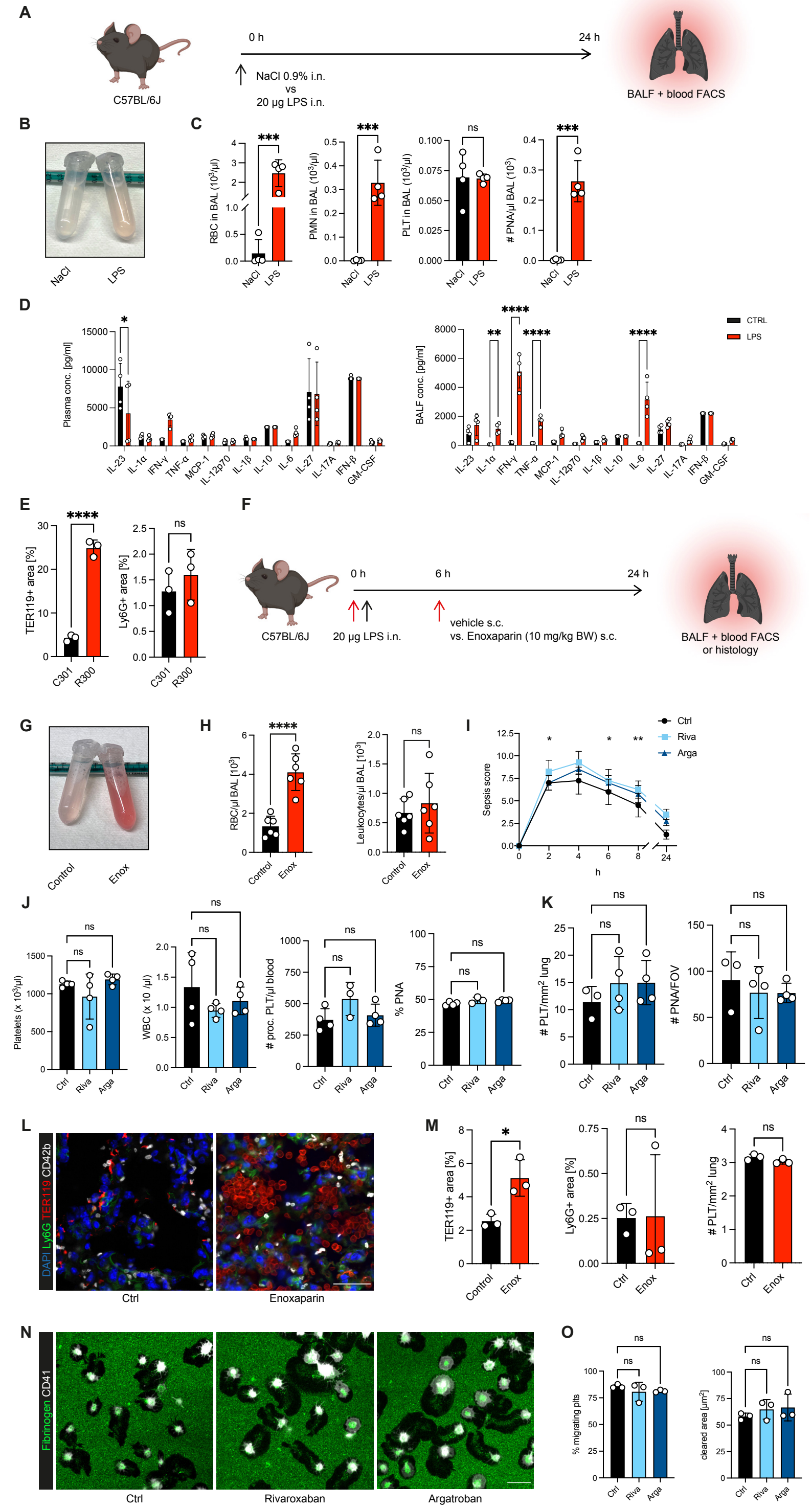

Suppl. Figure 2: The C1 multimer detects procoagulant platelets *in vitro* and *in vivo*

Suppl. Figure 3: Supporting data migration assay (I)

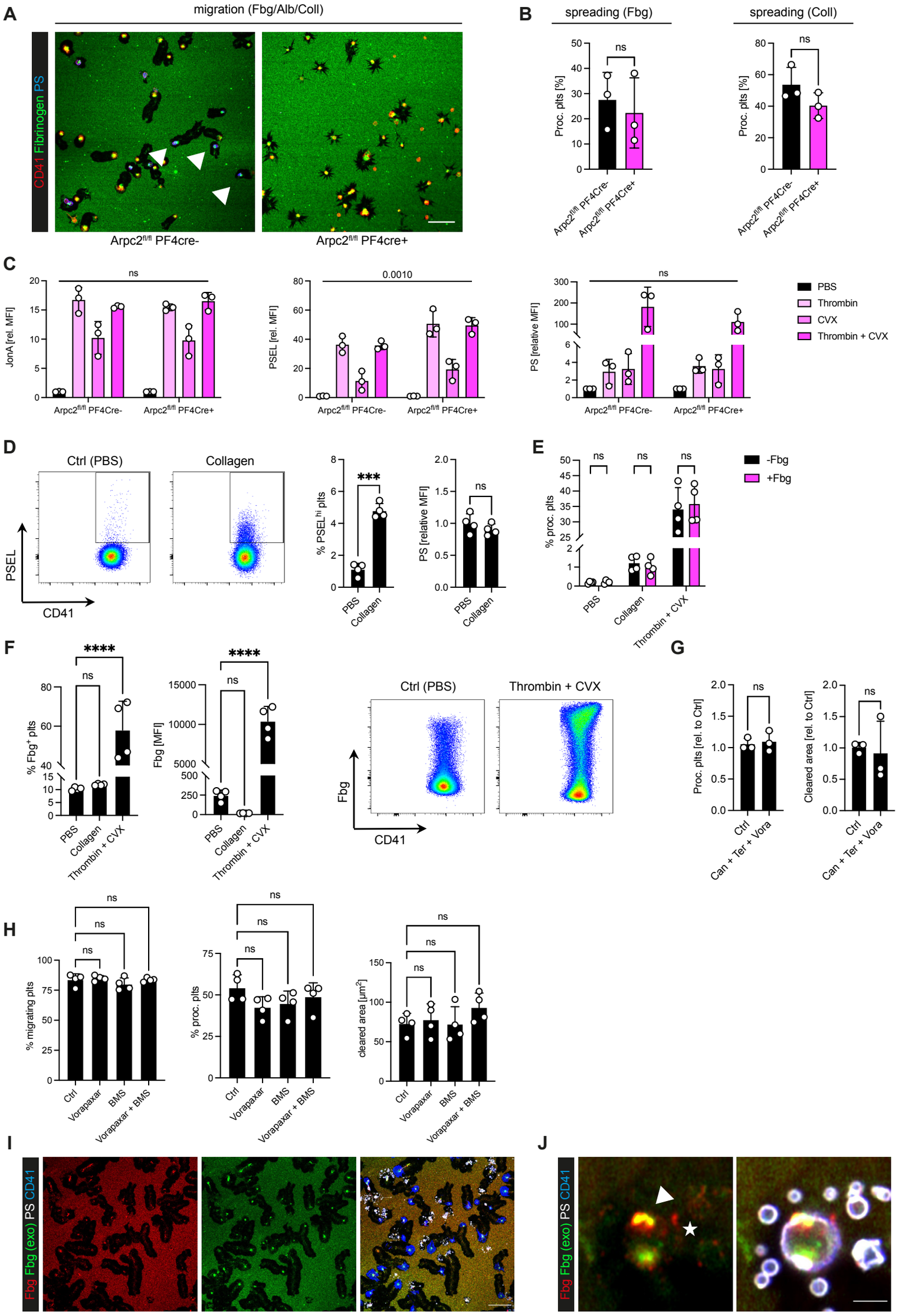

Suppl. Figure 4: Validation of PF4cre-CypD$^{fl/fl}$ and PF4cre-TMEM16F$^{fl/fl}$ mouse lines

Suppl. Figure 5: Supporting data CypD/TMEM16F ALI experiment

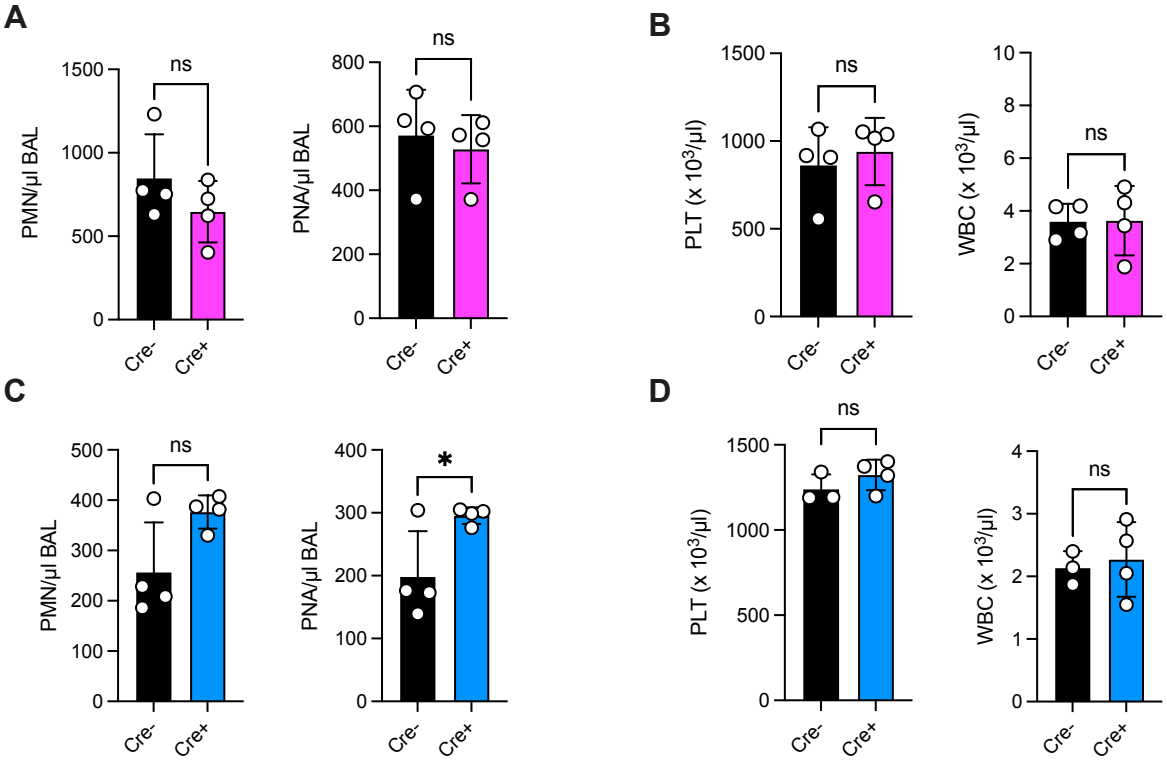

Suppl. Figure 6: Supporting data mechanosensing and calcium signaling

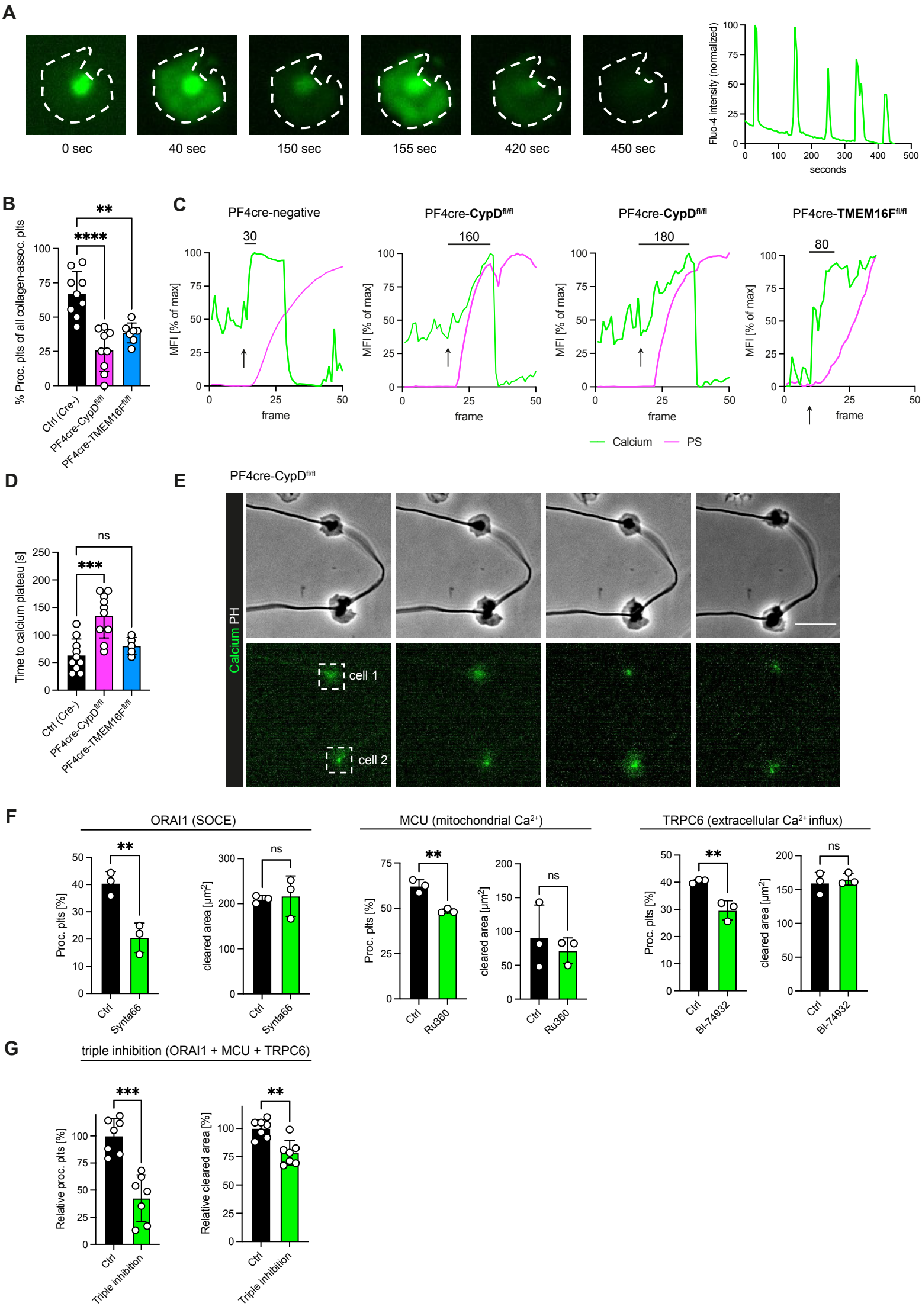

Suppl. Figure 7: Supporting data migration assay (II)

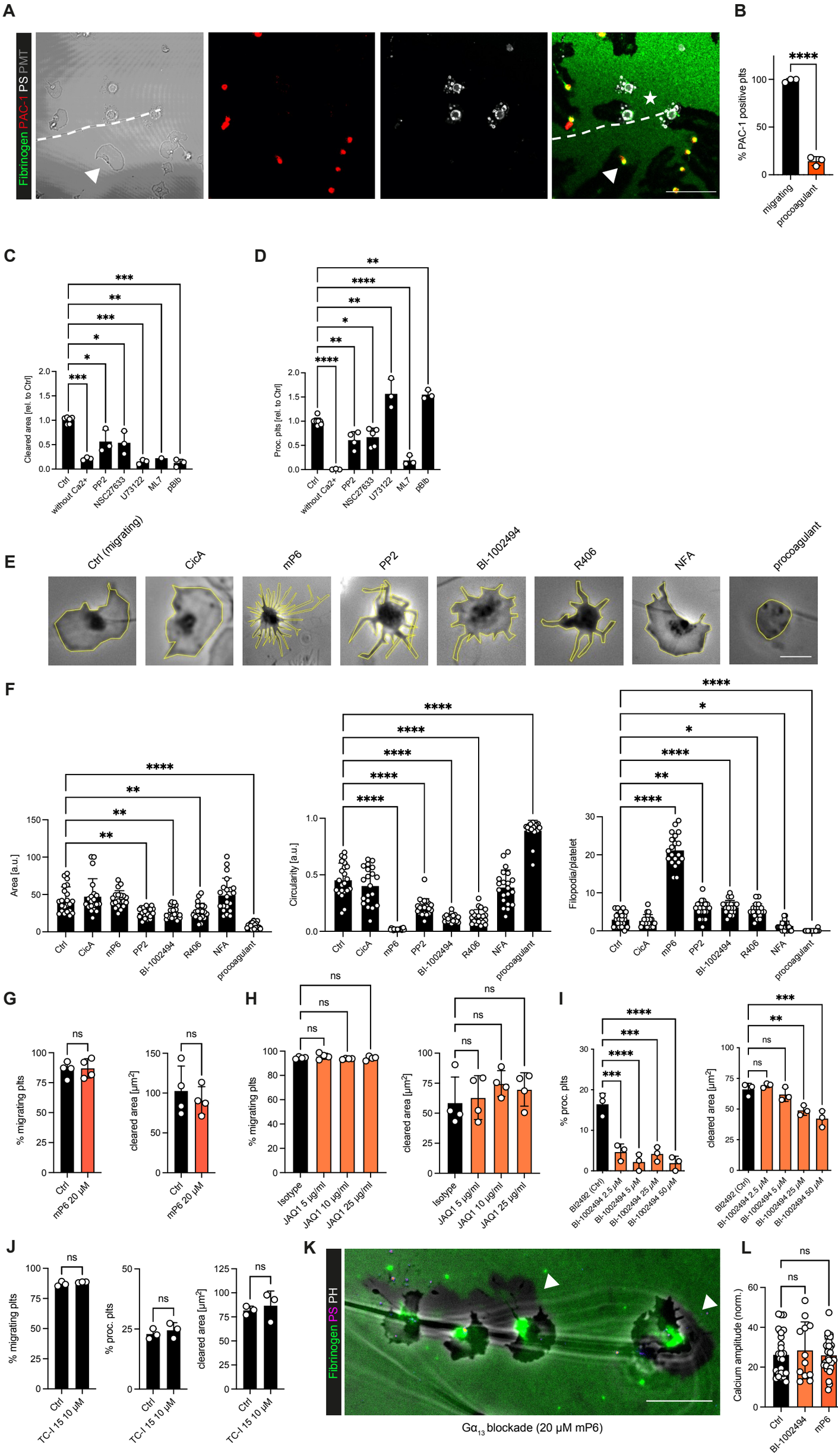

Suppl. Figure 8: Supporting *in vivo* and *in vitro* data for GPIIBIIIA and GPVI blockade

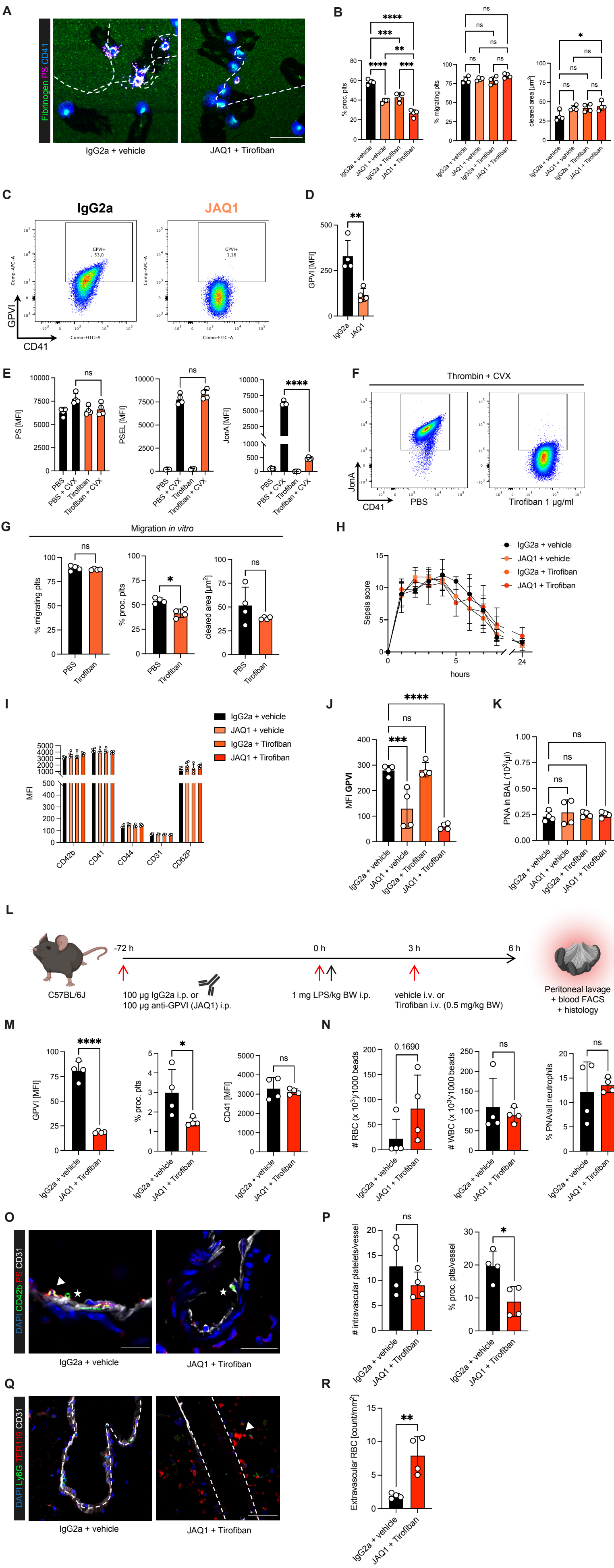

Suppl. Figure 9: Gating strategies

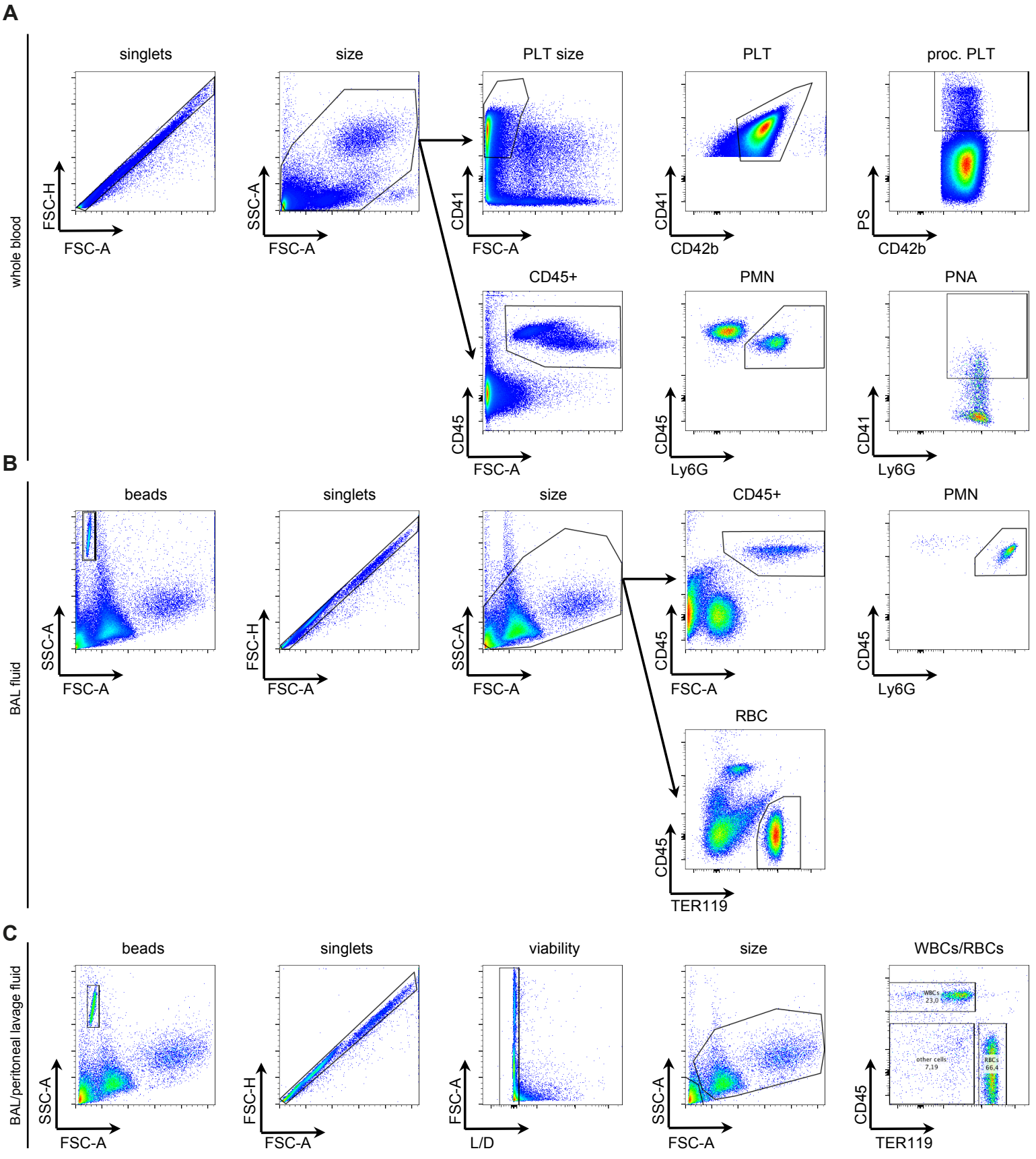

Part VII

References

1. Nicolai L, Massberg S. Platelets as key players in inflammation and infection. Current Opinion in Hematology. 2020;27(1):34-40. doi:10.1097/moh.0000000000000551
2. Gaertner F, Massberg S. Patrolling the vascular borders: platelets in immunity to infection and cancer. Nature Reviews Immunology. 2019;19(12):747-60. doi:10.1038/s41577-019-0202-z
3. Kaiser R, Escaig R, Nicolai L. Hemostasis without clot formation: how platelets guard the vasculature in inflammation, infection, and malignancy. Blood. 2023;142(17):1413-25. doi:10.1182/blood.2023020535
4. Scridon A. Platelets and Their Role in Hemostasis and Thrombosis—From Physiology to Pathophysiology and Therapeutic Implications. International Journal of Molecular Sciences. 2022;23(21):12772. doi:10.3390/ijms232112772
5. Koupenova M, Kehrel BE, Corkrey HA, Freedman JE. Thrombosis and platelets: an update. European Heart Journal. 2016:ehw550. doi:10.1093/eurheartj/ehw550
6. Kaiser R, Escaig R, Erber J, Nicolai L. Neutrophil-Platelet Interactions as Novel Treatment Targets in Cardiovascular Disease. Frontiers in Cardiovascular Medicine. 2022;8. doi:10.3389/fcvm.2021.824112
7. Nicolai L, Pekayvaz K, Massberg S. Platelets: Orchestrators of immunity in host defense and beyond. Immunity. 2024;57(5):957-72. doi:10.1016/j.immuni.2024.04.008
8. Gaertner F, Ahmad Z, Rosenberger G, Fan S, Nicolai L, Busch B, et al. Migrating Platelets Are Mechano-scavengers that Collect and Bundle Bacteria. Cell. 2017;171(6):1368-82.e23. doi:10.1016/j.cell.2017.11.001
9. Ali RA, Wuescher LM, Dona KR, Worth RG. Platelets Mediate Host Defense against *Staphylococcus aureus* through Direct Bactericidal Activity and by Enhancing Macrophage Activities. The Journal of Immunology. 2017;198(1):344-51. doi:10.4049/jimmunol.1601178
10. Chapman LM, Aggrey AA, Field DJ, Srivastava K, Ture S, Yui K, et al. Platelets Present Antigen in the Context of MHC Class I. The Journal of Immunology. 2012;189(2):916-23. doi:10.4049/jimmunol.1200580
11. Schrottmaier WC, Mussbacher M, Salzmann M, Assinger A. Platelet-leukocyte interplay during vascular disease. Atherosclerosis. 2020;307:109-20. doi:10.1016/j.atherosclerosis.2020.04.018
12. Kollef MH, Schuster DP. The Acute Respiratory Distress Syndrome. New England Journal of Medicine. 1995;332(1):27-37. doi:doi:10.1056/NEJM199501053320106
13. Zarbock A, Singbartl K, Ley K. Complete reversal of acid-induced acute lung injury by blocking of platelet-neutrophil aggregation. Journal of Clinical Investigation. 2006;116(12):3211-9. doi:10.1172/jci29499
14. Asaduzzaman M, Lavasani S, Rahman M, Zhang S, Braun OÖ, Jeppsson B, et al. Platelets support pulmonary recruitment of neutrophils in abdominal sepsis*. Critical Care Medicine. 2009;37(4):1389-96. doi:10.1097/CCM.0b013e31819ceb71
15. Rahman M, Roller J, Zhang S, Syk I, Menger MD, Jeppsson B, et al. Metalloproteinases regulate CD40L shedding from platelets and pulmonary recruitment of neutrophils in abdominal sepsis. Inflammation Research. 2012;61(6):571-9. doi:10.1007/s00011-012-0446-6
16. Bain BJ. Blood Cells: A Practical Guide: Barbara J. Bain; 2006.
17. Robier C. Platelet morphology. Journal of Laboratory Medicine. 2020;44(5):231-9. doi:10.1515/labmed-2020-0007
18. Frelinger A, Michelson A, Gremmel T. Platelet Physiology. Seminars in Thrombosis and Hemostasis. 2016;42(03):191-204. doi:10.1055/s-0035-1564835
19. Flaumenhaft R, Sharda A. 19 - Platelet Secretion. In: Michelson AD, editor. Platelets (Fourth Edition): Academic Press; 2019. p. 349-70.
20. Frojmovic MM, Milton JG. Human platelet size, shape, and related functions in health and disease. Physiological Reviews. 1982;62(1):185-261. doi:10.1152/physrev.1982.62.1.185
21. Allan HE, Vadgama A, Armstrong PC, Warner TD. Platelet ageing: A review. Thrombosis Research. 2023;231:214-22. doi:10.1016/j.thromres.2022.12.004
22. Rowley JW, Schwertz H, Weyrich AS. Platelet mRNA. Current Opinion in Hematology. 2012;19(5):385-91. doi:10.1097/moh.0b013e328357010e
23. Ajanel A, Campbell RA, Denorme F. Platelet mitochondria: the mighty few. Current Opinion in Hematology. 2023;30(5):167-74. doi:10.1097/moh.0000000000000772
24. Grichine A, Jacob S, Eckly A, Villaret J, Joubert C, Appaix F, et al. The fate of mitochondria during platelet activation. Blood Advances. 2023;7(20):6290-302. doi:10.1182/bloodadvances.2023010423

25. Denorme F, Campbell RA. Procoagulant platelets: novel players in thromboinflammation. American Journal of Physiology-Cell Physiology. 2022;323(4):C951-C8. doi:10.1152/ajpcell.00252.2022
26. Masselli E, Pozzi G, Vaccarezza M, Mirandola P, Galli D, Vitale M, et al. ROS in Platelet Biology: Functional Aspects and Methodological Insights. International Journal of Molecular Sciences. 2020;21(14):4866. doi:10.3390/ijms21144866
27. Melchinger H, Jain K, Tyagi T, Hwa J. Role of Platelet Mitochondria: Life in a Nucleus-Free Zone. Frontiers in Cardiovascular Medicine. 2019;6. doi:10.3389/fcvm.2019.00153
28. Berger G, Masse J, Cramer E. Alpha-granule membrane mirrors the platelet plasma membrane and contains the glycoproteins Ib, IX, and V. Blood. 1996;87(4):1385-95. doi:10.1182/blood.v87.4.1385.bloodjournal8741385
29. Raposo G, Marks MS, Cutler DF. Lysosome-related organelles: driving post-Golgi compartments into specialisation. Current Opinion in Cell Biology. 2007;19(4):394-401. doi:10.1016/j.ceb.2007.05.001
30. Li R. 10 - The Glycoprotein Ib-IX-V Complex. In: Michelson AD, editor. Platelets (Fourth Edition): Academic Press; 2019. p. 193-211.
31. Modderman PW, Admiraal LG, Sonnenberg A, Von Dem Borne AE. Glycoproteins V and Ib-IX form a noncovalent complex in the platelet membrane. Journal of Biological Chemistry. 1992;267(1):364-9. doi:10.1016/s0021-9258(18)48503-1
32. Clemetson K. A short history of platelet glycoprotein Ib complex. Thrombosis and Haemostasis. 2007;98(07):63-8. doi:10.1160/th07-05-0327
33. Simon DI, Chen Z, Xu H, Li CQ, Dong J-f, McIntire LV, et al. Platelet Glycoprotein Ibα Is a Counterreceptor for the Leukocyte Integrin Mac-1 (Cd11b/Cd18). Journal of Experimental Medicine. 2000;192(2):193-204. doi:10.1084/jem.192.2.193
34. Saboor M, Ayub Q, Ilyas S, Moinuddin. Platelet receptors; an instrumental of platelet physiology. Pak J Med Sci. 2013;29(3):891-6. doi:10.12669/pjms.293.3497
35. Bledzka K, Qin J, Plow EF. 12 - Integrin αIIbβ3. In: Michelson AD, editor. Platelets (Fourth Edition): Academic Press; 2019. p. 227-41.
36. Clemetson KJ, Clemetson JM. 9 - Platelet Receptors. In: Michelson AD, editor. Platelets (Fourth Edition): Academic Press; 2019. p. 169-92.
37. Furie B, Furie BC. The Molecular Basis of Platelet and Endothelial Cell Interaction with Neutrophils and Monocytes: Role of P-Selectin and the P-Selectin Ligand, PSGL-1. Thromb Haemost. 1995;74(07):224-7. doi:10.1055/s-0038-1642681
38. McEver RP, Cummings RD. Perspectives series: cell adhesion in vascular biology. Role of PSGL-1 binding to selectins in leukocyte recruitment. The Journal of clinical investigation. 1997;100(3):485-91.
39. Hamburger S, McEver R. GMP-140 mediates adhesion of stimulated platelets to neutrophils. Blood. 1990;75(3):550-4. doi:10.1182/blood.v75.3.550.550
40. Henn V, Slupsky JR, Gräfe M, Anagnostopoulos I, Förster R, Müller-Berghaus G, et al. CD40 ligand on activated platelets triggers an inflammatory reaction of endothelial cells. Nature. 1998;391(6667):591-4. doi:10.1038/35393
41. Zuchtriegel G, Uhl B, Puhr-Westerheide D, Pörnbacher M, Lauber K, Krombach F, et al. Platelets Guide Leukocytes to Their Sites of Extravasation. PLOS Biology. 2016;14(5):e1002459. doi:10.1371/journal.pbio.1002459
42. Betts MR, Brenchley JM, Price DA, De Rosa SC, Douek DC, Roederer M, et al. Sensitive and viable identification of antigen-specific CD8+ T cells by a flow cytometric assay for degranulation. Journal of Immunological Methods. 2003;281(1):65-78. doi:https://doi.org/10.1016/S0022-1759(03)00265-5
43. Brown EJ, Frazier WA. Integrin-associated protein (CD47) and its ligands. Trends in cell biology. 2001;11(3):130-5.
44. Burkhart JM, Vaudel M, Gambaryan S, Radau S, Walter U, Martens L, et al. The first comprehensive and quantitative analysis of human platelet protein composition allows the comparative analysis of structural and functional pathways. Blood. 2012;120(15):e73-e82. doi:10.1182/blood-2012-04-416594
45. Endemann G, Stanton LW, Madden KS, Bryant CM, White RT, Protter AA. CD36 is a receptor for oxidized low density lipoprotein. Journal of Biological Chemistry. 1993;268(16):11811-6. doi:10.1016/s0021-9258(19)50272-1
46. Haining EJ, Nicolson PLR, Onselaer M-B, Poulter NS, Rayes J, Thomas MR, et al. 11 - GPVI and CLEC-2. In: Michelson AD, editor. Platelets (Fourth Edition): Academic Press; 2019. p. 213-26.
47. Sugiyama T, Okuma M, Ushikubi F, Sensaki S, Kanaji K, Uchino H. A novel platelet aggregating factor found in a patient with defective collagen-induced platelet aggregation and autoimmune thrombocytopenia. Blood. 1987;69(6):1712-20. doi:10.1182/blood.v69.6.1712.1712

48. Kerrigan AM, Navarro-Nuñez L, Pyz E, Finney BA, Willment JA, Watson SP, et al. Podoplanin-expressing inflammatory macrophages activate murine platelets via CLEC-2. Journal of Thrombosis and Haemostasis. 2012;10(3):484-6. doi:10.1111/j.1538-7836.2011.04614.x
49. Rayes J, Jadoui S, Lax S, Gros A, Wichaiyo S, Ollivier V, et al. The contribution of platelet glycoprotein receptors to inflammatory bleeding prevention is stimulus and organ dependent. Haematologica. 2018;103(6):e256-e8. doi:10.3324/haematol.2017.182162
50. Hitchcock JR, Cook CN, Bobat S, Ross EA, Flores-Langarica A, Lowe KL, et al. Inflammation drives thrombosis after Salmonella infection via CLEC-2 on platelets. Journal of Clinical Investigation. 2015;125(12):4429-46. doi:10.1172/jci79070
51. Boulaftali Y, Hess PR, Getz TM, Cholka A, Stolla M, Mackman N, et al. Platelet ITAM signaling is critical for vascular integrity in inflammation. Journal of Clinical Investigation. 2013. doi:10.1172/jci65154
52. Lam FW, Vijayan KV, Rumbaut RE. Platelets and Their Interactions with Other Immune Cells. Comprehensive Physiology. 2015:1265-80. doi:10.1002/cphy.c140074
53. Nachman RL, Rafii S. Platelets, Petechiae, and Preservation of the Vascular Wall. New England Journal of Medicine. 2008;359(12):1261-70. doi:10.1056/nejmra0800887
54. Nieswandt B, Pleines I, Bender M. Platelet adhesion and activation mechanisms in arterial thrombosis and ischaemic stroke. Journal of Thrombosis and Haemostasis. 2011;9:92-104. doi:https://doi.org/10.1111/j.1538-7836.2011.04361.x
55. Nieswandt B, Watson SP. Platelet-collagen interaction: is GPVI the central receptor? Blood. 2003;102(2):449-61. doi:10.1182/blood-2002-12-3882
56. Furie B, Furie BC. Mechanisms of Thrombus Formation. New England Journal of Medicine. 2008;359(9):938-49. doi:10.1056/nejmra0801082
57. Ginsberg MH, Partridge A, Shattil SJ. Integrin regulation. Current Opinion in Cell Biology. 2005;17(5):509-16. doi:https://doi.org/10.1016/j.ceb.2005.08.010
58. Li Z, Delaney MK, O'Brien KA, Du X. Signaling During Platelet Adhesion and Activation. Arteriosclerosis, Thrombosis, and Vascular Biology. 2010;30(12):2341-9. doi:10.1161/atvbaha.110.207522
59. Gong H, Shen B, Flevaris P, Chow C, Lam SCT, Voyno-Yasenetskaya TA, et al. G Protein Subunit Gα13 Binds to Integrin αIIbβ3 and Mediates Integrin "Outside-In" Signaling. Science. 2010;327(5963):340-3. doi:10.1126/science.1174779
60. Yeaman MR, Yount NY, Waring AJ, Gank KD, Kupferwasser D, Wiese R, et al. Modular determinants of antimicrobial activity in platelet factor-4 family kinocidins. Biochim Biophys Acta. 2007;1768(3):609-19. doi:10.1016/j.bbamem.2006.11.010
61. Clark SR, Ma AC, Tavener SA, McDonald B, Goodarzi Z, Kelly MM, et al. Platelet TLR4 activates neutrophil extracellular traps to ensnare bacteria in septic blood. Nature Medicine. 2007;13(4):463-9. doi:10.1038/nm1565
62. Nicolai L, Schiefelbein K, Lipsky S, Leunig A, Hoffknecht M, Pekayvaz K, et al. Vascular surveillance by haptotactic blood platelets in inflammation and infection. Nature Communications. 2020;11(1):5778. doi:10.1038/s41467-020-19515-0
63. Mattheij NJA, Gilio K, Van Kruchten R, Jobe SM, Wieschhaus AJ, Chishti AH, et al. Dual Mechanism of Integrin αIIbβ3 Closure in Procoagulant Platelets. Journal of Biological Chemistry. 2013;288(19):13325-36. doi:10.1074/jbc.m112.428359
64. Agbani EO, Van Den Bosch MTJ, Brown E, Williams CM, Mattheij NJA, Cosemans JMEM, et al. Coordinated Membrane Ballooning and Procoagulant Spreading in Human Platelets. Circulation. 2015;132(15):1414-24. doi:10.1161/circulationaha.114.015036
65. Schmitt-Sody M, Metz P, Gottschalk O, Birkenmaier C, Zysk S, Veihelmann A, et al. Platelet P-selectin is significantly involved in leukocyte-endothelial cell interaction in murine antigen-induced arthritis. Platelets. 2007;18(5):365-72. doi:10.1080/09537100701191315
66. Verschoor A, Neuenhahn M, Navarini AA, Graef P, Plaumann A, Seidlmeier A, et al. A platelet-mediated system for shuttling blood-borne bacteria to CD8α+ dendritic cells depends on glycoprotein GPIb and complement C3. Nature Immunology. 2011;12(12):1194-201. doi:10.1038/ni.2140
67. Pease DC. An Electron Microscopic Study of Red Bone Marrow. Blood. 1956;11(6):501-26. doi:10.1182/blood.v11.6.501.501
68. Lefrançais E, Ortiz-Muñoz G, Caudrillier A, Mallavia B, Liu F, Sayah DM, et al. The lung is a site of platelet biogenesis and a reservoir for haematopoietic progenitors. Nature. 2017;544(7648):105-9. doi:10.1038/nature21706
69. Junt T, Schulze H, Chen Z, Massberg S, Goerge T, Krueger A, et al. Dynamic Visualization of Thrombopoiesis Within Bone Marrow. Science. 2007;317(5845):1767-70. doi:doi:10.1126/science.1146304

70. Nishimura S, Nagasaki M, Kunishima S, Sawaguchi A, Sakata A, Sakaguchi H, et al. IL-1α induces thrombopoiesis through megakaryocyte rupture in response to acute platelet needs. Journal of Cell Biology. 2015;209(3):453-66. doi:10.1083/jcb.201410052
71. Machlus KR, Italiano JE. The incredible journey: From megakaryocyte development to platelet formation. Journal of Cell Biology. 2013;201(6):785-96. doi:10.1083/jcb.201304054
72. Avecilla ST, Hattori K, Heissig B, Tejada R, Liao F, Shido K, et al. Chemokine-mediated interaction of hematopoietic progenitors with the bone marrow vascular niche is required for thrombopoiesis. Nature Medicine. 2004;10(1):64-71. doi:10.1038/nm973
73. Pitchford SC, Lodie T, Rankin SM. VEGFR1 stimulates a CXCR4-dependent translocation of megakaryocytes to the vascular niche, enhancing platelet production in mice. Blood. 2012;120(14):2787-95. doi:10.1182/blood-2011-09-378174
74. Hamad MA, Schanze N, Schommer N, Nührenberg T, Duerschmied D. Reticulated Platelets—Which Functions Have Been Established by In Vivo and In Vitro Data? Cells. 2021;10(5):1172. doi:10.3390/cells10051172
75. Karpatkin S, Charmatz A. Heterogeneity of human Platelets. Journal of Clinical Investigation. 1969;48(6):1073-82. doi:10.1172/jci106063
76. Kienast J, Schmitz G. Flow cytometric analysis of thiazole orange uptake by platelets: a diagnostic aid in the evaluation of thrombocytopenic disorders. Blood. 1990;75(1):116-21. doi:10.1182/blood.v75.1.116.116
77. Hirsh J, Glynn MF, Mustard JF. The effect of platelet age on platelet adherence to collagen. Journal of Clinical Investigation. 1968;47(3):466-73. doi:10.1172/jci105743
78. Detwiler TC, Odell TT, McDonald TP. Platelet size, ATP content, and clot retraction in relation to platelet age. American Journal of Physiology-Legacy Content. 1962;203(1):107-10. doi:10.1152/ajplegacy.1962.203.1.107
79. Bongiovanni D, Han J, Klug M, Kirmes K, Viggiani G, Von Scheidt M, et al. Role of Reticulated Platelets in Cardiovascular Disease. Arteriosclerosis, Thrombosis, and Vascular Biology. 2022;42(5):527-39. doi:10.1161/atvbaha.121.316244
80. Allan HE, Hayman MA, Marcone S, Chan MV, Edin ML, Maffucci T, et al. Proteome and functional decline as platelets age in the circulation. Journal of Thrombosis and Haemostasis. 2021;19(12):3095-112. doi:10.1111/jth.15496
81. Schmitt A, Guichard J, Massé J-M, Debili N, Cramer EM. Of mice and men. Experimental Hematology. 2001;29(11):1295-302. doi:10.1016/s0301-472x(01)00733-0
82. An O, Deppermann C. Platelet lifespan and mechanisms for clearance. Current Opinion in Hematology. 2024;31(1).
83. Handtke S, Thiele T. Large and small platelets—(When) do they differ? Journal of Thrombosis and Haemostasis. 2020;18(6):1256-67. doi:10.1111/jth.14788
84. Quach ME, Chen W, Li R. Mechanisms of platelet clearance and translation to improve platelet storage. Blood. 2018;131(14):1512-21. doi:10.1182/blood-2017-08-743229
85. Soslau G, Giles J. The loss of sialic acid and its prevention in stored human platelets. Thrombosis Research. 1982;26(6):443-55. doi:10.1016/0049-3848(82)90316-4
86. Wei M, Wang PG. Chapter Two - Desialylation in physiological and pathological processes: New target for diagnostic and therapeutic development. In: Zhang L, editor. Progress in Molecular Biology and Translational Science. 162: Academic Press; 2019. p. 25-57.
87. McArthur K, Chappaz S, Kile BT. Apoptosis in megakaryocytes and platelets: the life and death of a lineage. Blood. 2018;131(6):605-10. doi:10.1182/blood-2017-11-742684
88. Kodama T, Takehara T, Hikita H, Shimizu S, Shigekawa M, Li W, et al. BH3-only Activator Proteins Bid and Bim Are Dispensable for Bak/Bax-dependent Thrombocyte Apoptosis Induced by Bcl-xL Deficiency. Journal of Biological Chemistry. 2011;286(16):13905-13. doi:10.1074/jbc.m110.195370
89. Josefsson EC. Platelet intrinsic apoptosis. Thrombosis Research. 2023;231:206-13. doi:10.1016/j.thromres.2022.11.024
90. Suzuki J, Denning DP, Imanishi E, Horvitz HR, Nagata S. Xk-Related Protein 8 and CED-8 Promote Phosphatidylserine Exposure in Apoptotic Cells. Science. 2013;341(6144):403-6. doi:10.1126/science.1236758

Part VIII

Acknowledgements

To my TAC members,

I am grateful for your supervision, your guidance and your interest in my projects. I believe that I am lucky to have been guided by people at the top of their fields. Even though I would have liked to finish my main project prior to my thesis submission, nevertheless, I am glad how far I have progressed with all my projects.

I express my eternal gratitude to Leo, my supervisor, as his motivation and passion towards science has been infectious. From the start I have been encouraged to be independent and become responsible. Leo has been an amazing supervisor as he was approachable and gave me the space to work on my own. I am happy to have had the support to explore all my ideas and the chance to grow into a stronger person, confident in my work. And I must thank Leo for paying for the expensive lab setups I needed for the project. *Leo, it has been a pleasure working with you!*

I am thankful to Charo for her expertise, and her contributions to ALL of my projects. My projects would not have finished without her involvement. I am grateful for her interest and her ideas in my projects.

I am happy to have had the support of Prof. Massberg, and his continued interest in my projects. His positive feedback has always uplifted me, and it is truly amazing how he has taken time out for me out of his busy schedule.

Finally, I would like to thank Prof. Scheiermann, for his interest in the circadian rhythm project and for contributing ideas at every meeting. Thank you for imparting your knowledge, and asking the right questions whenever necessary, as this definitely made the project stronger.

To my colleagues,

You all have been the foundation of my mental strength, and the support I needed on the intense days of my experiments. You have definitely tried to ensure that I participate in social outings and parties when I only wanted to chill at home. I am grateful for the most amazing laughs, intense science discussions, and bets on when I would have handed in my thesis.

I am very grateful to Rainer, for being almost like a mentor and a friend. He has always been happy to share his expertise and help with experiments whenever I needed and he is the most responsive person I know. I am grateful to have him as a colleague and a friend, as he has always motivated me to pursue more and encouraged me to reach my full potential.

I want to thank Marie, for teaching me all I know in the lab. I am happy that I learned all the animal models from a vet like her, as I learned the true importance of doing ethical experiments. Even though we did not have enough time, your calm demeanor was the perfect match for my restlessness during experiments.

Dario is my lab bestie and definitely the person who knows my hurdles well. I truly appreciate the sarcastic relationship we have, and he truly is a gem of an Italian, imparting his culture especially when he is doing surgeries! I am glad that I have you as a friend, but more as a colleague because without you I would have had to do all the surgeries myself, and I should not be good at everything. Jokes aside, thank you for your friendship and scientific support!

I must thank my colleagues, Nadja, Alejandro, Luke, Sezer, Robin, Maité, Flavio, Filip, Evan, Julia, Lulu and Bing for the great fun we had. I want to thank: Alejandro and Nadja for arranging holiday trips for us and being the life of the parties, Luke for being Luke, Sezer for the tastiest food and believing that I can submit my PhD by summer 2024, Robin for the fun drinks, Maité for being a sweetheart, Flavio for the funniest talks and Filip for his deep outlook on life, Lulu and Bing for being the nicest friends, and Evan the funny med student that sneaked into the group of PhDs. I am lucky that I have been blessed with such great company, and I know that they are genuinely happy and proud of my progress.

I am also thankful for the contributions of Fabian, Amar, Magdalena, Abhinaya and Shaan in my projects. Fabian has performed all the proteomics & accompanying analysis and has become a great friend over the last 4 years. I could not have proceeded so far without his support. I want to thank Amar for collaborating on the sea horse analyzer, and who also became a great friend. I am grateful for his scientific contributions. Magdalena has definitely made my life easier with her assistance in my projects. Abhinaya was very funny & great company, and contributed immensely to my projects. Shaan has definitely used his in vitro expertise to help in all the projects and help wrap up the Aging project.

I am very grateful to Micha, Hellen, Dom, Zeljka, Anna, Basti, Susanne, Julia and Denise as the lab is incomplete without their contributions!

To my family and my friends,

I am who I am today because my family. I get to be who I want to be because of my friends.

Abbu, this PhD is for you, your dream. I remember when I was at least 7 years old, you told me that it is your dream that I do a PhD when I am older, and that I be the best at whatever I study. Thank you for being my cheerleader. Ammu, I dedicate my hard work to you, for all your sacrifices and effort. Thank you for being a great mother, and giving the life I live today. I am happy that I can talk to you anytime about anything: lab, life, work. You always say what I need to hear.

To my big brothers. I feel so proud and lucky to have you two in my life. Borobhaiya, you have practically raised me, and are the reason I was able to come here and study. You have ensured at every step, that I am independent and ready to take on any opportunity that comes my way. *My achievements are yours.* Razi bhaiya, from a very young age I have tried to copy you, walk like you and talk like you. Your sacrifices made it possible for me to pursue my dreams. I am happy that I have you as a friend now. *I have been able to succeed because of you.*

To my Borna bhabi, thank you for being a huge part of my life, and making sure I enjoy my life. I love our "Cha" time and "adda". Thank you for my lovely nephews and niece, and ensuring that I get to spend enough time with them. To my Keya bhabi, thank you for your positive calm outlook and making the tastiest food ever. I enjoy our long talks and "adda".

To Ma, thank you for being the coolest mother-in-law ever, who regularly showers me with love and gifts. Thank you for considering me as a responsible person and sharing everything with me. I am grateful to all my-in-laws who had welcomed me with their warm hearts and made me feel so loved and blessed.

I want to thank all of my friends for their friendship, love and support. Sarah, Sanika, Shagoofa, Kakon, Reza, Cinderella, Sarah, Hélène and Hesham. I am the most grateful to my long distance best friend, Sarah, for her unconditional love and support since we were 12. It was hard for both of us to be separated and go years without seeing each other. I am grateful to Hélène for making sure I keep in contact and maintain a social life. I enjoy our deep conversations about life and science. Hesham, practically a family member to us, has been especially supportive since my masters. I am very grateful for his love and support, not only to me but also towards my family and in-laws.

Last but not the least, I thank my husband, for being there for me, at my best and at my very worst. Thanks for understanding, why I needed to pull so many late nighters at work (now you definitely understand). Thank you for your patience, love and support. *For all that I have done, am doing and will do, I cannot do it without you.*